NEW YORK POWER AUTHORITY
123 MAIN STREET
WHITE PLAINS, NY 10601

TECHNICAL REPORT TR-5321-1
REVISION 0

MARK 1 CONTAINMENT PROGRAM

PLANT-UNIQUE ANALYSIS REPORT OF THE TORUS SUPPRESSION CHAMBER

FOR

JAMES A. FITZPATRICK
NUCLEAR POWER PLANT

JULY 27, 1983

TELEDYNE ENGINEERING SERVICES

130 SECOND AVENUE
WALTHAM, MASSACHUSETTS 02254
617-890-3350

ABSTRACT

The work summarized in this report was undertaken as a part of the Mark 1 Containment Long-Term Program. It includes a summary of the analysis that was performed, the results of the analysis and a description of 19 significant modifications that were made to the structure and internals to increase safety margins.

In all cases, the stresses reported in this document meet the allowable levels as defined in the structural acceptance criteria (Reference 3). The methods and assumptions used in this analysis are in strict accordance with USNRC NUREG 0661 (Reference 2), except as noted in the text. The modifications described in this report are also in compliance with NUREG 0661, unless otherwise noted.

TABLE OF CONTENTS

TABLE OF CONTENTS (CONTINUED)

TABLE OF CONTENTS (CONTINUED)

TABLE OF CONTENTS (CONTINUED)

TABLE OF CONTENTS (CONTINUED)

FIGURES AND TABLES

Figures:

FIGURES AND TABLES (CONTINUED)

FIGURES AND TABLES (CONTINUED)

1.0 GENERAL INFORMATION

The purpose of the Mark 1 Torus Program is to evaluate the effects of hydrodynamic loads resulting from a loss of coolant accident and/or an SRV discharge on the torus structure. This report summarizes the results of extensive analysis on the Fitzpatrick torus structure and reports safety margins against established criteria. The content of this report deals with the torus shell, external support system, vent header system and internal structures. Analysis and results for piping attached to the torus (including shell penetrations and internal piping), for the SRV line (except for the submerged portion and tee-quencher), and for the SRV line vent pipe penetration will be presented in a separate piping report, TR-5321-2.

The criteria used to evaluate the torus structure is the ASME Boiler & Pressure Vessel Code, Section III, Division 1, with addenda through Summer 1977 (Reference 11) and Code Case N-197. Modifications were done under Section XI of the ASME Code and meet the Summer 1978 Edition of Section III for design, materials, fabrication, installation and inspection.

A great many technical reports have been written and issued as a part of this program. These reports provide detailed descriptions of the phenomena, the physics controlling the phenomena, calculational methods and detailed procedures for plant unique load calculations. Several of these documents are listed as references in this report. The approach of this report will be to reference these documents, wherever possible, and to avoid a restatement of the same information.

A major part of this program has dealt with providing plant-unique load calculation procedures (Reference 1 is an example of this). In most cases, the loads used to support the analysis were calculated in strict accordance with those procedures, as amended by NUREG 0661 (Reference 2). In some cases, optional methods have been used; these methods are specifically referenced in

Program documentation. Examples of these are the use of plant-unique SRV test data to calibrate SRV analysis, and use of plant unique quarter scale pool swell movies to refine certain water impact and froth loads. In a few cases, analysis assumptions have been made that do not appear in Program documentation; these are identified in the text.

Extensive structural analysis was performed as a part of this evaluation. The major analysis was for dynamic response to time-varying loads. Analysis for static and thermal conditions also form a part of this work. The computer code used to perform almost all of this analysis was the STARDYNE code, as marketed by Control Data Corporation (CDC). STARDYNE is a fully qualified and accepted code in this industry; details of the code are available through CDC. Cases where a computer code other than STARDYNE is used will be identified in the text. All dynamic analysis used damping equal to 2% of critical, unless stated otherwise.

As an aid in processing the large amounts of calculated data, post-processors for the STARDYNE program were written and used. These programs were limited in function to data format manipulations and simple combinations of load or stress data; no difficult computational methods were included.

The loads and load combinations considered in this program required special consideration to determine the appropriate levels of ASME Code application. Reference 3 was developed to provide this standard. Table 5-1 of Reference 3 is the basis for all the evaluation work in this report; it is reproduced in this report as Table 1. This table shows 27 load combinations that must be considered for each structure. The number actually becomes several times that when we consider the many different values associated with various SRV discharge conditions. The approach used in the final evaluation of structures is to reduce this large number to a relatively small number of cases by conservative bounding. For example, load combinations including SSE seismic, have a higher allowable than the same combination with OBE seismic.

For these cases, our first evaluation attempt is to consider the SSE combination against the OBE allowables. If this produces an acceptable result, those numbers are reported as final. This procedure results in many cases where safety margins are understated; this is the case for most of the results.

As an aid in correlating discussion of particular load analyses to detailed program documentation, most analysis described in this report has been referenced directly to a paragraph in the Load Definition Report (Reference 1). This has been done by identifying the applicable LDR paragraph in parenthesis immediately following the title of the load. This referencing directs the reader to a more detailed description of the load than can be included in this report.

2.0 PLANT DESCRIPTION

2.1 General Description

The configuration of the Fitzpatrick torus structure is shown in Figures 2-1 and 2-2.

Figure 2-1 shows a plan view of the torus. It is made up of the sixteen (16) mitred sections, connected to the drywell by eight (8) equally spaced vent pipes. It is supported by two external columns and an intermediate saddle at each of sixteen places, as shown. The columns and saddles are connected to the basemat floor with anchor bolts. Four earthquake restraints, spaced equally around the torus, connect the belly of the torus to the basemat (Figure 3-10).

Figure 2-2 shows some of the inside arrangement. Ring girders reinforce the outer shell at each of the sixteen planes defined by the external support system. The vent header system is supported off of the ring girders and is directly connected to the drywell via the vent pipes. The opening where the vent pipe penetrates the torus shell is sealed by a bellows. The ring girder also supports the spray header, SRV tee-quencher and a partial catwalk. Figures 2-3 to 2-21 show several details of the torus structure. Table 2.0 lists several of the plant specific dimensions.

2.2 Recent Modifications

Over the period of the past few years, many modifications have been made to the Fitzpatrick torus, both to increase its strength and also to mitigate the hydrodynamic loads. The modifications are illustrated and listed in the composite sections of Figures 2-3 and 2-4, along with their installation dates. A description and illustration of each individual modification follows:

2.2.1 Modifications to Reduce Hydrodynamic Loads

Drywell Pressurization System (ΔP System)

Installation of a system to maintain a pressure differential between torus and drywell was the first modification of this Program. The system is illustrated in Figure 2-5. It is designed to maintain a minimum positive pressure difference of 1.7 psi between the vent system (drywell) and the airspace inside the torus. The result of this pressure difference (ΔP) is to depress the water leg in the downcomers and reduce the water slug that must be cleared, if rapid pressurization of the drywell occurs. Early generic testing in the Program demonstrated that this was an effective means to reduce shell pressures related to DBA pool swell. The 1.7 psi pressure difference was selected as the basis for the Fitzpatrick plant unique quarter-scale pool swell tests and is intended to be the normal operating condition of the plant. As illustrated in Figure 2-5, pressure differential is maintained by using the nitrogen inerting system to pressurize the drywell to 1.7 psi; the torus remains at ambient pressure. No pumping or additional piping is involved.

Vent Header Deflector

The vent header deflector at Fitzpatrick is illustrated in Figures 2-6 and 2-7. It is a 30-inch pipe with a one-inch wall.

The deflector extends under the belly of the vent header to protect the vent header from direct water impact during pool swell. It does this by shadowing the most sensitive part of the vent header and by separating and diverting the rising pool before it can reach the vent header. This deflector was included in the plant unique pool swell tests for Fitzpatrick to provide accurate vent header loading for detailed analysis.

SRV Tee-Quencher

A tee-quencher has been installed at the discharge end of each main steam relief line to replace the existing ramsheads. The quencher and its support is illustrated in Figure 2-8. The quencher serves to divide the SRV discharge bubble into hundreds of smaller bubbles and to distribute them over an entire bay. This division and distribution of SRV discharge has been shown in generic testing to reduce torus shell pressure by factors of two or more when compared to ramshead pressures. The plant-unique characteristics of these devices at Fitzpatrick were determined by in-plant testing after their installation.

The quencher support is also illustrated in Figure 2-8. It is a 20-inch schedule 120 pipe welded to the ring girder, as shown.

Temperature Monitoring System & RHR Return Lines

The addition of a pool temperature monitoring system and an elbow to the discharge end of the RHR return lines are both intended to assure proper operation of the SRV quenchers. These modifications are illustrated in Figure 2-9, 2-10, 2-14 and 2-21.

The temperature monitoring system senses pool temperature through a set of 16 thermowells set around the inside wall of the torus (Figures 2-14 and 2-21). They are averaged to provide pool bulk temperature. The system is hard wired to a console in the control room.

The elbows on the RHR return lines were added to provide pool circulation during periods of extended SRV blowdown. Circulation of the pool with these lines assures that local-to-bulk temperature differences will be minimized and that SRV quencher performance will be maintained during extended discharge. These two RHR return lines were further modified by re-

routing them to the ring girders. The ring girders react drag loads on these lines and also provide for reactions due to elbow discharge loads (Figure 2-10).

Additional SRV Vacuum Breakers

Each of the 11 SRV discharge lines at Fitzpatrick has been fitted with one, ten-inch vacuum breaker, in addition to the original small vacuum breaker. This modification minimizes the temporary formation of the high water leg in the SRV line which could occur after an initial actuation; and thereby limits the high clearing loads which could occur if a second actuation occurred at that time. The location of these devices is different on each SRV line due to space constraints and is not illustrated.

Modification of Submerged Piping

Early analysis showed that some of the submerged piping inside the torus might experience high drag loads which could produce unacceptable stress levels. Three such lines were identified; they are

1. RCIC return lines (eight-inch diameter).
2. Condensate return lines (ten-inch diameter).
3. RHR return lines (described previously - two lines).

Two cases required rerouting; all required additional support to the ring girder. The modifications are illustrated in Figures 2-10, 2-11, and 2-12.

Early analysis also showed that the mitre joint on the HPCI return line might reach unacceptable stress levels. This was a direct consequence of the high stress intensification associated with the fabricated mitre joint. The line was modified by the addition of an elbow in place of the mitre. The modification is illustrated in Figure 2-20.

In addition, the eight vent (one-inch diameter) drain lines were cut off and capped above the pool.

2.2.2 Modifications to Strengthen the Structure

Torus Support Saddles and Anchor Bolts

Support saddles were added under each ring girder as shown in Figure 2-13. The saddles, support columns and ring girder all lie in the same plane and react all vertical loads on the torus - most of the load is reacted by the saddle.

The saddle is constructed of 1½-inch SA 516 GR 70 steel plates, welded to the torus shell and resting on the concrete basemat. It is restrained from upward motion by six pairs of two-inch Williams rock bolts, set 24-inches into the basemat. The anchor bolt restraints are set with a small clearance to allow for normal radial growth of the torus due to temperature changes. Sliding of the saddle is accommodated by lubrite plates between the saddle and basemat.

Column to Anchor Bolts

In addition to the six pairs of anchor bolts that attach to the saddles, there are four anchor bolts attached to each column base plate. These bolts are identical to the saddle anchors and are set with the same 24-inch embedment.

Downcomer Tie-Rods and Vent Header Gussets

The downcomer tie-rods and vent header gussets are illustrated in Figure 2-15.

The tie-rods are constructed from 2½-inch schedule 40 pipe and provide greatly increased capacity to downcomer lateral loads than the original tie bars. They are attached to the downcomers with specially fabricated 24-inch pipe clamps, constructed from 3/4-inch steel. The clamps are prevented from sliding on the downcomers by welded steel clips both above and below the clamp.

The gussets between the downcomers and vent header are necessary to reduce local intersection stresses due to chugging lateral loads on the downcomers. They are constructed from ½-inch thick 516 GR 70 steel plate, and are welded to the vent header and downcomers.

Catwalk Modification

The catwalk at Fitzpatrick would have required major modifications to avoid overstress during pool swell impact and fallback; the extent of the required modifications was considered unacceptable. Accordingly, the entire catwalk was removed except for three bays, centered under the equipment access hatch, as illustrated in Figure 2-16. The center section of the remaining catwalk is in a non-vent bay and includes a small platform that extends toward the center of the torus. Modifications to this part of the catwalk include:

- Addition of four new diagonal supports back to the ring girder (three-inch schedule 80 pipes).
- Replacement of the support for the extension platform.
- Replacement of the handrails with wire rope to reduce drag loads.

Figures 2-17, 7-1 and 7-2 also illustrate the catwalk structure.

Internal Spray Header Modification

The internal spray header at Fitzpatrick is located above the vent header as shown in Figure 2-3. It was originally supported at every second ring girder (eight places around the torus) with full anchors. The system was modified by the addition of an additional restraint at each of the intermediate ring girders. These new supports provide lateral and vertical restraint but allow rotation and axial motion.

The original installation also included supports on the spray header branch lines near the penetrations; these were not modified.

The modification is illustrated in Figure 2-19.

Monorail

A high capacity monorail was installed inside the Fitzpatrick torus for use in handling materials. The monorail extends completely around the torus except for two bays where piping systems are installed. It is illustrated in Figures 2-18 and 7-5.

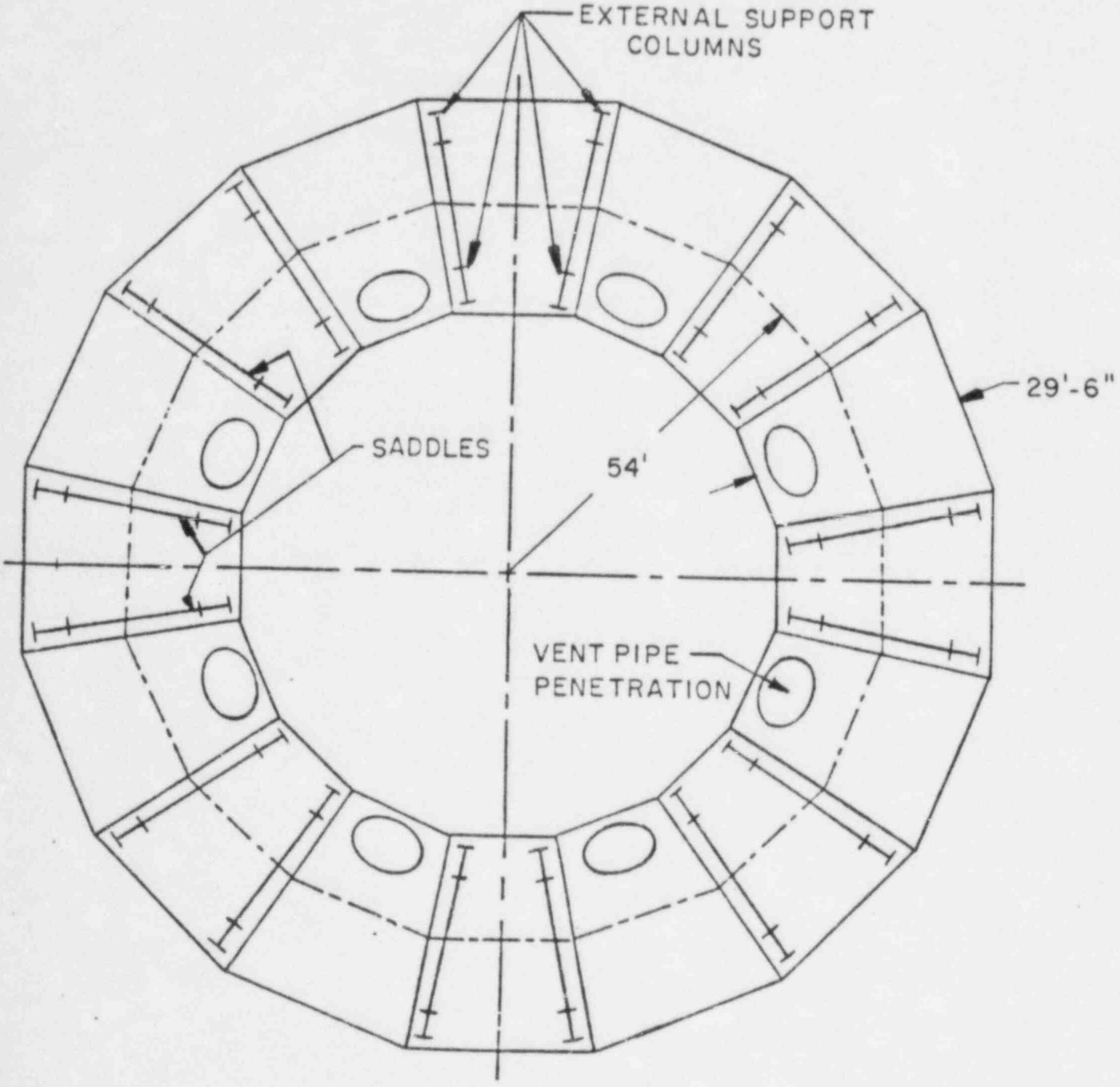

FIG. 2-1
TORUS PLAN VIEW

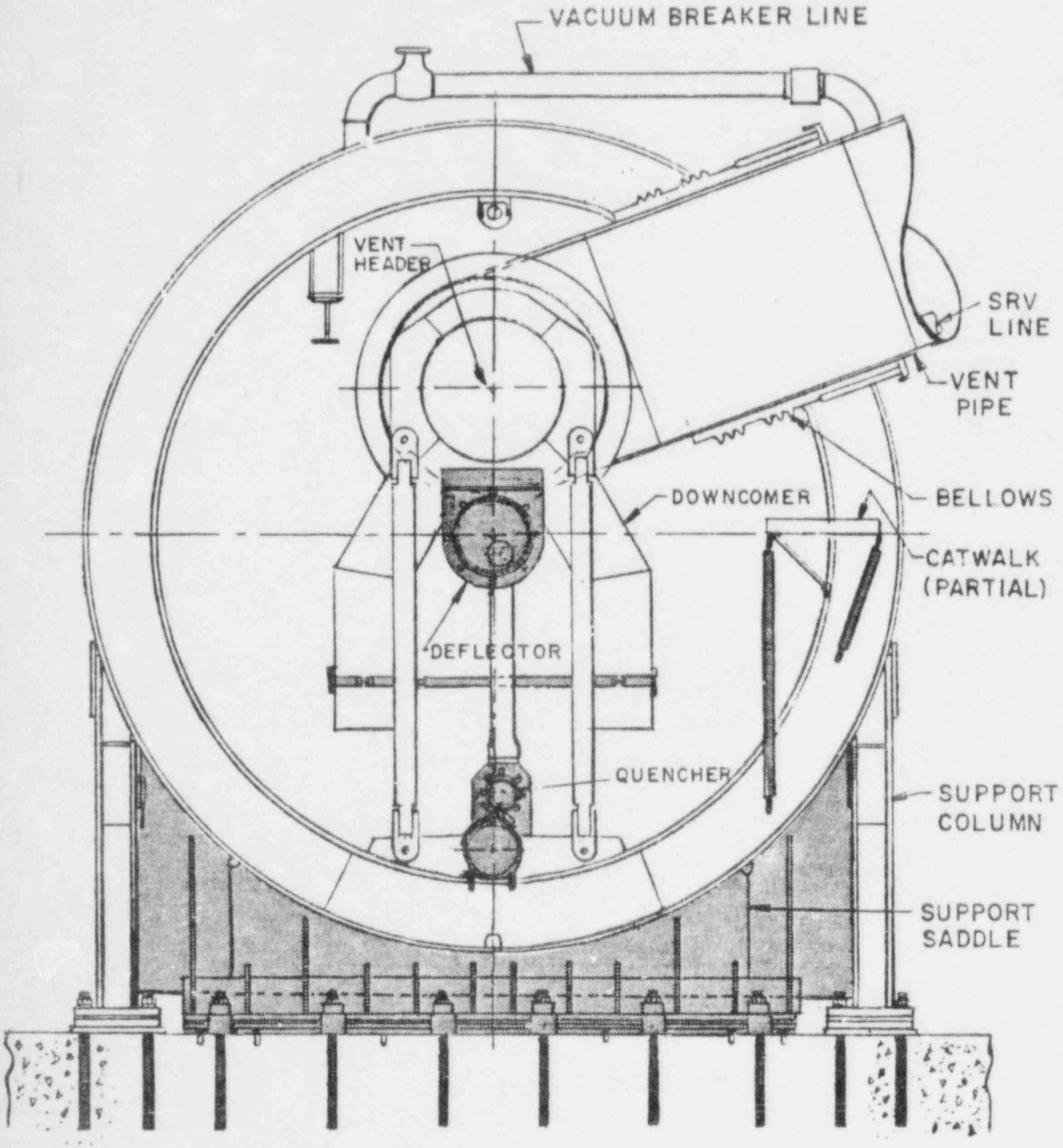

= MODIFICATIONS

FIG. 2-2

TORUS COMPOSITE CROSS SECTION FITZPATRICK

KEY FOR FIGURES 2-3 AND 2-4

	Modification	Completion Date
1.	Mitre Joint Saddles	8/80
2.	Saddle Anchor Bolts	8/80
3.	Downcomer Tie Straps	8/80
4.	Vent Header Deflector	8/80
5.	Vent Header/Downcomer Stiffening	2/82
6.	Monorail	6/80
7.	Catwalk Strengthen & Partial Removal	2/82
8.	Ring Girder, Drain Hole	Complete
9.	Drywell/Wetwell ΔP Control	11/77
10.	Temperature Monitoring System	Complete
11.	Safety Relief Line, Vacuum Breakers & Supports	12/81
12.	SRV Tee-Quencher	12/81
13.	Tee-Quencher Support	12/81
14.	RHR Return Line Elbow	12/81
15.	Modify HPCI Line	12/81
16.	Relocate RCIC Line 8"	12/81
17.	Vent Header Drain	Complete
18.	Relocation of 10" Condensate Line	Complete
19.	Spray Header Support	Complete

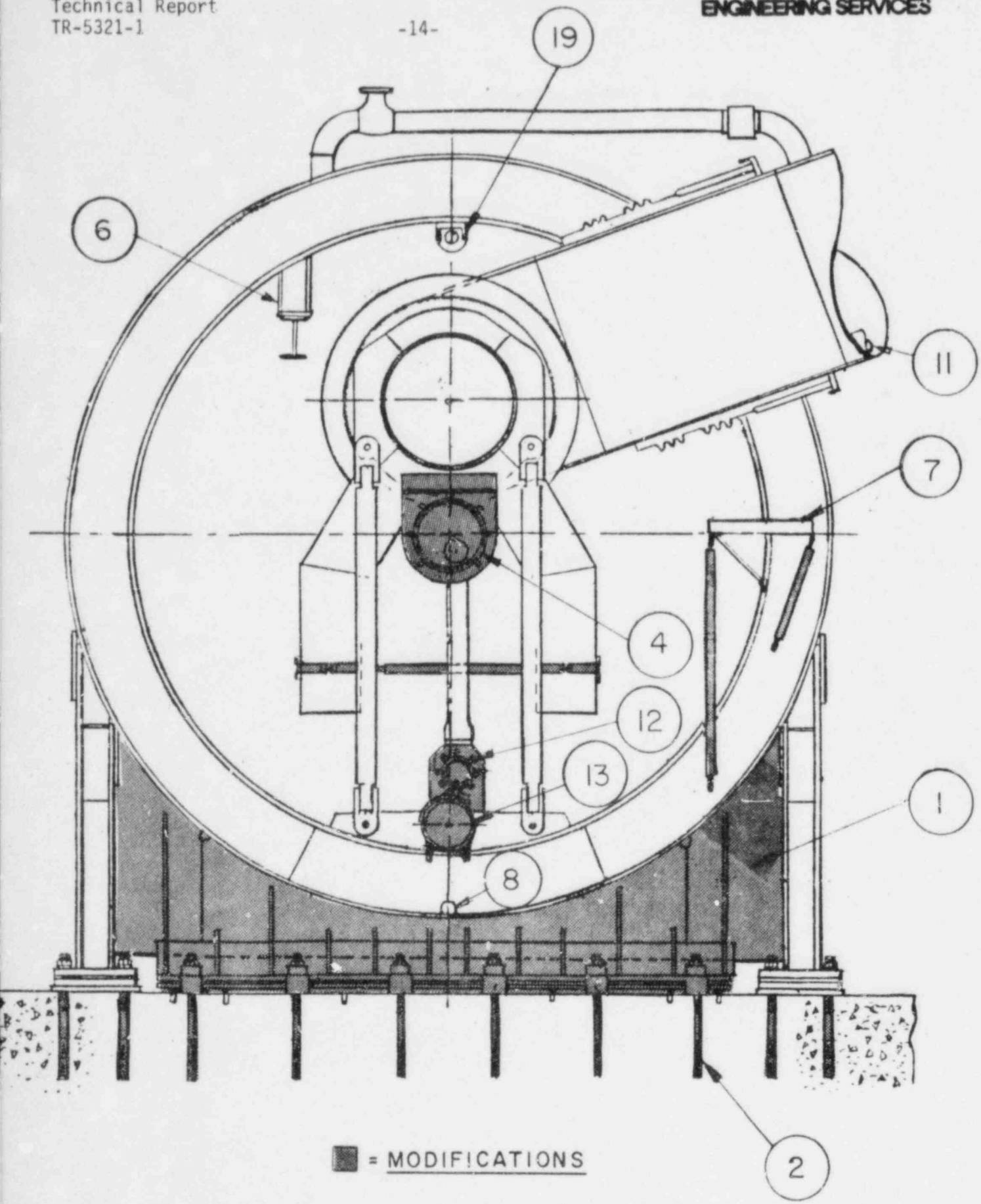

FIG. 2-3
FITZPATRICK TORUS MODIFICATIONS
CROSS-SECTION AT RING GIRDER

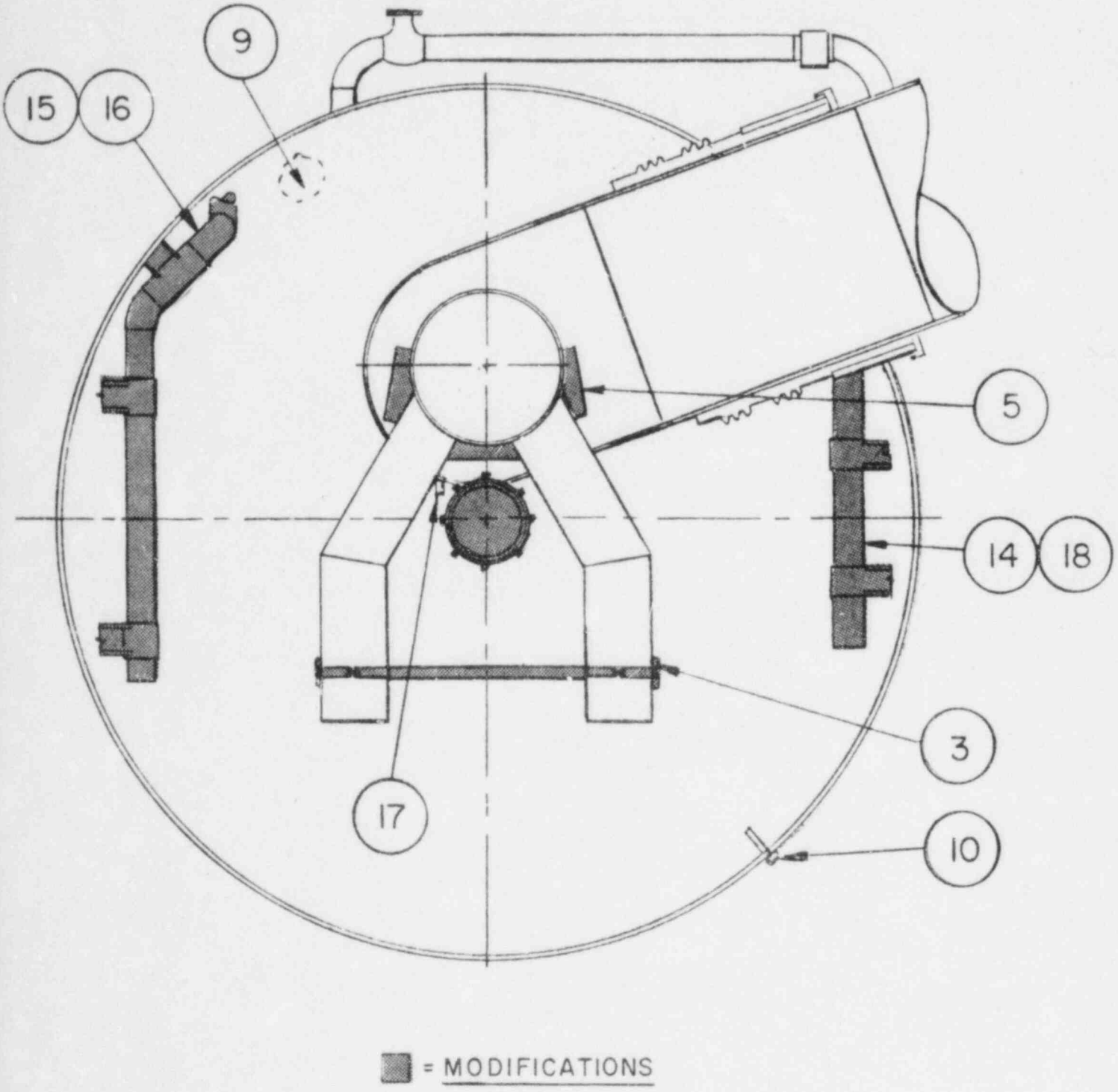

FIG. 2-4
FITZPATRICK TORUS MODIFICATIONS
CROSS-SECTION AT MID BAY

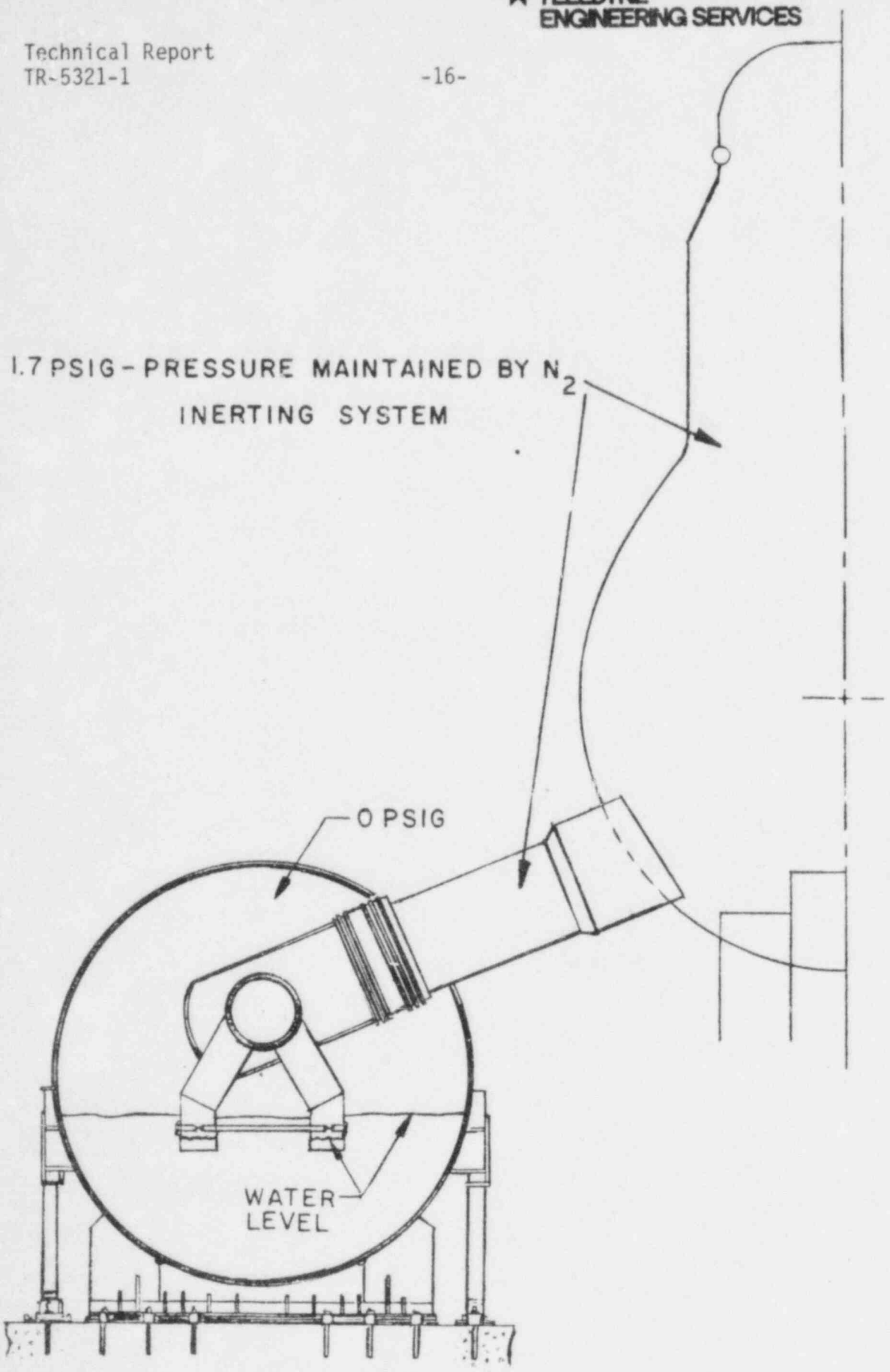

FIG. 2-5

A.P. PRESSURIZATION SYSTEM

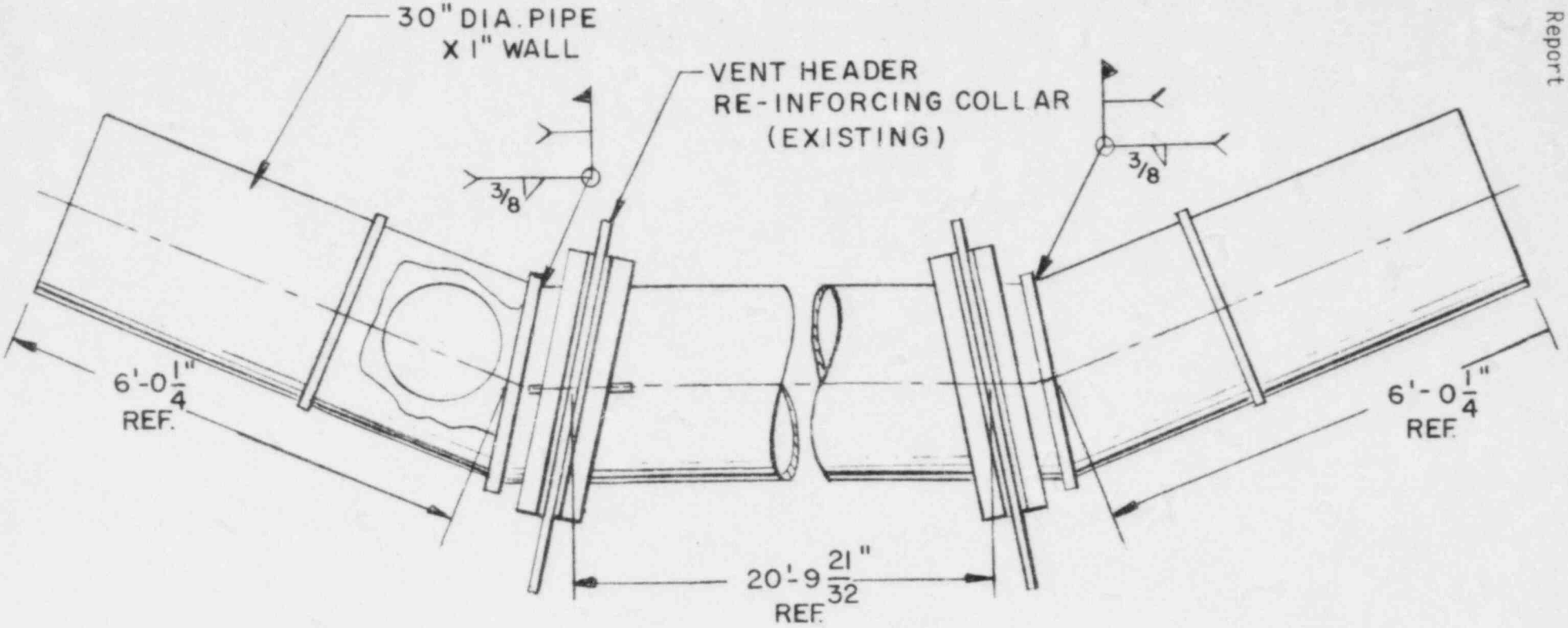

FIG. 2-6

VENT HEADER DEFLECTOR

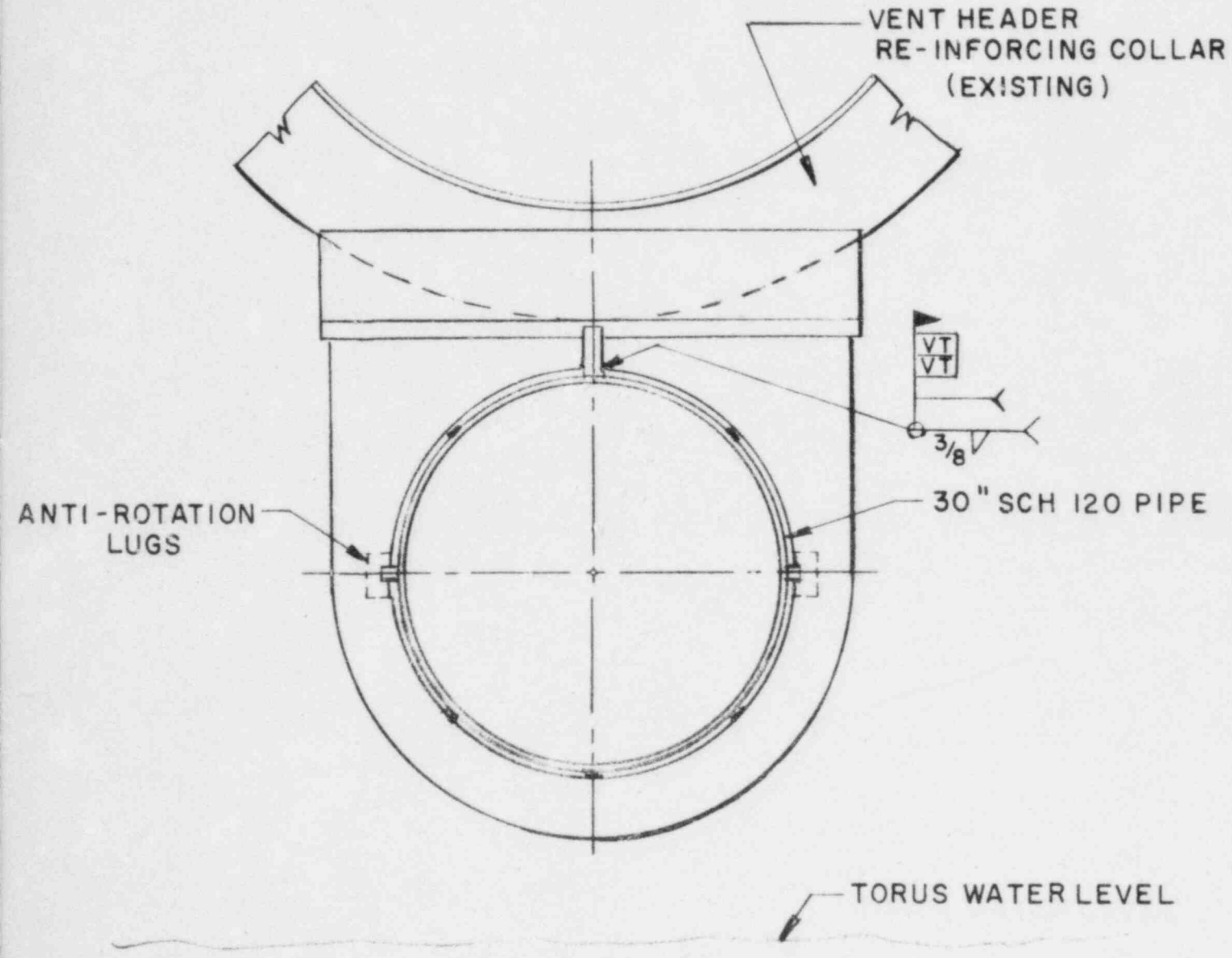

FIG. 2-7

VENT HEADER DEFLECTOR ATTACHMENT

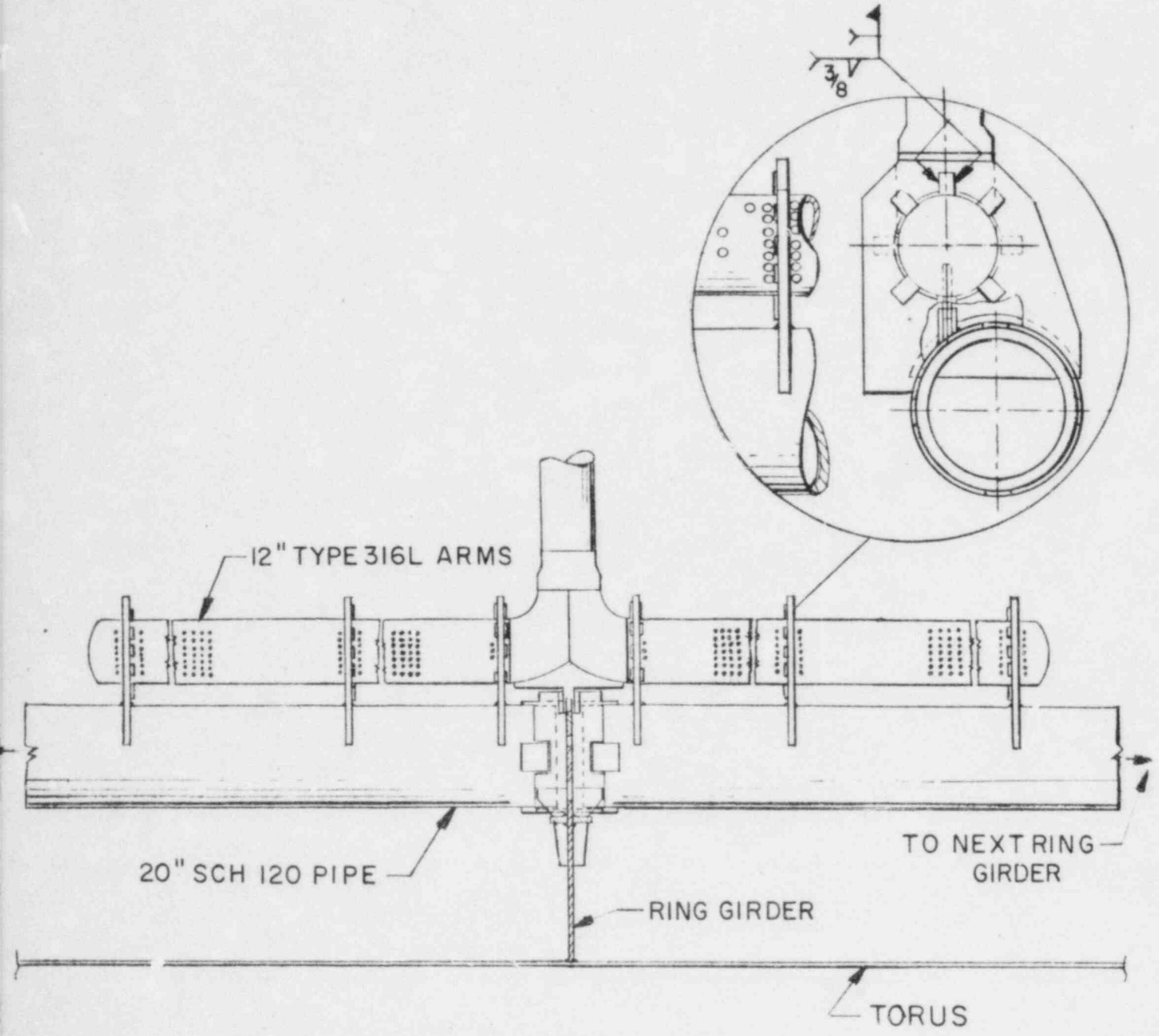

FIG. 2-8

SRV TEE QUENCHER & SUPPORT

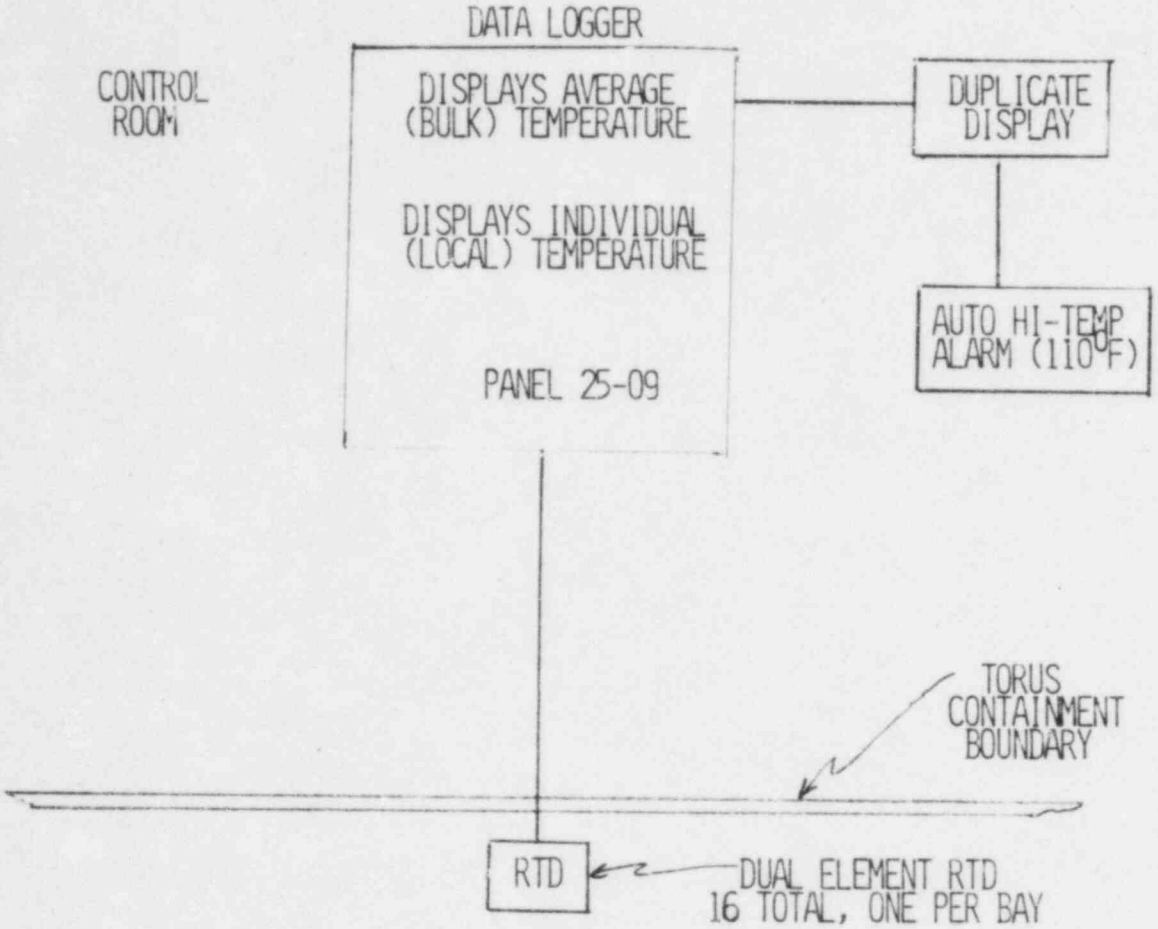

FIGURE 2-9: POOL TEMPERATURE MONITORING SYSTEM

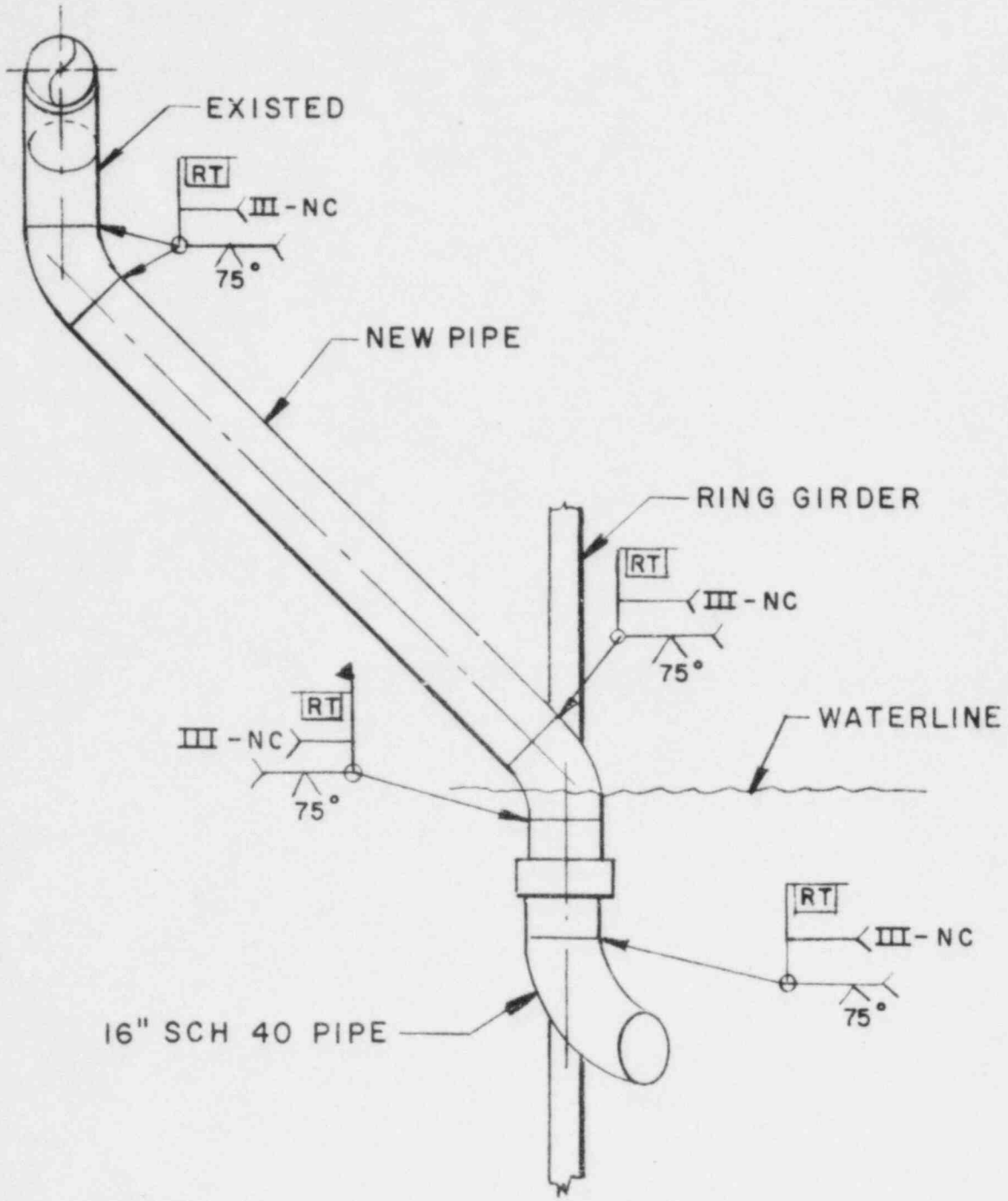

FIG. 2-10
RHR RETURN LINE ELBOW & SUPPORT

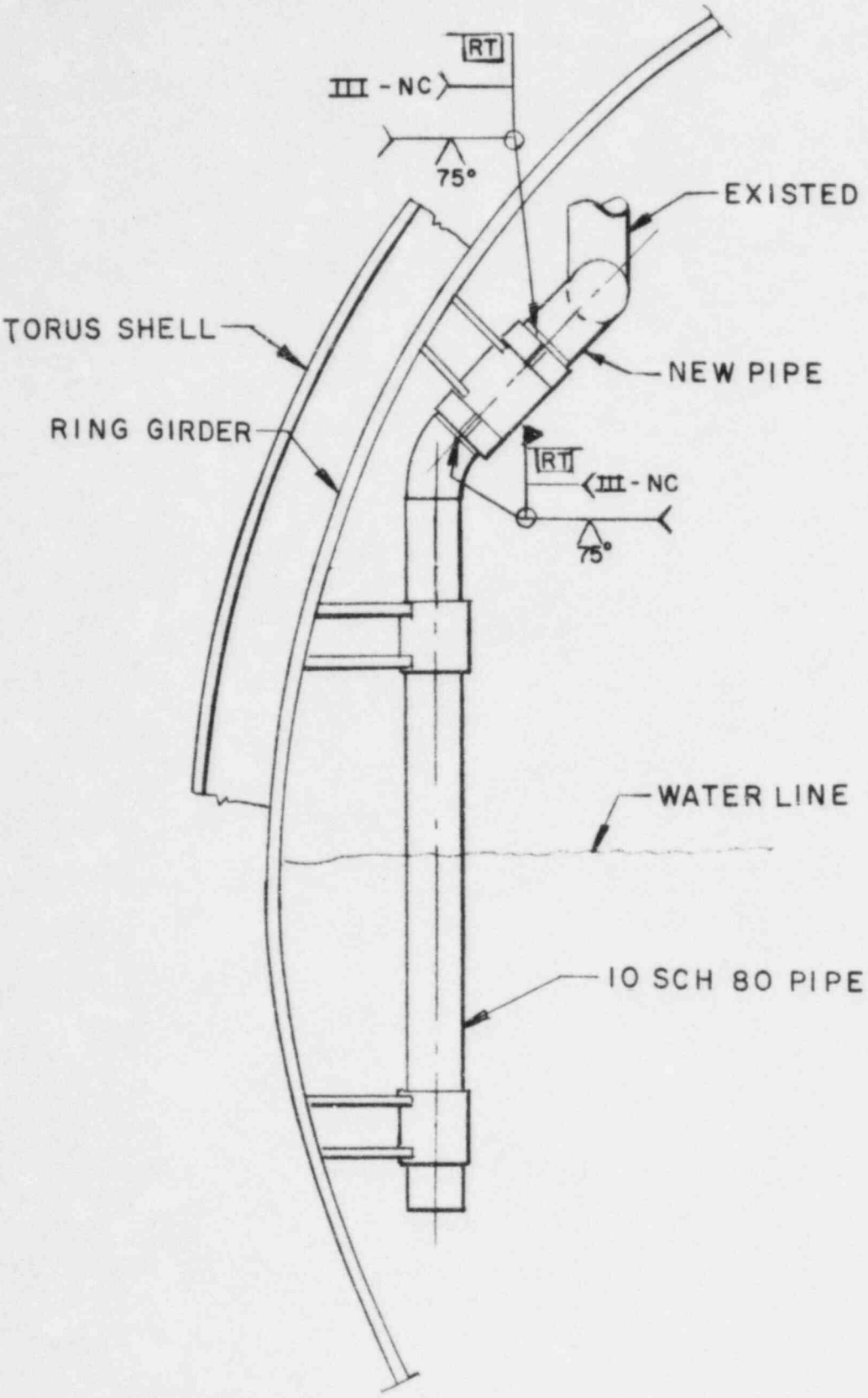

FIG. 2-11
RCIC RETURN LINE MODIFICATION

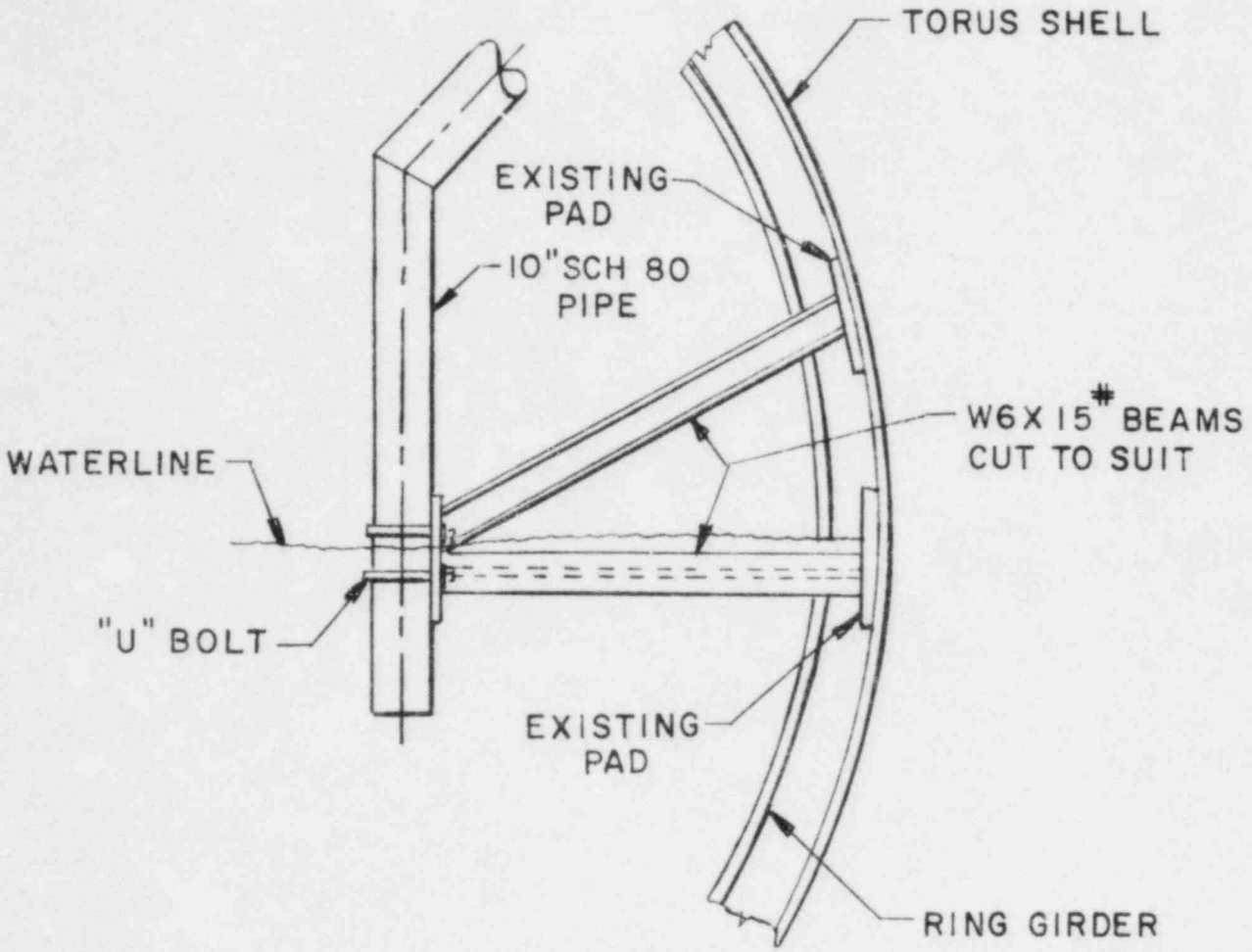

FIG. 2-12
10" CONDENSATE DRAIN LINE

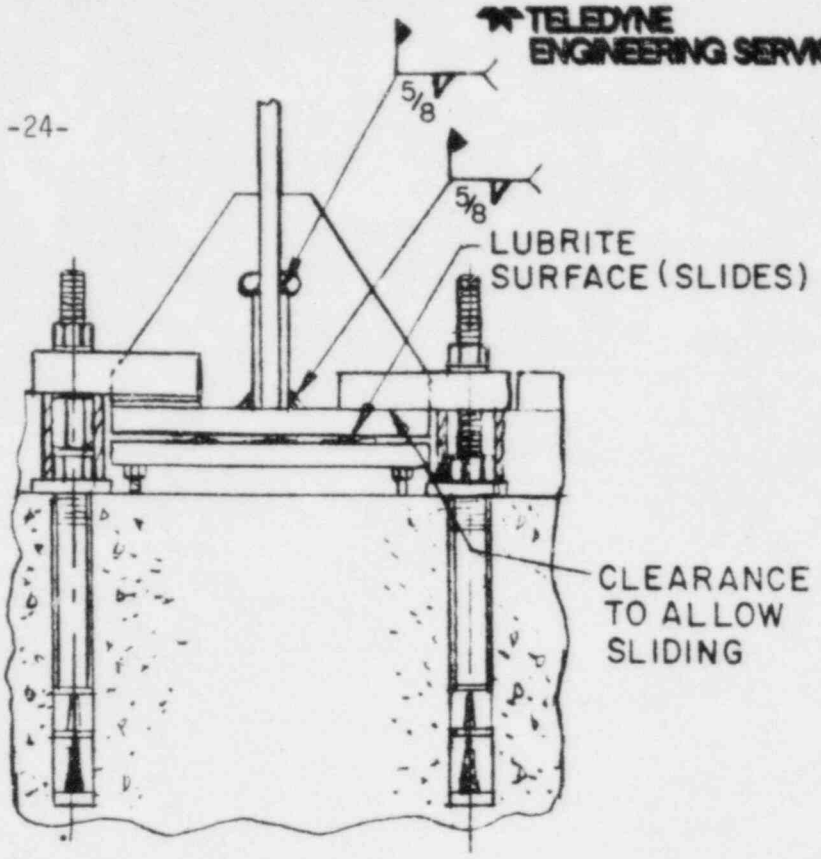

SECTION A-A

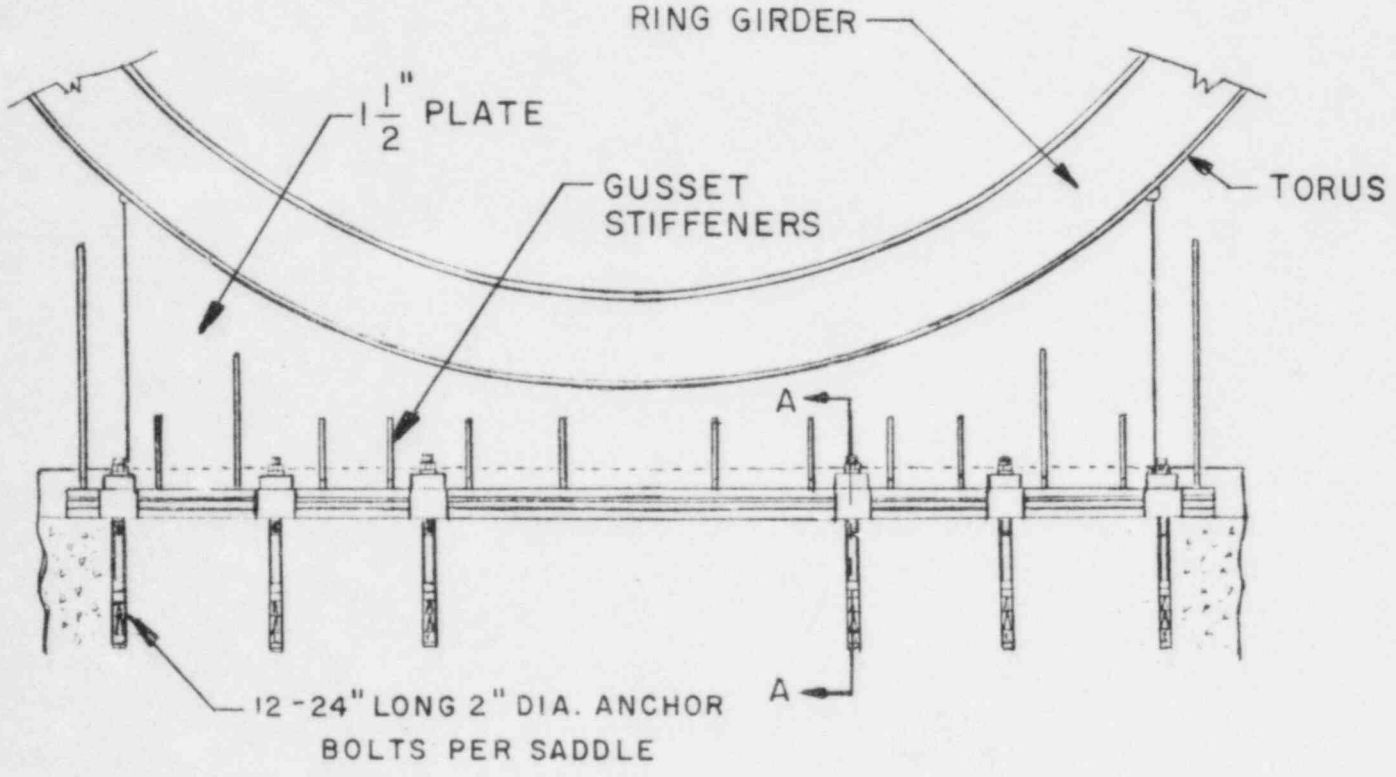

FIG. 2-13

TORUS SUPPORT SADDLES & SADDLE ANCHORS

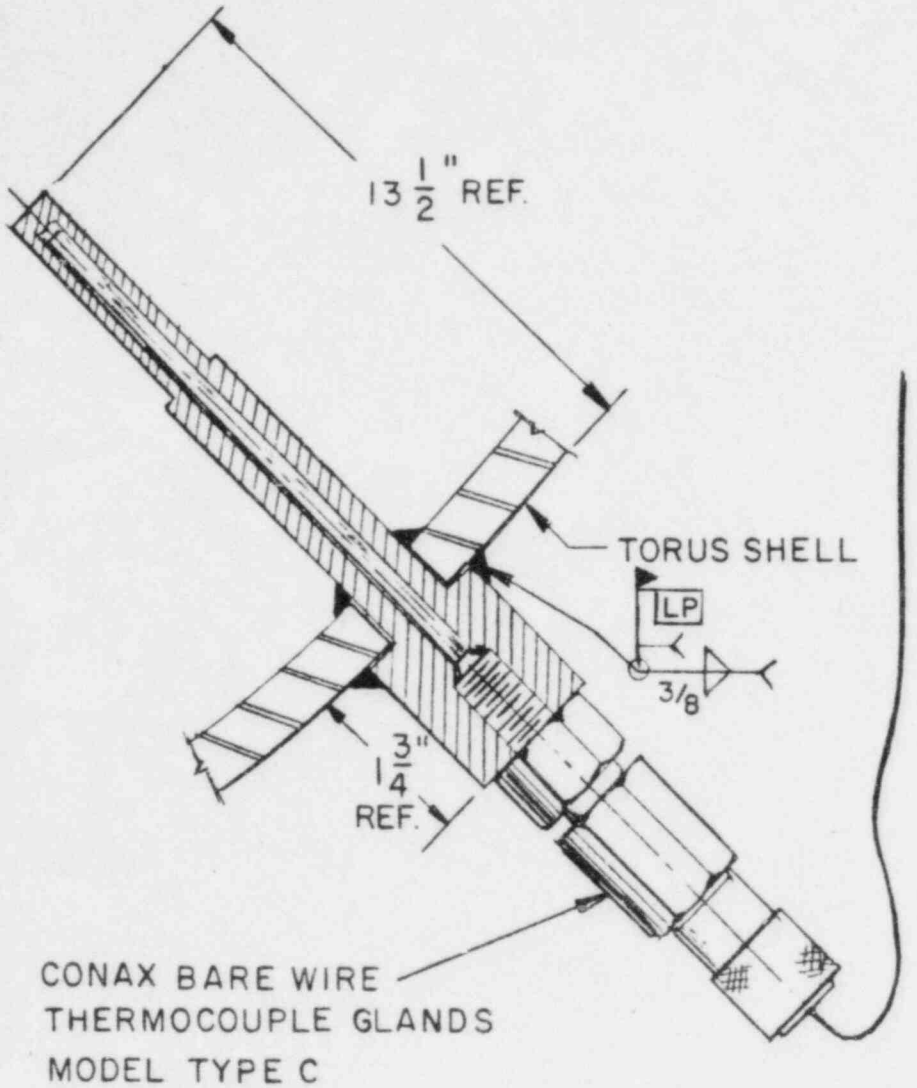

FIG. 2-14

THERMOWELL DETAIL

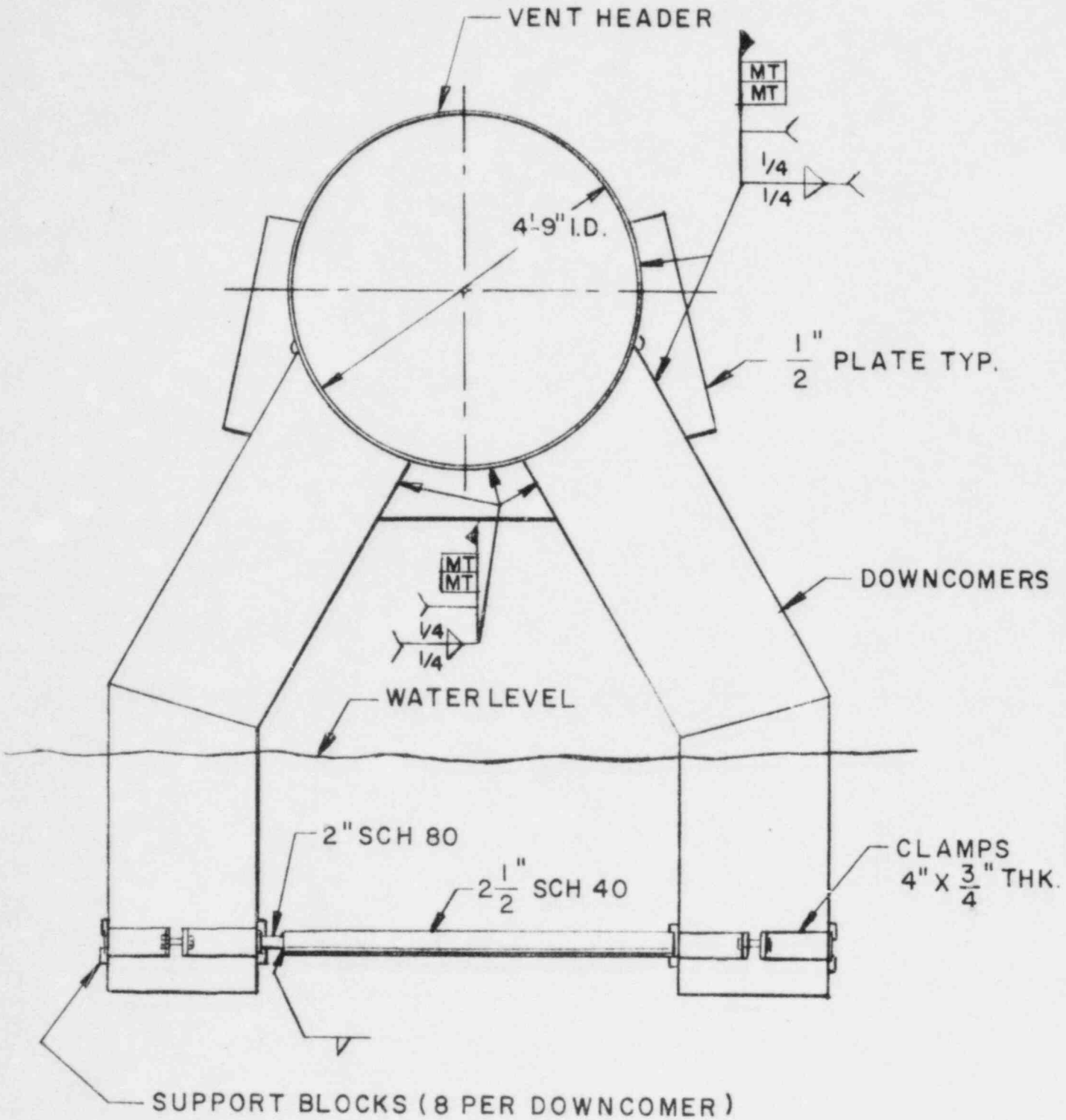

FIG. 2-15

DOWNCOMER TIE-ROD & GUSSET MODIFICATION

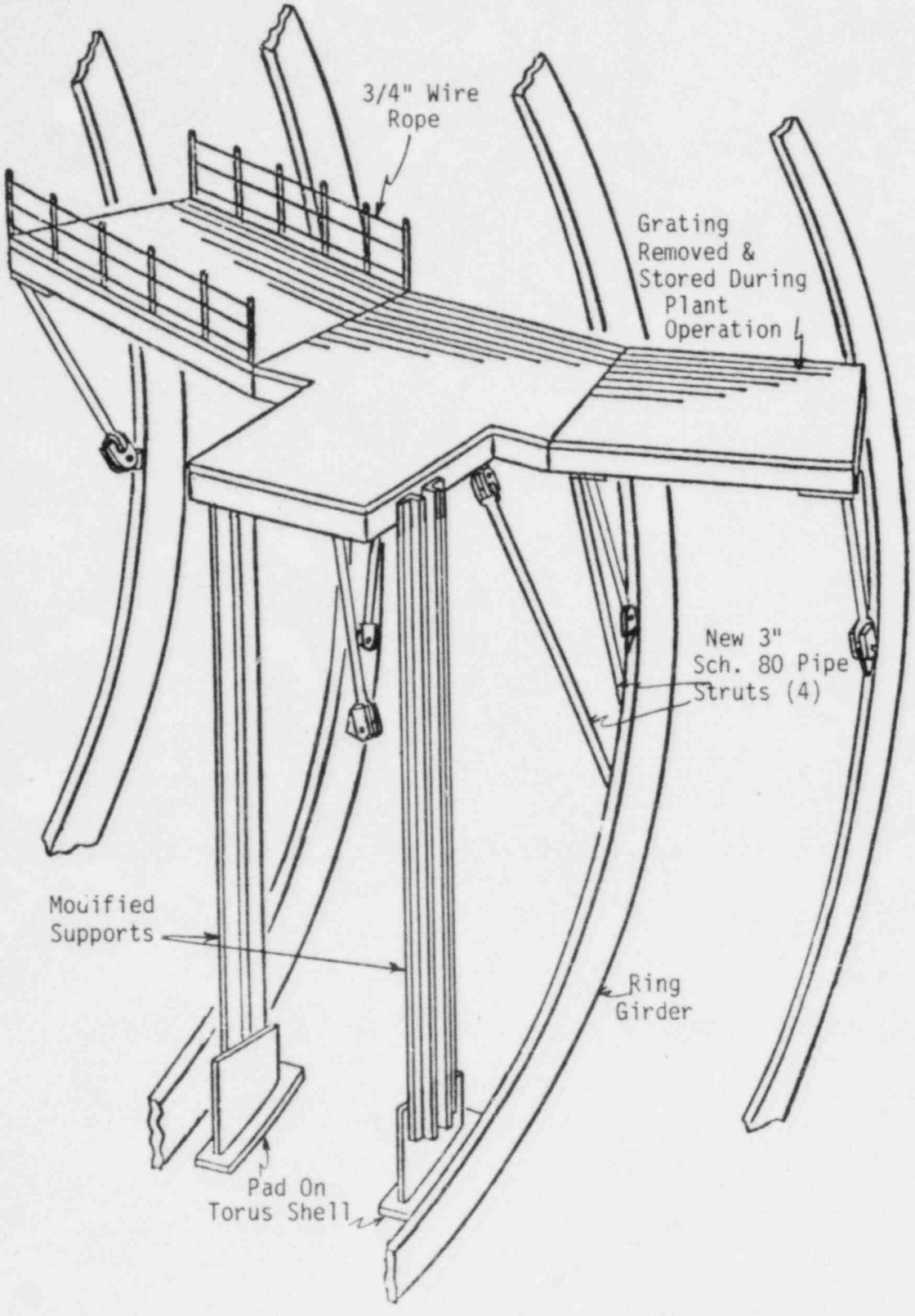

FIG 2-16

CATWALK & HANDRAIL MODIFICATION

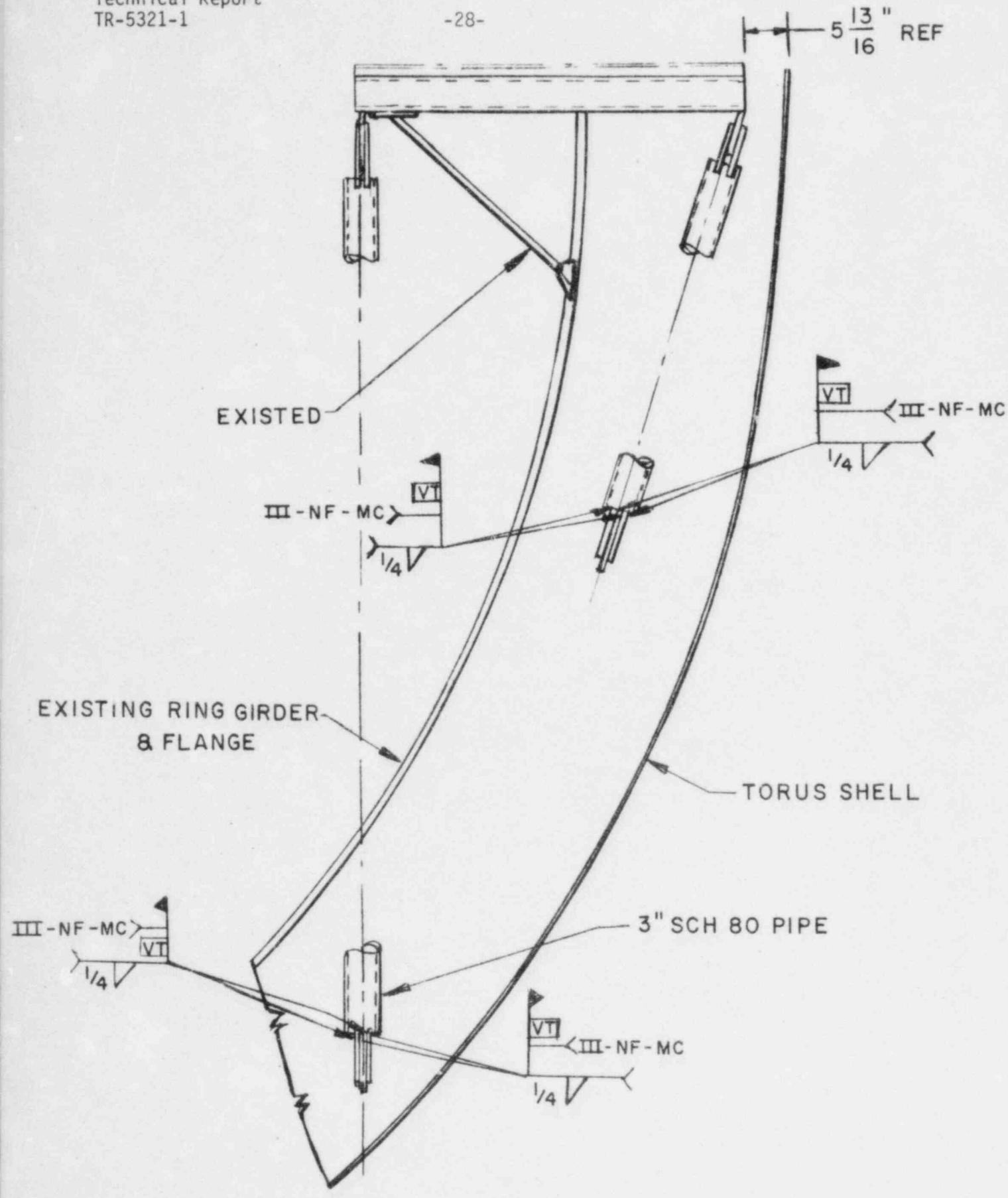

FIG. 2-17

CATWALK MODIFICATION

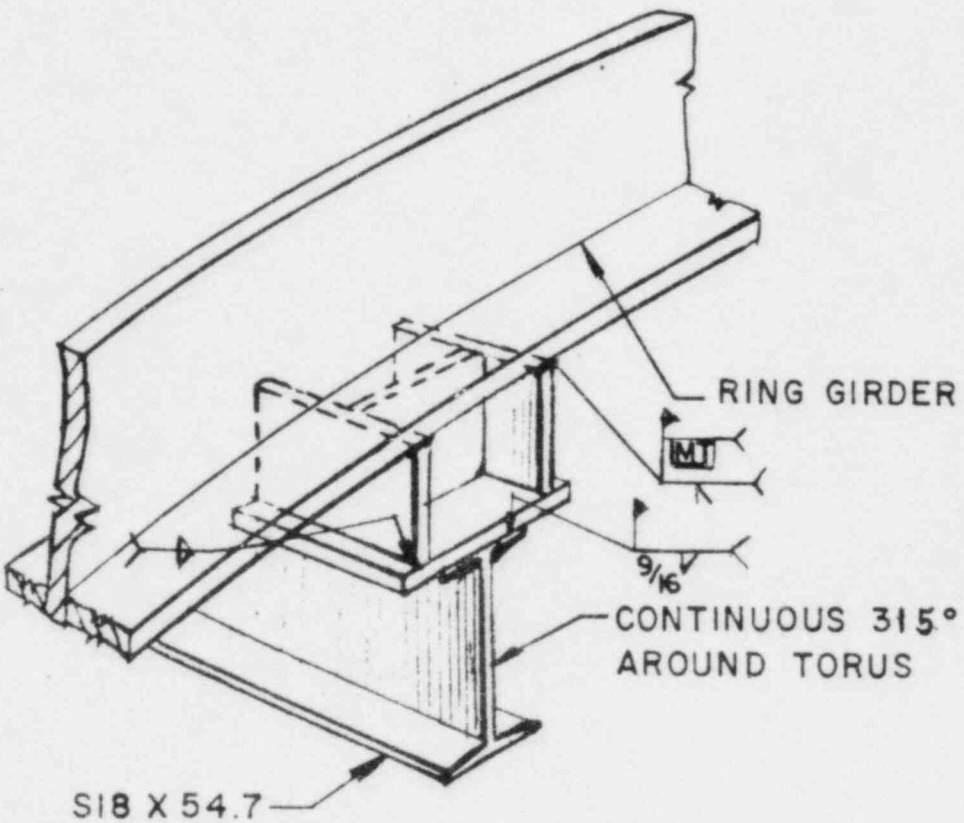

FIG. 2-18
MONORAIL

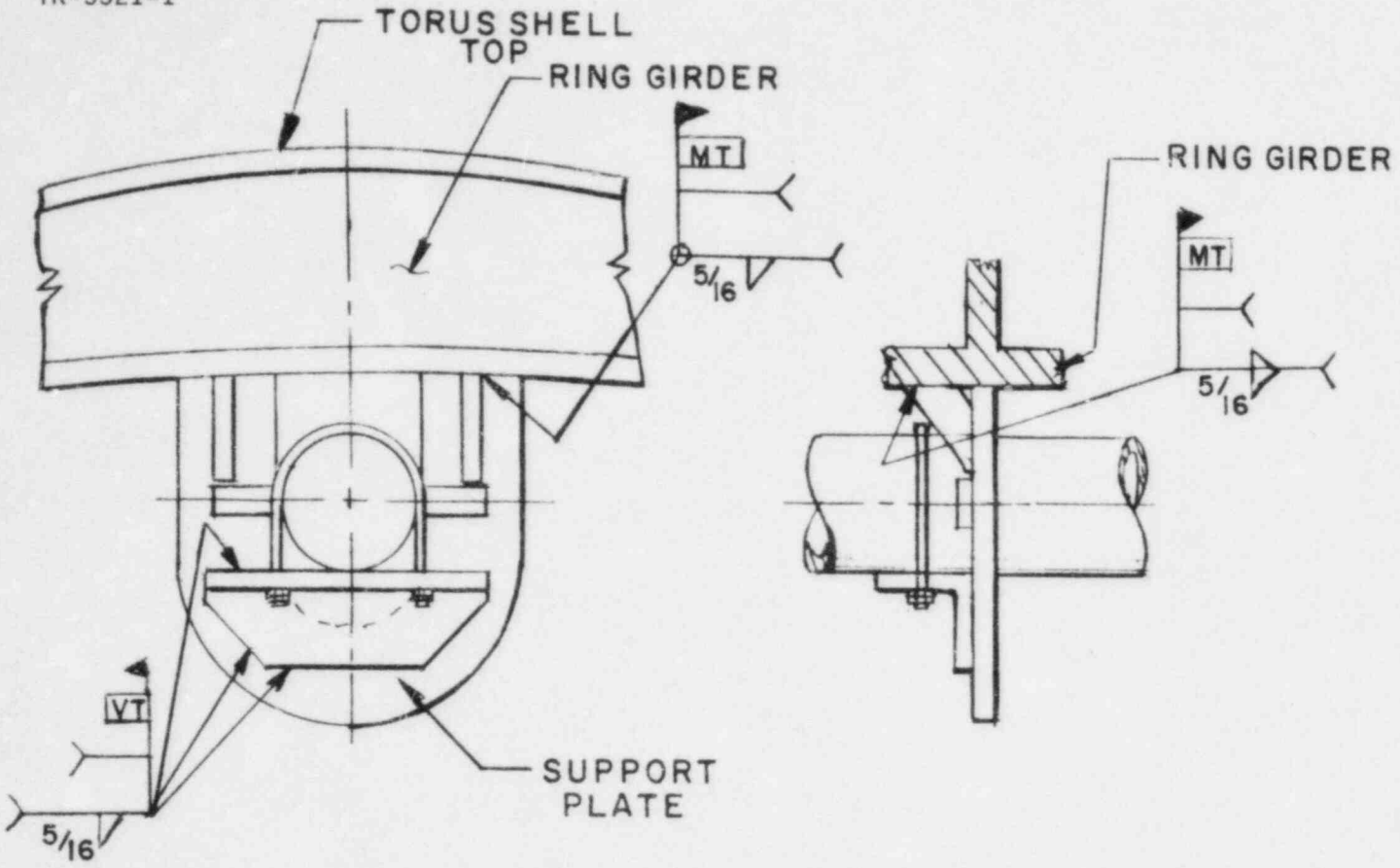

NEW SUPPORT

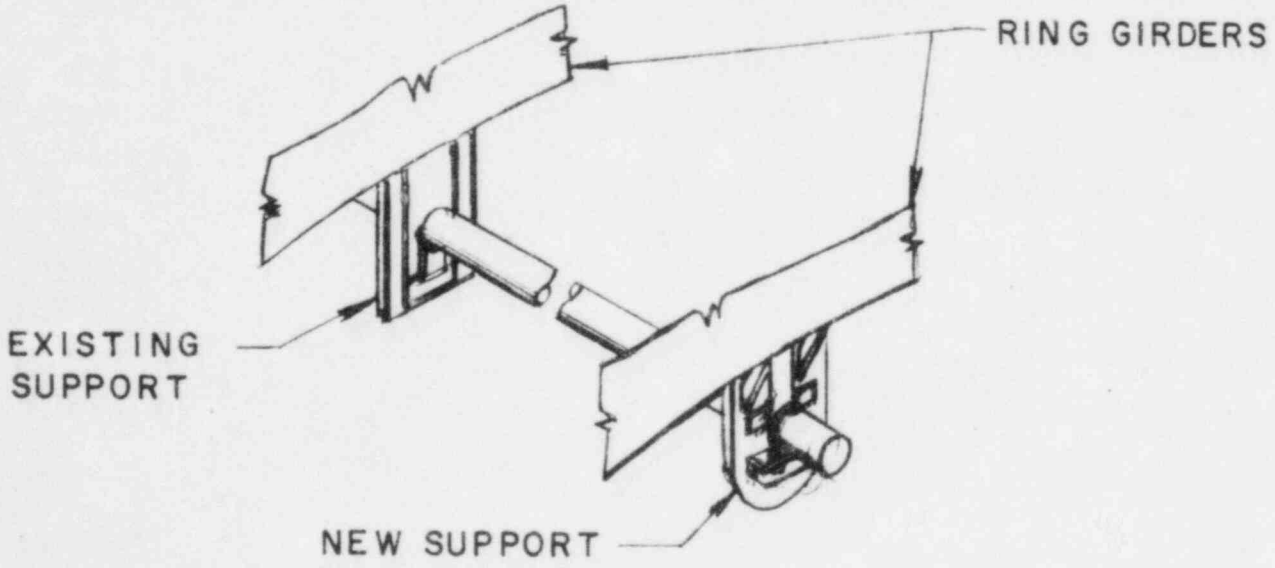

FIG. 2-19

TORUS SPRAY HEADER SUPPORT MODIFICATIONS

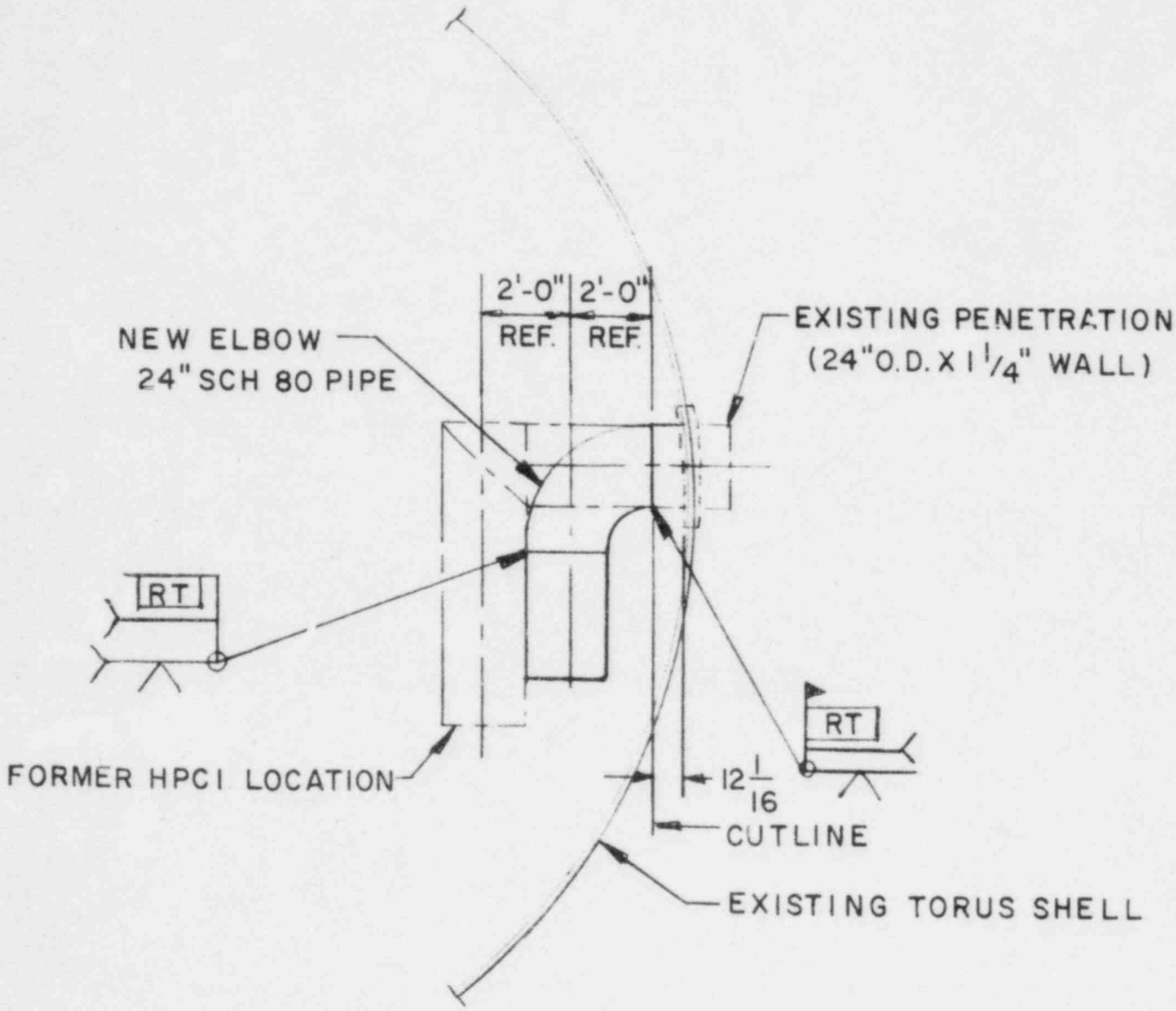

FIG. 2-20

HPCI MITRE JOINT MODIFICATION

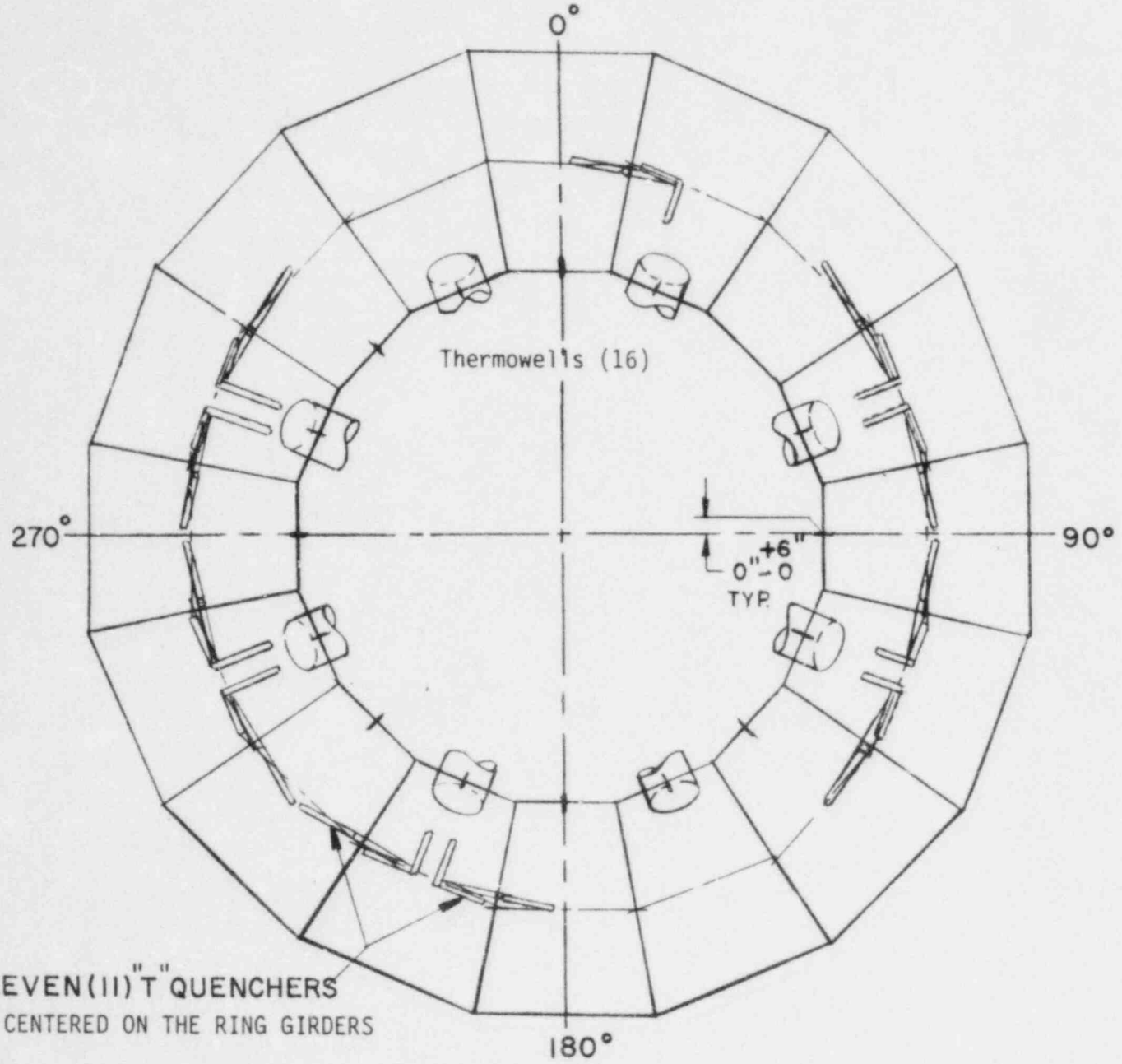

TOTAL THERMOWELLS = 16

FIG. 2-21

THERMOWELL LOCATIONS - FITZPATRICK

3.0 CONTAINMENT STRUCTURE ANALYSIS - OUTER SHELL & EXTERNAL SUPPORT SYSTEM (INCLUDING ANCHORS)

The containment structure section of this report includes the analysis and evaluation of the following structures:

Torus Shell
Support Columns
Column-To-Torus Weld
Support Saddles
Saddle-To-Torus Weld
Earthquake Restraints & Attachment
Anchor (tie-down) System

3.1 Computer Models

Analysis of the containment structures was accomplished using the computer models shown in Figure 3-1 to Figure 3-4. The detailed shell model shown in Figure 3-1 was used to calculate the effects of all loads on shell stress, as well as all symmetric loads on the support and anchor system. The beam model shown in Figure 3-4 was used to determine the effects of asymmetric loads on the support system. Asymmetric loads on the torus structure are horizontal earthquake, SRV and chugging. Evaluation of the support system considered the combined effect of symmetric and asymmetric loads in accordance with the load combination table (Table 1).

The detailed finite element model shown in Figure 3-1 simulates one-half of the non-vent bay. It is bounded by the ring girder on one end and the mid-bay point on the other. The vent header system is assumed to be dynamically uncoupled from the shell by the support saddles and is not included in this model. This model was constructed with the assumption that the small offset that exists between the ring girder and mitre joint will not affect results; accordingly, the offset is not included in the model.

This model includes 641 structural nodes, 736 plate elements and 362 dynamic degrees of freedom. Symmetric boundary conditions were used at both ends of the model.

The model was modified for various load calculations to account for differences in the percent of the water mass that is effective for that load event. In all cases, modeling of the water mass was accomplished using a 3-D virtual mass simulation as an integral part of the structural analysis. The percent of water mass used is identified in the discussion of each load calculation that follows.

The 360^{o} beam model of the torus is shown in Figure 3-4. This model was used to evaluate the effects of lateral loads on the support system and earthquake restraint system. The beam element properties were selected to simulate combined bending and shear stiffness of the sections. Water mass was lumped with the structure weight on the wetted nodes.

3.2 Loads Analysis

3.2.1 Pool Swell Loads (4.3.1 & 4.3.2)

Analysis for pool swell loads was done using the finite element model shown in Figure 3-1. This was a dynamic analysis performed in the time domain by applying a force time history, to simulate the pressure-time histories of the pool swell event to each node on the computer model. Input pressure-time histories were varied in both the longitudinal and radial directions in accordance with the information in References 1, 10 and 2. Typical pressure-time history curves are shown in Figures 3-5 through 3-7. (These pressure-time histories are taken directly from Reference 10, before adjustment, as required by Reference 2. Therefore, the amplitudes shown are slightly different than the loads used in the analysis).

The computer analysis was run for two different pool swell conditions, full $\triangle P$ and zero $\triangle P$. Figures 3-5 through 3-7 show comparative

values and time histories for the two cases. The only difference between the analyses was the input loads; the models were identical. Details of the full load distribution can be found in References 1 and 10.

Plant-unique quarter scale pool swell tests showed that the effective water mass was less than 100% after bubble breakthrough and was slightly different for both zero and full ΔP conditions (Reference 4). The water mass used in the computer simulation was constant throughout the analysis and was set at the average of the two reduced masses identified in the quarter scale tests. The reduced and average mass values are given in Table 3. This simplification in water mass analysis is consistent with the relatively slow (pseudo-static) nature of the pool swell load. This simplification only affects the inertial (frequency) calculation; the effects of weight are accurately calculated for each load and time in the deadweight analysis.

3.2.2 Condensation Oscillation - DBA (4.4.1)

Analysis for condensation oscillation (CO) was also done with the structual model shown in Figure 3-1.

The condensation oscillation shell load is specified as a spectrum of pressures in 1 Hz bands (Reference 1). The analysis for this load was performed by considering the effects of unit loads at each load frequency (harmonic analysis) and then scaling and combining the individual frequency effects to determine total stress at selected elements. The three variations in the CO spectrum (Reference 1) were evaluated by re-scaling the results of the unit load analysis. 100% of the water mass was used for all CO analysis. A plant-unique factor was applied to the nominal condensation oscillation pressures as discussed in Reference 1; the factor is listed in Table 3.

The combination of individual harmonic stresses into total element stress was done by considering frequency contributions at 31 Hz and

below. The actual combination was done by adding the absolute value of the four highest harmonic contributors to the SRSS combination of the others for shell stress. Loads on the support and anchor system were determined by adding the absolute value of the three highest harmonic contributors to the SRSS of the others. These combination methods and use of the 31 Hz cutoff are the result of extensive numerical evaluation of full scale test data, which is reported and discussed in References 6 and 14, and in Appendix 2 of this report.

3.2.3 Chugging

3.2.3.1 Pre-Chugging & IBA/CO (4.5.1.2 & 4.4.1)

The pre-chug load was evaluated for both the symmetric and asymmetric distribution described in Reference 1. Results for the symmetric pre-chug analysis were also used for IBA/CO as described in paragraph 4.4 of Reference 1.

Results for symmetric pre-chug were developed directly from the unit-load harmonic analysis done for CO. The results of that analysis were scaled to 2 psi (the pre-chug pressure) and all frequencies in the pre-chug range were scanned to determine the highest possible stresses.

Analysis for asymmetric pre-chug was performed using the beam model in Figure 3-4 by applying the unbalanced lateral load through the prescribed frequency range.

3.2.3.2 Post Chugging (4.5.1.2)

Post chugging is defined as a spectral load across a wide band, similar in nature to the CO, but much lower in amplitude. Analysis done on one of the TES plants produced very low stresses and loads that were bounded by pre-chug values. The analyses for pre- and post chug produced these results for maximum shell stress:

Maximum Shell Stress

Shell Membrane Stress

Pre-Chug	1284 psi
Post Chug	774 psi[1]

1. Based on frequencies to 30 Hz - sum of 4 maximum + SRSS of others.

Additional work published in Reference 12 showed that pre-chug bounded post chug (to 50 Hz) for column and saddle loads (Table 5-1, Ref. 12). It also showed that $P_L + P_b$ stress due to post chug exceeded pre-chug by 53%.

TES analysis for post chug used the pre-chug stress values. The pre-chug stress may be increased by 53% to account for the 30 to 50 Hz contribution and they will still meet allowable stress.

No further post chug analysis was done for the shell. This position was also influenced by the fact that post chug stresses were very small.

3.2.4 SRV Discharge

Calculation of stresses, due to SRV line discharge pressures, were also done using the finite element model in Figure 3-1. The loading function used for this analysis was based on data collected from in-plant SRV testing in this facility. Testing was done in general accordance with the guidelines given in Reference 2. In these tests, pressure amplitude and frequency were recorded and compared to calculated values for the test conditions. Factors were developed that related test to calculated values for both

amplitude and frequency (See Appendix 1). These factors were then applied to calculated load values for other SRV conditions; the structural analyses were performed using these adjusted values. Appendix 1 discusses the in-plant test and analysis in more detail. A typical set of SRV shell pressures is shown in Figure 3-8.

The method of modeling the water mass in the SRV computer model was the subject of extensive study in this program. Initial attempts to reproduce measured stresses by applying measured pressures to the computer models failed. After considerable study of the nature of the SRV phenomena itself, and the differences between it and the pool swell related loads, it appeared that a dry structure analysis should produce acceptable correlation. The method was tested and correlation of calculated-to-measured shell stress was excellent. The dry structure analysis method was subsequently used as a basis for all SRV analysis.

3.2.5 Deadweight, Thermal & Internal Pressure

Deadweight, thermal and internal pressure analyses were done using the computer model shown in Figure 3-1. Resulting stresses were calculated and considered for all elements on the model.

For the thermal analysis, conduction into the columns and saddles from the torus was considered. Convection from the columns and saddles to ambient produced a calculated temperature gradient in these elements. The torus water, internals and shell were all assumed at the same temperature.

3.2.6 Seismic

Seismic analysis for shell stress was done by applying static G levels to the model in Figure 3-1. Load orientation and values were adjusted for vertical and horizontal earthquakes in accordance with Table 3.

The effects of lateral seismic loads on the support system were determined using the model in Figure 3-4. The effective water mass used in this (lateral) analysis was adjusted in line with test results which showed that net dynamic reaction loads due to the water mass were substantially less than those obtained from static application of the seismic acceleration. A discussion of this fact can be found in Reference 7; the effective water mass used can be found in Table 3 of this report.

3.2.7 Fatigue Analysis

Fatigue analysis of the torus shell and external support system is described here. Analysis of the shell at piping penetrations will be described in TES report TR-5321-2, when the piping analysis is complete.

The fatigue analysis of the shell and support system was a conservative one, which was based on applying a stress concentration factor of 4.0 on the most highly stressed elements for each load case. In the case of the support system only, the column-to-torus and saddle web-to-torus welds were considered, since they have higher stresses than the rest of the support system. The process is conservative because:

- It applies the maximum stress concentration (4.0), recognized by Section III of the ASME Code to all elements (Reference 11).

  and

- It adds the maximum stress for each load case even though they do not usually occur at the same element.

The procedure used in this analysis consists of the following steps.

1. For a given load, locate the maximum component-level stresses (S_x, S_y, S_{xy}) for the free shell, local shell, and the supports.

2. For these locations, establish the stress intensity ranges and the approximate number of cycles.

3. Repeat the process for all other loads in the load combination.

4. Add the stress ranges for all loads, independent of sign.

5. Multiply these total stress ranges by 4.0 (the SIF).

6. Calculate the alternating stress intensity and complete the fatigue analysis in compliance with Reference 11.

Fatigue analysis resulting from chugging after an SBA was done assuming that the operator would use a procedure to end chugging after 15 minutes. Plant procedures are presently under study to provide for this action.

3.3 Results and Evaluation

Results are reported for each structural element of the containment system for the controlling load combination. Controlling load combinations are the ones that produce the smallest margins against the allowable stress - not necessarily the highest stress.

All load combinations listed in Table 1 have been considered. As stated previously, most results include some level of bounding analysis and, therefore, understate the margins which actually exist.

3.3.1 Torus Shell

Results of shell stress due to individually applied loads were calculated and maintained on a component stress level until all the load combinations were formed. Stress intensities were then calculated from these total component-level values.

The controlling load combinations for the shell at Fitzpatrick are Cases 14 and 20 in Table 1, these are:

Case 14 IBA.CO + SRV + Seismic (SSE) + Pressure + Weight

Case 20 DBA.CO + Pressure + Weight + Seismic (SSE)

These load combinations control all categories of shell stress, although the location of the elements is different for the different types of stress. The following table summarizes the controlling stresses. Approximate locations of the controlling stresses are shown in Figure 3-9.

CONTROLLING SHELL STRESSES - FITZPATRICK

TYPE OF STRESS	LOCATION	ACTUAL STRESS (psi)	ALLOWABLE STRESS (psi)
Membrane (Pm) (Case 20)	Free Shell Element 17	13,776	19,300
Local (Pl) (Case 14)	Local Shell Element 160	8,807	28,950
Membrane + Bending (Case 20)	Free Shell Element 19	14,146	28,950
Stress Range (Case 14)	Local Shell Element 148	27,895	69,900

Compressive Buckling - Acceptable (see below)

Compressive Buckling Reference 13 discusses the results of analytical studies and tests on Mark 1 torus structures to determine their compressive buckling capabilities. The report concludes that SRV is the dynamic load which presents the maximum chance of compressive buckling failure; but, that a safety factor of seven still exists for an applied SRV pressure of +29.3/-22.6 psi. The maximum worst-case SRV shell pressures for Fitzpatrick are +7.8 psi and -5.0 psi, which are lower than those used in the referenced study. Based on this, compressive buckling stresses are considered to be acceptable for the Fitzpatrick torus.

FATIGUE EVALUATION - FITZPATRICK

CUMULATIVE USAGE FACTOR SUMMARY

(STRESS INTENSIFICATION FACTOR 4.0)

ELEMENT	NORMAL OPERATING	EVENT TYPE SBA/IBA	EVENT TYPE DBA
19	.000	.001	.001
148	.001	.006	.038

3.3.2 Support Columns & Weld to Torus Shell

The controlling load case for the support columns and the column base joint is case 16 of Table 1:

Pool Swell (0 $\triangle$ P) + Weight

and case 25 for the attachment weld to the shell.

Pool Swell (full $\triangle$ P) + Seismic (SSE) + SRV + Weight

For these load cases, the following controlling conditions were identified:

SUPPORT COLUMN - CONTROLLING AXIAL CONDITION

COLUMN	LOAD DIRECTION	CONTROLLING CONDITION	ACTUAL FACTOR	ALLOWABLE FACTOR
Inner	Down	Axial & Bending	.55	1.0
Outer	Down	Axial & Bending	.65	1.0

COLUMN BASE JOINT

LOCATION	LOAD DIRECTION	CONTROLLING STRESS	ACTUAL STRESS	ALLOWABLE STRESS
Tiedown Clamping Plate	Up	Bending	18.8 ksi	28.5 ksi

COLUMN-TO-SHELL WELD

LOCATION	LOAD DIRECTION	CONTROLLING STRESS	ACTUAL STRESS	ALLOWABLE STRESS
Inner	Down	Shear	15.82 K/in	24.13 K/in
Outer	Down	Shear	16.96 K/in	24.13 K/in

3.3.3 Support Saddles & Shell Weld

Stress levels in the saddle structure are very low for downward loads. The controlling stress occurs in the saddle clamping plate (which connects the saddle to the anchor bolts) during the upward loads associated with load case 21 in Table 1. Controlling stresses in the saddle-to-shell weld occur during downward loads associated with case 25. These cases include:

Case 21

DBA.CO + SRV + Weight

Case 25

Pool Swell (full $\triangle P$) + SRV + Weight + Seismic (SSE)

Controlling stresses and loads for these cases are:

SADDLE STRESSES

LOCATION	TYPE STRESS	ACTUAL LOAD	ALLOWABLE LOAD
Clamping Plate	Bending	51.7 kips	75 kips

SADDLE-TO-SHELL WELD

LOCATION	TYPE STRESS	ACTUAL STRESS	ALLOWABLE STRESS
Outside End	Shear	12.04 K/in	13.65 K/in

3.3.4 Earthquake Restraints & Attachments

The earthquake restraint system is illustrated in Figure 3-10. The controlling load case for this system is the one that produces the largest lateral load. This is case 15 which includes:

Chugging + SRV + SSE

All three of these loads have been selected to produce the highest lateral load on one earthquake restraint; contributions from the individual loads were added directly.

The controlling stress results follow:

EARTHQUAKE RESTRAINT

STRESS LOCATION	STRESS TYPE	ACTUAL STRESS	ALLOWABLE STRESS
Attachment to Concrete	Concrete Shear	10 psi	65 psi

ATTACHMENT WELD

STRESS LOCATION	STRESS TYPE	ACTUAL STRESS	ALLOWABLE STRESS
Base of tie plates	Shear	1,443 psi	21,000 psi

3.3.5 Anchor (Tie-Down) System

The load combination which produces the highest upload and minimum margin on the anchor bolts is case 21 for the saddle anchors:

DBA.CO + SRV + Weight

and load case 16 for the column anchors:

Pool Swell (zeroΔP) + Weight

For these cases, the anchor bolts with the smallest margin of safety (accounting for as-built conditions) are:

SADDLE ANCHOR BOLT

ACTUAL MAXIMUM LOAD	MAXIMUM CAPACITY	FACTOR OF SAFETY
51.7 K/bolt	264 K/bolt	5.1

COLUMN ANCHOR BOLTS

LOCATION	ACTUAL MAXIMUM LOAD	MAXIMUM CAPACITY	FACTOR OF SAFETY
Inside Column	44.2 K	258 K	3.96
Outside Column	65 K	258 K	3.96

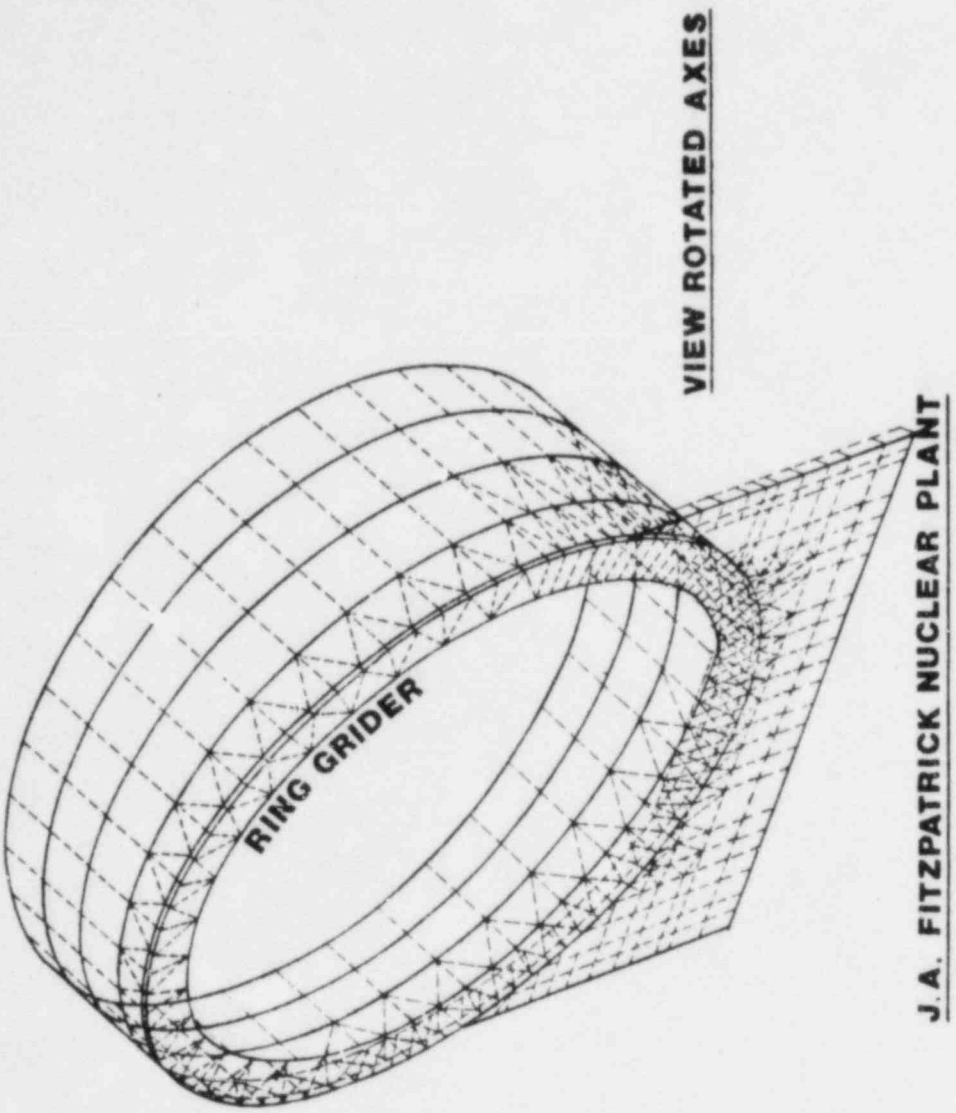

FIGURE 3.1 DETAILED SHELL MODEL

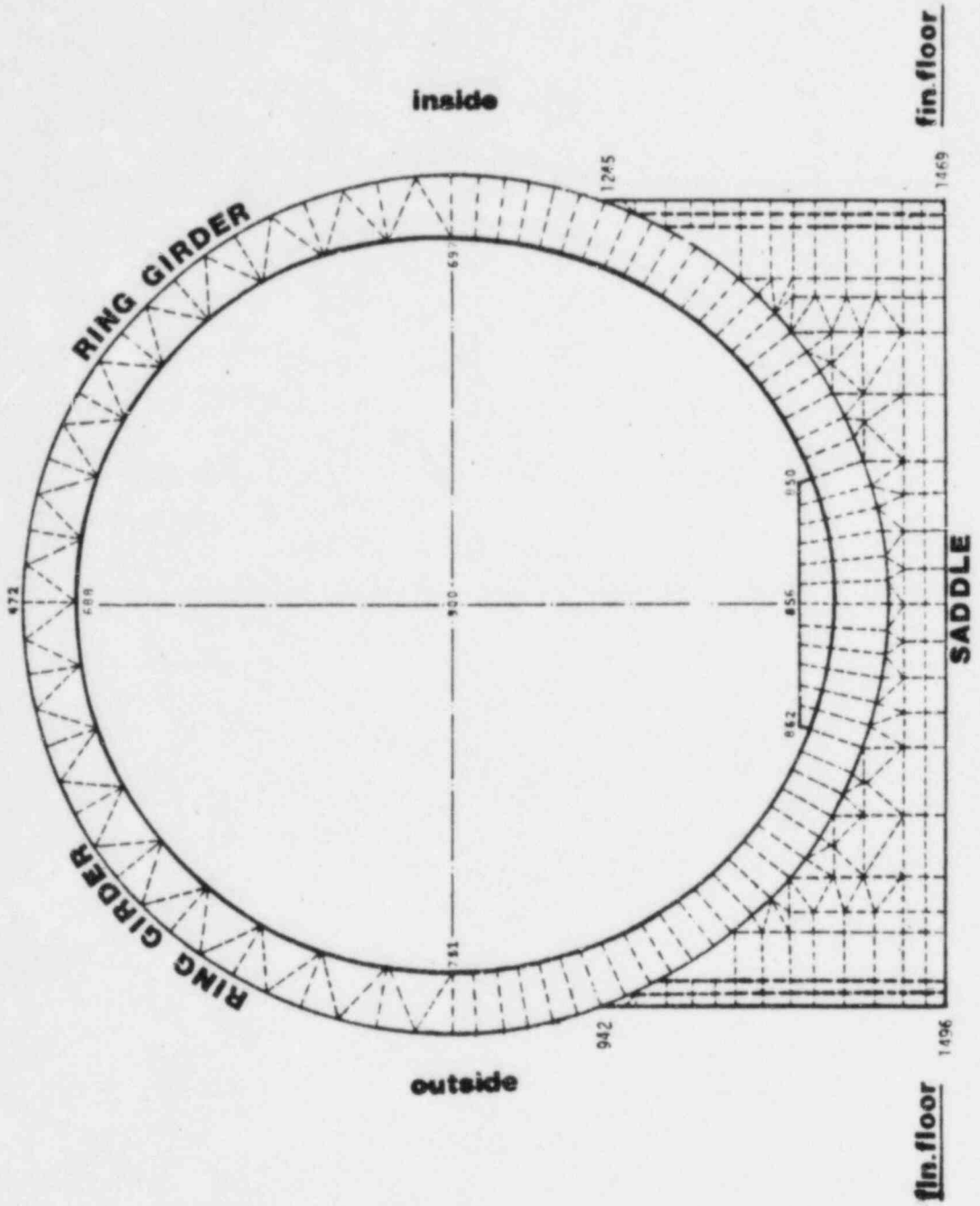

FIGURE 3.2 TORUS SHELL MODEL

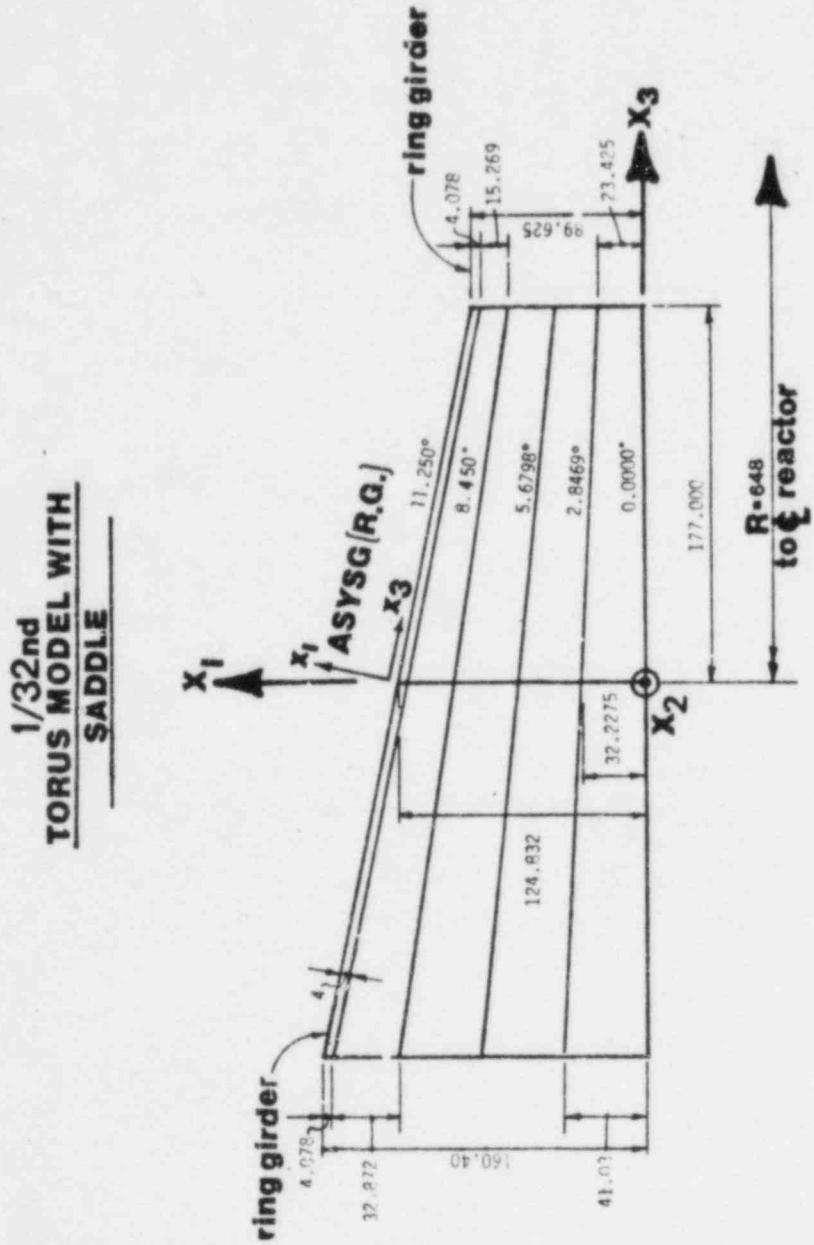

FIGURE 3.3 DETAILED SHELL MODEL

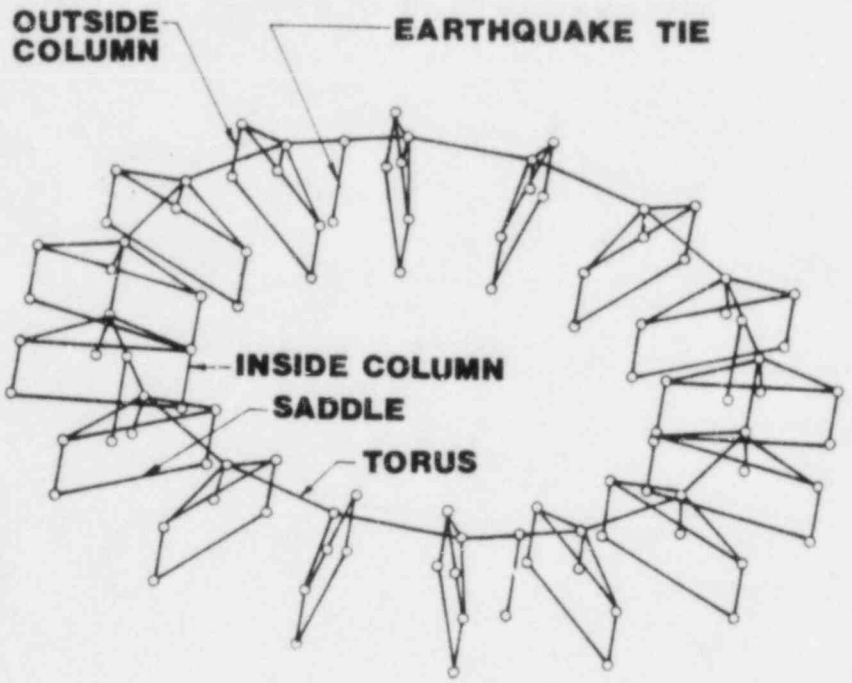

FIGURE 3.4 360° TORUS BEAM MODEL

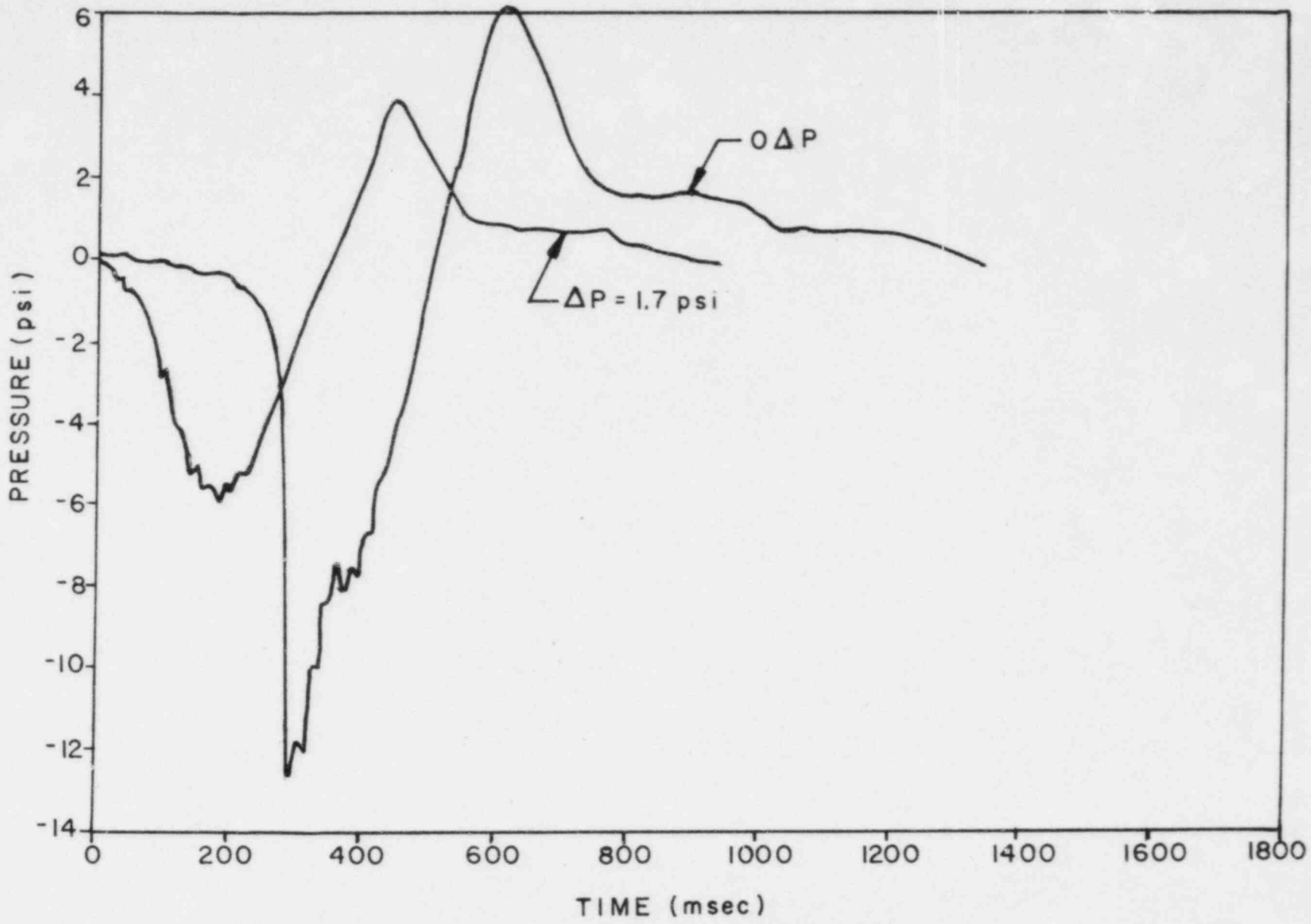

FIG. 3-5
POOL SWELL - NET TORUS VERTICAL LOAD - FITZPATRICK

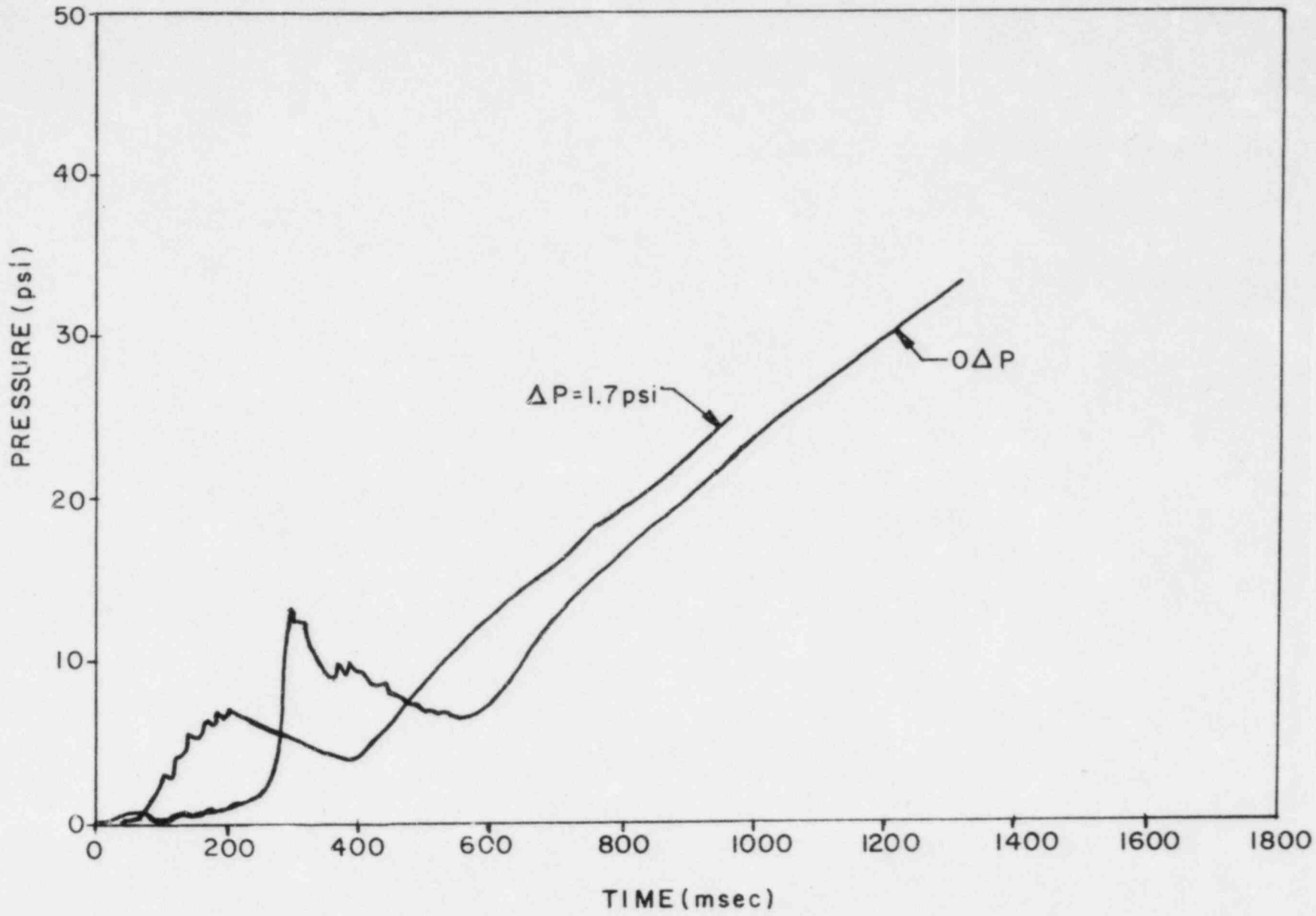

FIG.3-6
POOL SWELL - AVERAGE SUBMERGED PRESSURE - FITZPATRICK

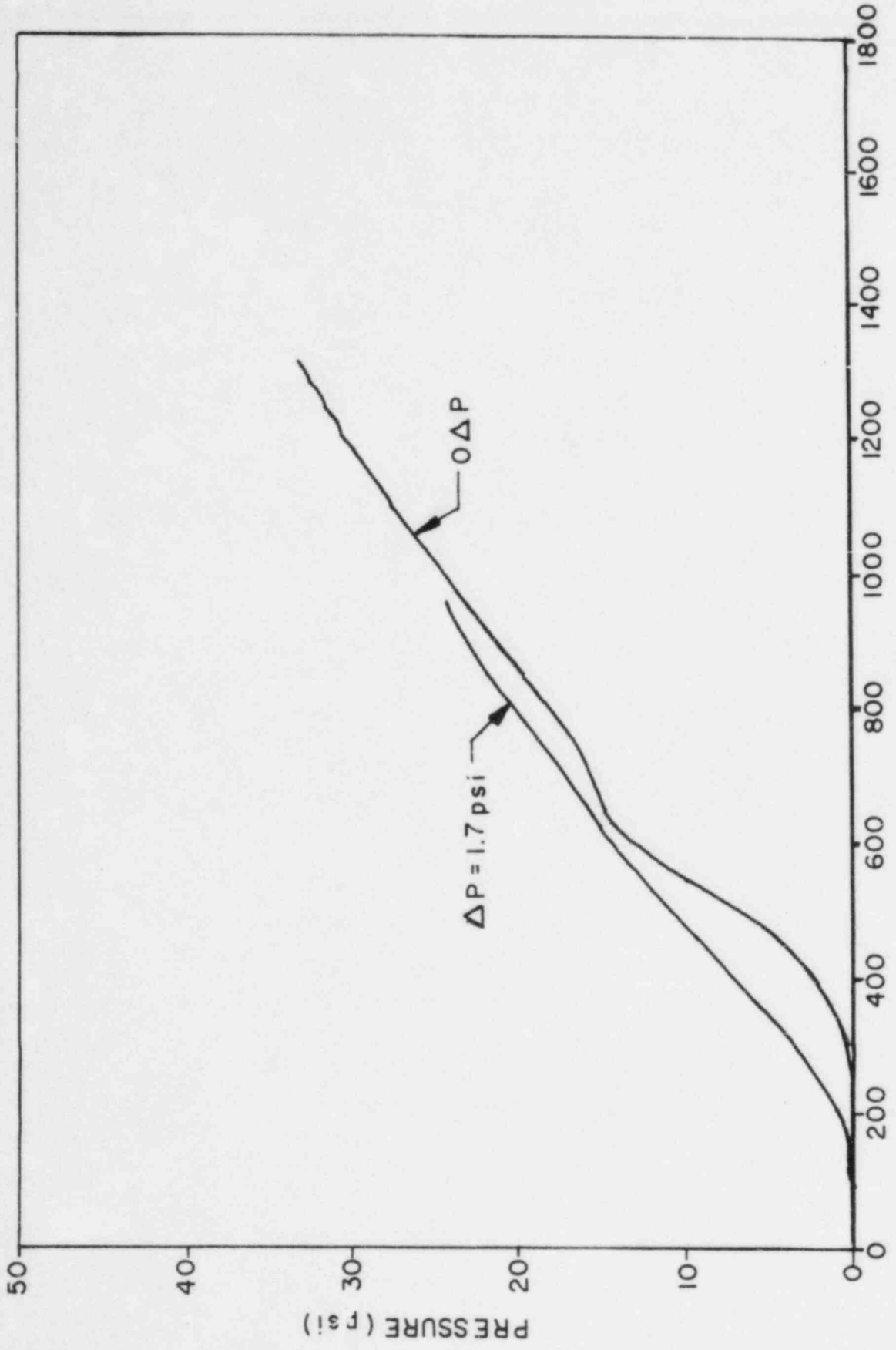

FIG. 3-7

POOL SWELL - TORUS AIR PRESSURE - FITZPATRICK

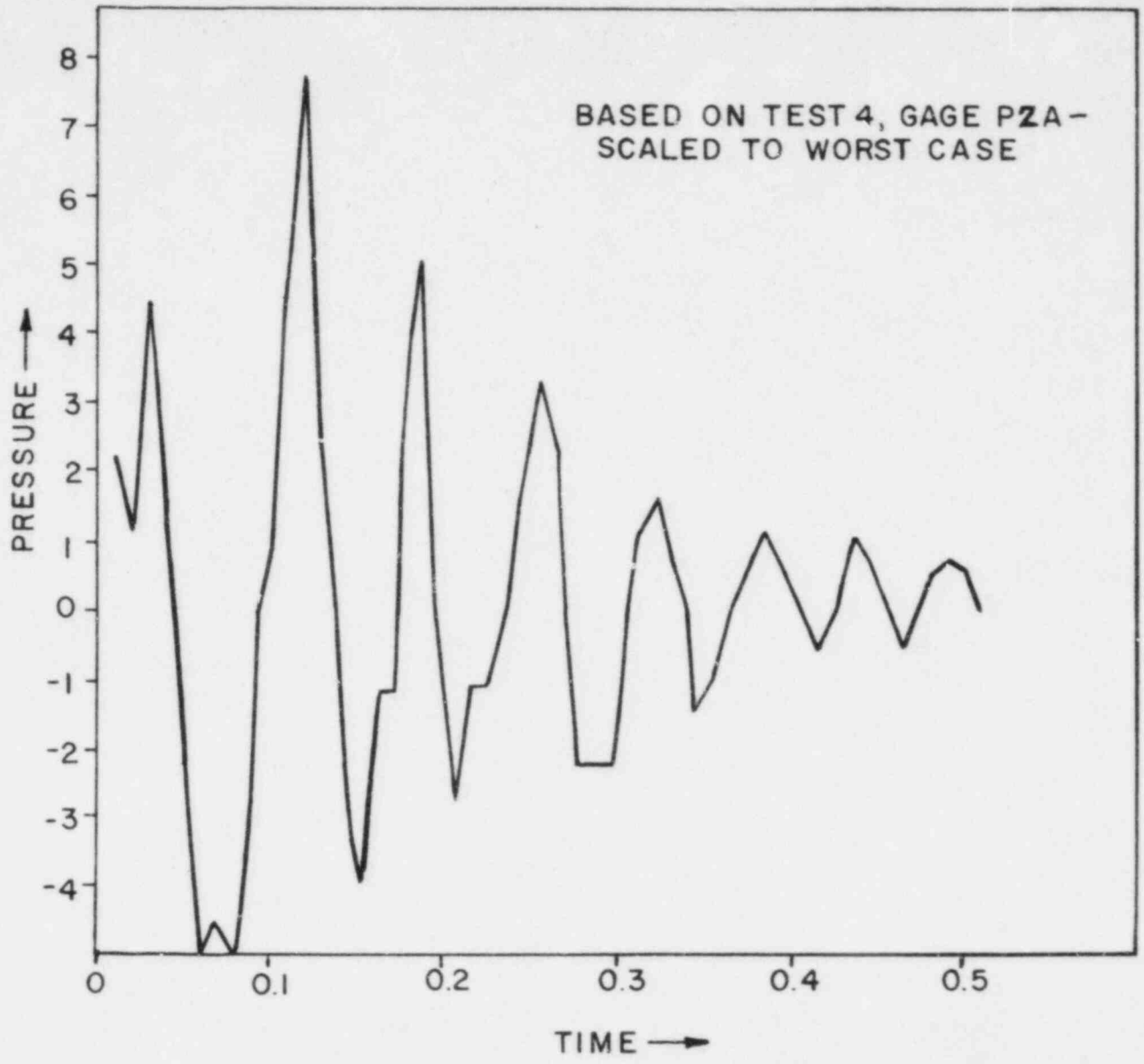

FIG. 3-8
TYPICAL SRV SHELL PRESSURE - FITZPATRICK

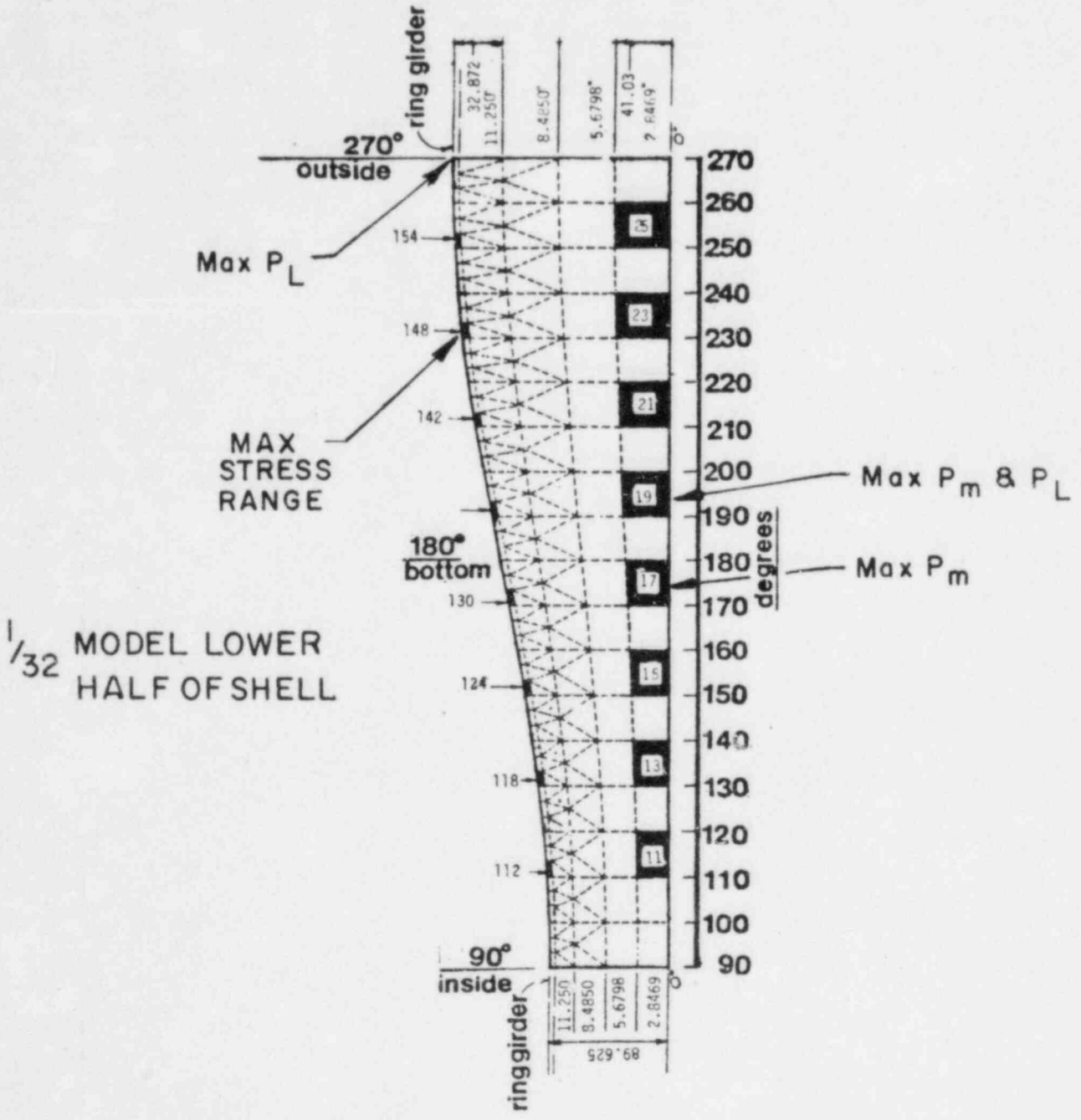

FIG. 3-9

MAXIMUM SHELL STRESS LOCATIONS – FITZPATRICK

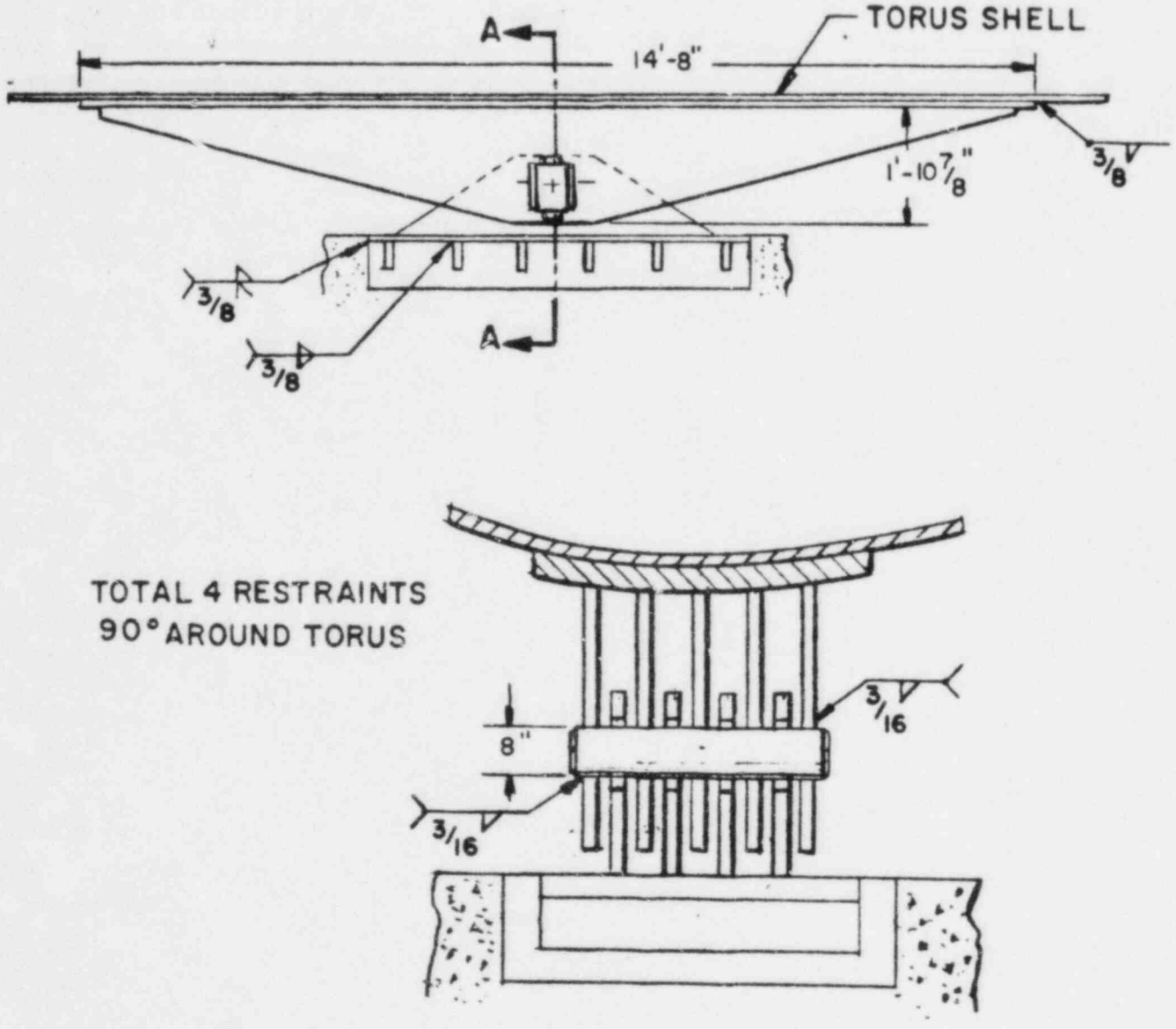

SECTION A-A

FIG. 3-10

EARTHQUAKE RESTRAINT SYSTEM

4.0 VENT HEADER SYSTEM

4.1 Structural Elements Considered

The vent header system, as defined in this section, includes the following structural components:

a. Vent Header (V.H.)
b. Main Vent Pipe (V.P.)
c. Downcomers (D.C.)
d. Downcomer Tie Bars
e. Deflector
f. Vent Header Support Columns & Attachments
g. VH/DC Intersection
h. VH/VP Intersection
i. VP/Drywell Intersection
j. Vent Header Mitre Joint

The main vent bellows are considered in Section 7.0.

4.2 Computer Models

Two computer models provided the means to analyze the vent header system; they are shown in Figures 4-1 through 4-4.

The first of these is a detailed shell model (Figures 4-1 to 4-3), which includes a highly detailed representation of one-half of the header in a non vent bay, complete with four downcomers.

The model also includes an approximate representation of one-half of the vent bay; this was intended to provide the proper boundary conditions and stiffness transition near the non-vent bay. The vent bay half of the

model was not used for stress determination. This large finite element model was used primarily to determine shell stresses in the non-vent bay; some other uses are discussed in the following text. It was used for both static and dynamic analysis and provided detailed stress gradient information in the downcomer/vent header intersection region.

The second vent header model is the beam model shown in Figure 4-4. This model represents a full vent bay, complete with vent pipe and downcomers; as well as a half non-vent bay on either side. It was used to determine boundary loads on the vent system components to support a more detailed stress analysis of those components. This model was used to define loads on the following elements:

- Vent Header Support Columns
- Vent Pipe/Vent Header Intersection
- Vent Pipe/Drywell Intersection
- Vent Header Mitre Joint
- Main Vent Pipe

The loads and moments taken from the beam model were used in further analysis to determine stresses. The calculation methods used for these stresses are:

- VH support columns - hand analysis
- VP/VH intersection - applied stress multipliers (stress intensification factors) from Reference 7
- VP/drywell intersection - used stress multipliers from - Reference 16 (Bijlaard)
- Mitre joint - used stress multipliers from detailed shell model (Figure 4-1)
- Main vent pipe - hand analysis

The beam model used a stiffness representation of the VP/VH intersection taken from Reference 7. Attachment stiffness between the vent pipe and drywell was calculated using References 17 and 18.

Pool swell water impact on the vent header deflector was calculated with a hand analysis. The impact forces were applied statically to a beam model and a dynamic load factor was applied (see Figure 4-5).

4.3 Loads Analysis

4.3.1 Pool Swell Loads

4.3.1.1 Pool Swell Water Impact

Analysis for stresses due to pool impact and drag was done using both computer models.

Determination of shell stresses was done with the detailed model in Figure 4-1. For this analysis, force time histories based on QSTF test data was used (References 4 and 10). These time histories were applied at 100 nodal points on the shell model and the dynamic response of the structure was calculated. Relative timing between loadings (Reference 1) was maintained to preserve accurate representation of longitudinal and circumferential wave sweep. Stresses in the vent header/downcomer intersection, as well as in the free shell areas, were taken directly from this model. Stresses in the downcomer tie bars were also taken from this model. Analysis was done for both full and zero ΔP impacts.

The beam model (Figure 4-4) was also used to determine stress from pool swell impact and drag. This was done with a time history dynamic analysis using loads developed by integrating the impact pressures over small areas and reducing them to nodal forces. Approximately

95 nodes along the length of the beam model were dynamically loaded in this analysis, including loads on the VP/VH intersection and vent pipe. The results of this analysis were used to define boundary loads on VP/VH intersection, mitre joint and other elements as listed in Section 4.2. Stress analysis for these elements was performed using the methods indicated in Section 4.2.

4.3.1.2 Pool Swell Thrust (4.2)

Pool swell thrust forces are defined as dynamic forces at each bend or mitre in the vent system, and are a consequence of the flowing internal fluids. Analysis for these loads was done using the beam model and applying the loads statically. This is consistent with the slow nature of the applied pressure forces.

The calculation was performed with the maximum value of all thrust forces applied simultaneously; this is a conservative condition.

4.3.1.3 Pool Swell Drag Loads (4.3.7 & 4.3.8)

The vent header support columns are loaded by forces from LOCA-jet and LOCA bubble drag. By inspection, it was concluded that LOCA-jet loads would not combine with water impact on the vent system due to differences in timing and, therefore, would not contribute to the maximum stress calculations - LOCA jet forces were not considered further.

LOCA bubble forces were calculated and the maximum normal components (radial and longitudinal) were applied simultaneously to conservatively bound the bending moments on the support column. These peak values were applied statically at the midpoint of the column. Stress calculations were done by hand.

4.3.2 Chugging Loads

4.3.2.1 Downcomer Lateral Loads (4.5.3)

Reference 1 identifies downcomer lateral loads as static equivalents with random orientation in the horizontal plane. The major consequence of this loading is to produce high local stress in the VH/downcomer intersection. The detailed shell model (Figure 4-1) was used to identify stresses in the downcomer intersection due to static loads applied at the base of the downcomer. Frequencies of the first downcomer response mode were taken from a dynamic analysis on the same model (Figure 4-1) with the downcomers full of water to the operating level. This frequency was necessary to determine the proper dynamic scale factor to apply to the static load.

The stress results from the statically applied load were used as a basis for a fatigue evaluation of the intersection in accordance with Reference 1.

4.3.2.2 Chugging - Synchronized Lateral Loads

The random nature of the downcomer lateral chugging load provides for all combinations of alternate force orientations on adjacent pairs of downcomers. Various load combinations were examined to determine stress levels in the vent header and mitre joint as a result of these loads. The cases considered are shown in Figure 4-6.

These cases were considered by applying static loads to the beam model (Figure 4-4) and determining final stresses as described in Section 4.2.

4.3.2.3 Internal Pressure (4.5.4)

Three vent system internal pressures exist during chugging. They are:

- Gross vent system pressure - a .7 Hz oscillating pressure with a maximum value of 5.0 psi. This pressure acts on the entire vent system.

- Acoustic vent system pressure - a sinusoidal pressure varying from 6.9 to 9.5 Hz at a maximum value of 3.5 psi. This pressure affects the entire vent system.

- Acoustic downcomer pressure oscillation - a 40-50 Hz pressure at 13 psi that produces only hoop stress in the downcomers.

Responses to these pressures were estimated using hand analysis and were determined to be substantially less than those resulting from internal vent system pressures during pool swell. The values associated with pool swell pressures were used in all combined load cases involving chugging pressures; this produces conservative results.

4.3.2.4 Submerged Structure Drag (Support Columns only)

Examination of the load combinations that include chugging makes it clear that these cannot control maximum stress level in the support columns; combinations that include vent header water impact will produce much higher stresses. For this reason, stresses in the vent header support columns were not calculated for chugging drag.

Drag forces on the downcomers and downcomer tie bars are already included in the Downcomer Lateral Loads, which were based directly on test data.

4.3.3 Condensation Oscillation - DBA

4.3.3.1 Downcomer Dynamic Load (4.4.3.2)

The downcomer dynamic load, due to condensation oscillation, is a sinusoidal pressure variation that can be equal or unequal in the two downcomers forming a pair.

The unequal pressure case produces a net lateral load on the downcomer much like chugging. The major considerations for this load are stresses in the downcomer intersection due to a net lateral load on one pair of downcomers and a more general stress case where loads on adjacent downcomer pairs are phased to produce gross lateral loads on the vent system or torsion in the vent header.

The horizontal component of the CO downcomer load produces the same type of loading on the vent system as the CH lateral load, in terms of the stress analysis. A comparison of the magnitudes and frequencies of these two loads shows that stresses resulting from CH horizontal loads will bound CO horizontal loads.

The CO downcomer load also produces a vertical component of load, which is not present during CH. The effects of this load were evaluated by static analysis of the detailed vent header model (Figure 4-1) and consideration of dynamic amplification effects, using the beam model (Figure 4-4). This evaluation showed that the combined effects of the CO downcomer load (horizontal and vertical components) would still be bounded by CH lateral loads.

Based on this, CH lateral load results were conservatively used in all load cases in place of CO downcomer loads.

4.3.3.2 Vent System Loads (4.4.4)

Vent system loads consist of a sinusoidal pressure in the vent header and downcomers superimposed on a static pressure. The dynamic pressure in the downcomers is used to calculate hoop stress only.

Stresses for all pressure loads were based on hand analysis using static analysis. The static analysis assumption is consistent with the low frequency of the applied pressure and the fact that the ring modes of the structure are very high.

4.3.3.3 Thrust Forces (4.2)

Stresses resulting from CO thrust forces were conservatively taken from the pool swell thrust calculations and applied to all C.O. load cases (para. 4.3.1.2).

4.3.3.4 Drag Forces on Support Columns

Inspection of approximate total loads on support columns due to CO, CH, and pool swell showed that condensation oscillation would not contribute to the maximum column load, due to differences in timing. No detailed analysis was performed.

4.3.4 Condensation Oscillation - IBA

Stresses and loads resulting from IBA condensation oscillation are bounded in all cases by either DBA condensation oscillation or chugging. No detailed analysis was performed for IBA condensation oscillation.

4.3.5 SRV Loads

4.3.5.1 SRV Drag Loads

An SRV discharge produces drag loads which act on the vent header support columns, downcomers, and downcomer tie bars. Analysis for drag loads on these structures was based on data collected during in-plant SRV tests.

Data collected during these tests was scaled to correct it for the appropriate SRV conditions and then applied to the structural model to determine the resulting stress. A more detailed discussion of this procedure is provided in Appendix 1.

4.3.6 Other Loads

Deadweight and seismic stresses in the vent system were calculated using the beam model of Figure 4-4.

Seismic stresses were calculated by statically applying the acceleration values in Table 3.

Thermal stresses were determined for the steady state application of maximum vent system temperature, using hand analysis.

4.4 Results and Evaluation

Results are reported for each structural element of the vent system for the controlling load combination. Controlling load combinations are the ones that produce the smallest margins against the allowable stress, not necessarily the highest stress. All load combinations listed in Table 1 have been considered.

As stated previously, most results include some level of bounding analysis and, therefore, understate the margins which actually exist.

4.4.1 Vent Header - Downcomer Intersection

The controlling load on the vent header-downcomer intersection, both for maximum stress and fatigue, is the downcomer lateral load due to chugging. The worst load combination in which this load appears is case 15 of Table 1. This cases consists of:

Chugging (IBA) + Seismic (SSE) + Weight + Presssure + Thrust + SRV

For this case, the following stress occurs at a point 90^{o} from the plane of a downcomer pair. It is primarily the result of a longitudinal chugging force on the downcomer.

TYPE OF STRESS	ACTUAL STRESS	ALLOWABLE STRESS
Combined Maximum Stress	35,303 psi	37,635 psi

4.4.2 Vent Header - Vent Pipe Intersection

The controlling load on the vent header/vent pipe intersection occurs as a result of pool swell water impact. The controlling load condition is case 25 in Table 1 which includes:

Pool Swell (full$\triangle$P) + Thrust + Seismic (SSE) + Weight + SRV Pressure

TYPE OF STRESS	ACTUAL STRESS	ALLOWABLE STRESS
Combined Maximum Stress	26,748 psi	28,950 psi

This load case was formed using a 0△P load, and was evaluated to a level A allowable. This conservative evaluation was performed to eliminate the need to evaluate several other vent header load cases.

4.4.3 Vent Header Support Columns and Attachments

The controlling load combination for the vent header support columns and the clevis joints at each end is case 25, Table 1. This case includes:

Pool Swell (full△P) + Seismic (SSE) + Weight + Thrust + SRV

As before, the evaluation was conservatively performed using 0 △P loads and a level A allowable.

Controlling stress in the support column is:

TYPE OF STRESS	ACTUAL STRESS	ALLOWABLE STRESS
Axial in Column (tension)	17,420 psi	18,000 psi

Controlling stress in the clevis joint at the end of the support column is:

LOCATION	STRESS TYPE	ACTUAL STRESS	ALLOWABLE STRESS
Clevis Plate	Shear	13,015 psi	15,200 psi

4.4.4 Downcomer Tie-Bars and Attachments

The controlling load combination for stresses in the downcomer tie bar and attachments is case 25, in Table 1. The major load is associated with pool swell impact on the crotch region of the downcomers which produces tensile loads in the tie bar.

The controlling case includes:

Pool Swell Impact (full ΔP) + SSE Seismic + SRV + Weight + Pressure + Thrust

Zero ΔP pool swell loads and service level allowables were conservatively used in this analysis.

The controlling stress is:

LOCATION	STRESS TYPE	ACTUAL STRESS	ALLOWABLE STRESS
Tie Bar Clamp	Bending	10,614 psi	22,240 psi

4.4.5 Vent Header Deflector and Attachments

The major load on the vent header deflector occurs as a result of pool swell water impact. The controlling load condition is case 25 in Table 1 which includes:

Pool Swell (full ΔP) + SSE Seismic + Weight + SRV

The controlling stress in the deflector is:

LOCATION	STRESS TYPE	ACTUAL VALUE	ALLOWABLE VALUE
Center of the Long Span	Bending	6,236 psi	16,500 psi

The controlling stress for the attachments is:

LOCATION	STRESS TYPE	ACTUAL VALUE	ALLOWABLE VALUE
Fillet Weld	Shear	10,662 psi	18,000 psi

4.4.6 Main Vent/Drywell Intersection

The major load on the drywell penetration occurs as a result of chugging. The controlling load condition is case 21 in Table 1 which includes:

Chugging + Seismic (SSE) + Weight + Pressure (Drywell)

The controlling stress is:

TYPE OF STRESS	ACTUAL STRESS	ALLOWABLE STRESS
Primary and Secondary	23,664 psi	69,900 psi

The effects of all loads from the vent system, and the pressure load were considered using Reference 16. Information regarding stresses due to seismic and thermal response of the drywell was taken from the Fitzpatrick FSAR update (Reference 19).

The controlling stress is:

TYPE OF STRESS	ACTUAL STRESS	ALLOWABLE STRESS
Primary and Secondary	17,724 psi	69,900 psi

The total vent-to-drywell intersection stress is:

TYPE OF STRESS	ACTUAL STRESS	ALLOWABLE STRESS
Primary and Secondary	41,388 psi	69,900 psi

4.4.7 Vent Header, Main Vent & Downcomers - Free Shell Stresses

It was established by inspection of the computer results that large safety margins existed in free shell regions and that minimum safety margins would be controlled by local shell stresses. No further work was done for free shell stress in these structures.

4.4.8 Vent Header - Mitre Joint

The controlling load on the vent header mitre joint occurs as a result of pool swell water impact. The controlling load condition is case 25 in Table 1 which included:

Pool Swell (full $\triangle P$) + Thrust + Seismic (SSE) + Weight + SRV + Pressure

TYPE OF STRESS	ACTUAL STRESS	ALLOWABLE STRESS
Combined Maximum Stress	18,935 psi	28,950 psi

4.4.9 Fatigue Evaluation

The fatigue analysis of the vent system is a conservative one which assumes that all maximum stresses occur simultaneously, and that all cycles reach these maximum values. The duration of the major loads in this analysis is 900 seconds, the length of chugging associated with an SBA/IBA event.

The procedure used in this analysis consists of the following steps:

- For a given load and component, locate the highest stress.

- For this location, establish the stress range.
- Repeat this process for all other loads in the load combination.
- Add the stress ranges for all loads.
- Multiply this total stress range by the appropriate stress intensification factor.
- Calculate stress intensity and determine the allowable number of stress cycles.
- Determine the usage factor, using the methods of Reference 11.

The fatigue evaluation was performed for all high stress areas in the vent system. The major load, contributing to the fatigue evaluation is chugging following a DBA. The controlling load case is case 21 in Table 1, which includes:

IBA.CH + Seismic (SSE) + SRV + Weight

The controlling usage factor for the vent system is:

VENT SYSTEM FATIGUE RESULTS

LOCATION	ACTUAL USAGE FACTOR	ALLOWABLE USAGE FACTOR
Vent Header Support	.98	1.0

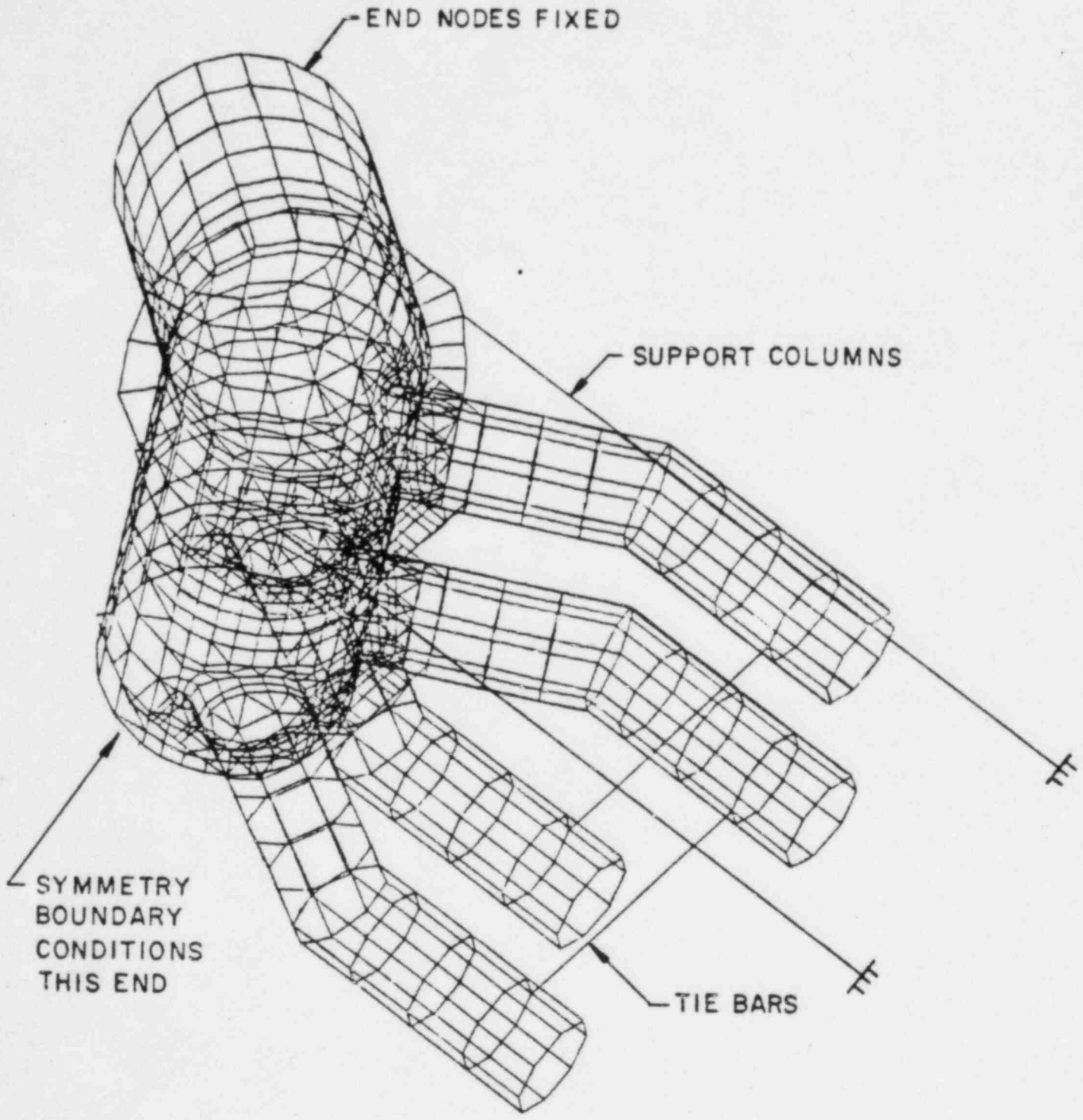

FIG. 4-1

VENT HEADER MODEL

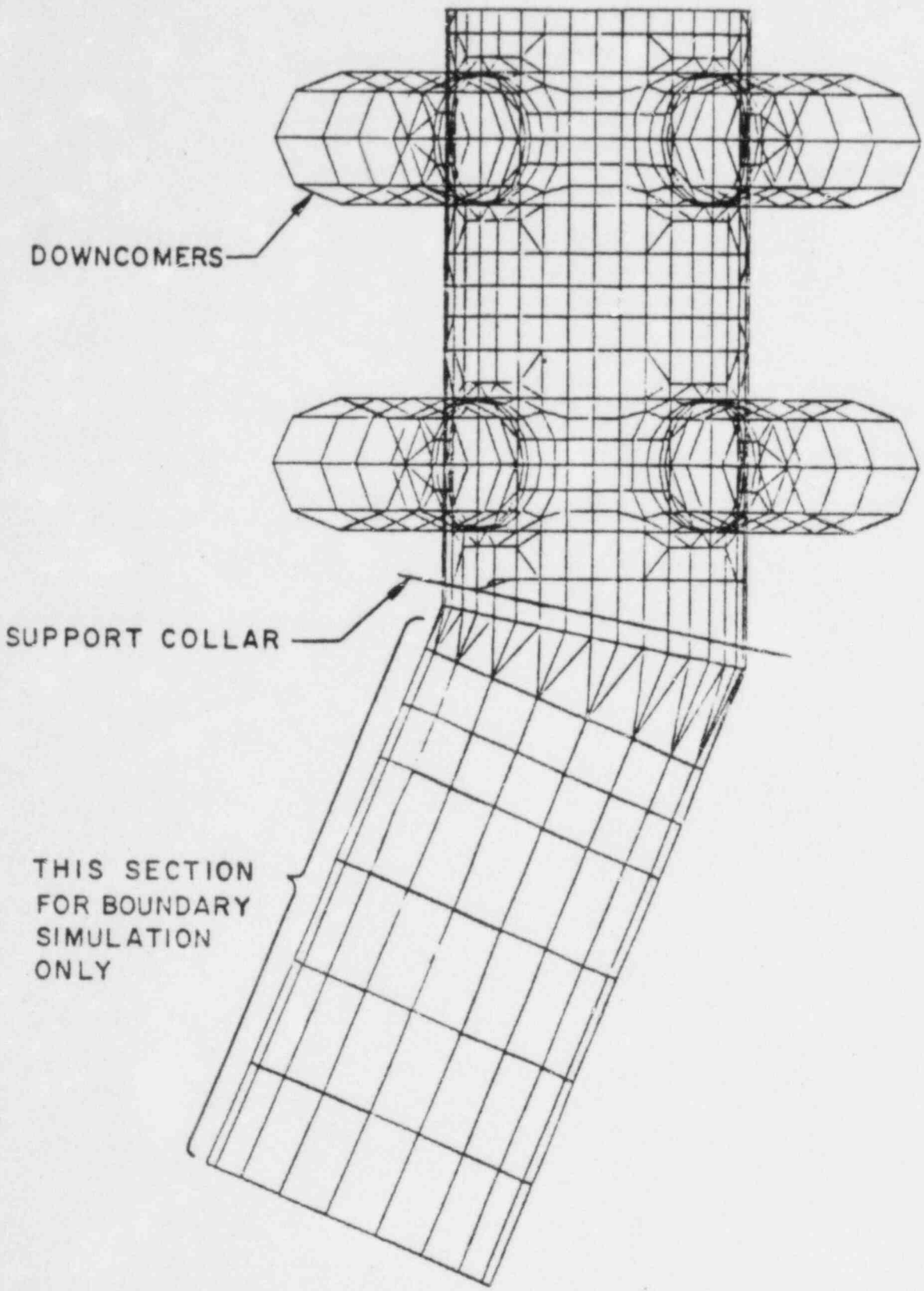

FIG. 4-2

DETAILED VENT HEADER MODEL

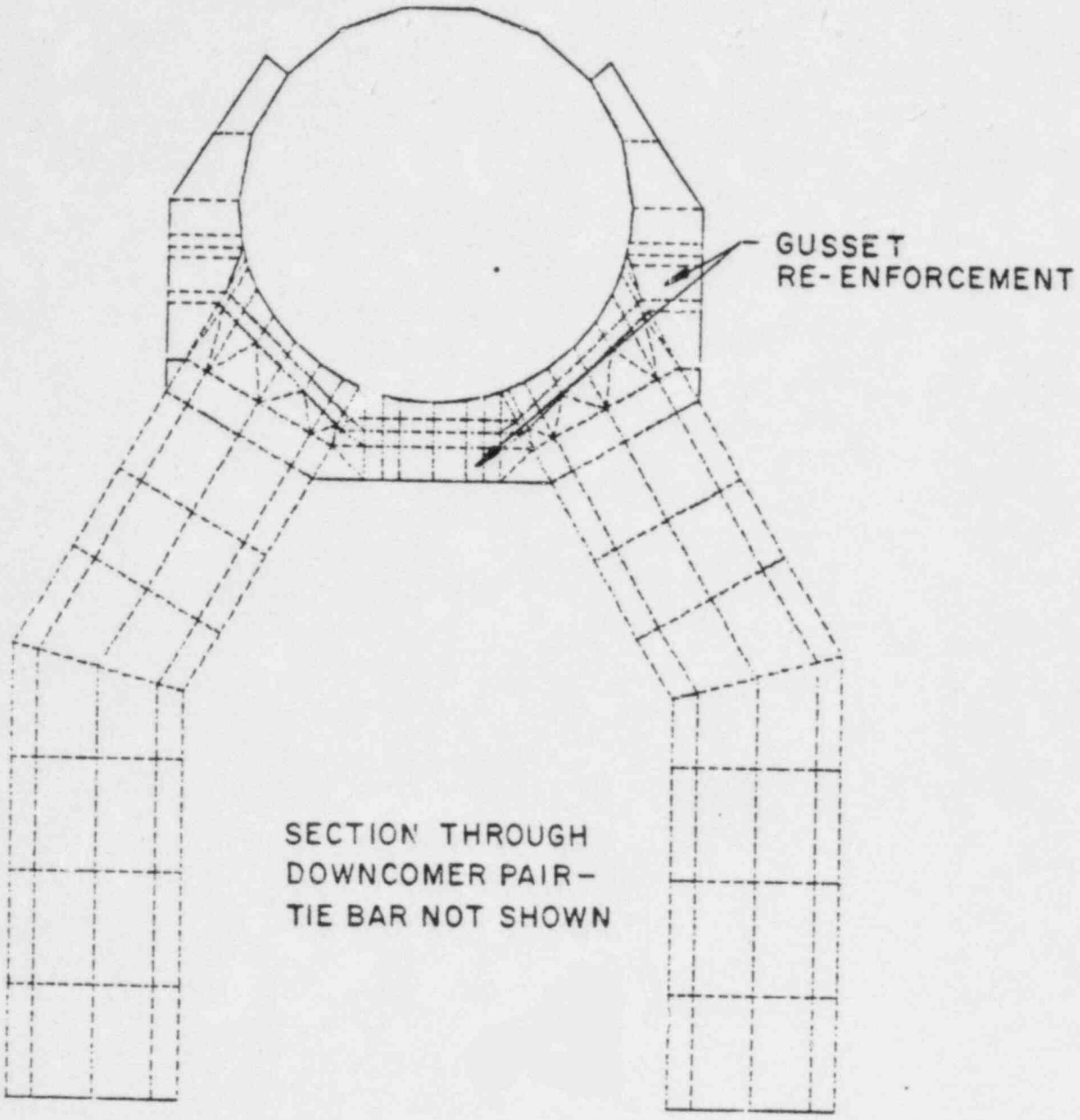

FIG. 4-3

DETAILED VENT HEADER MODEL

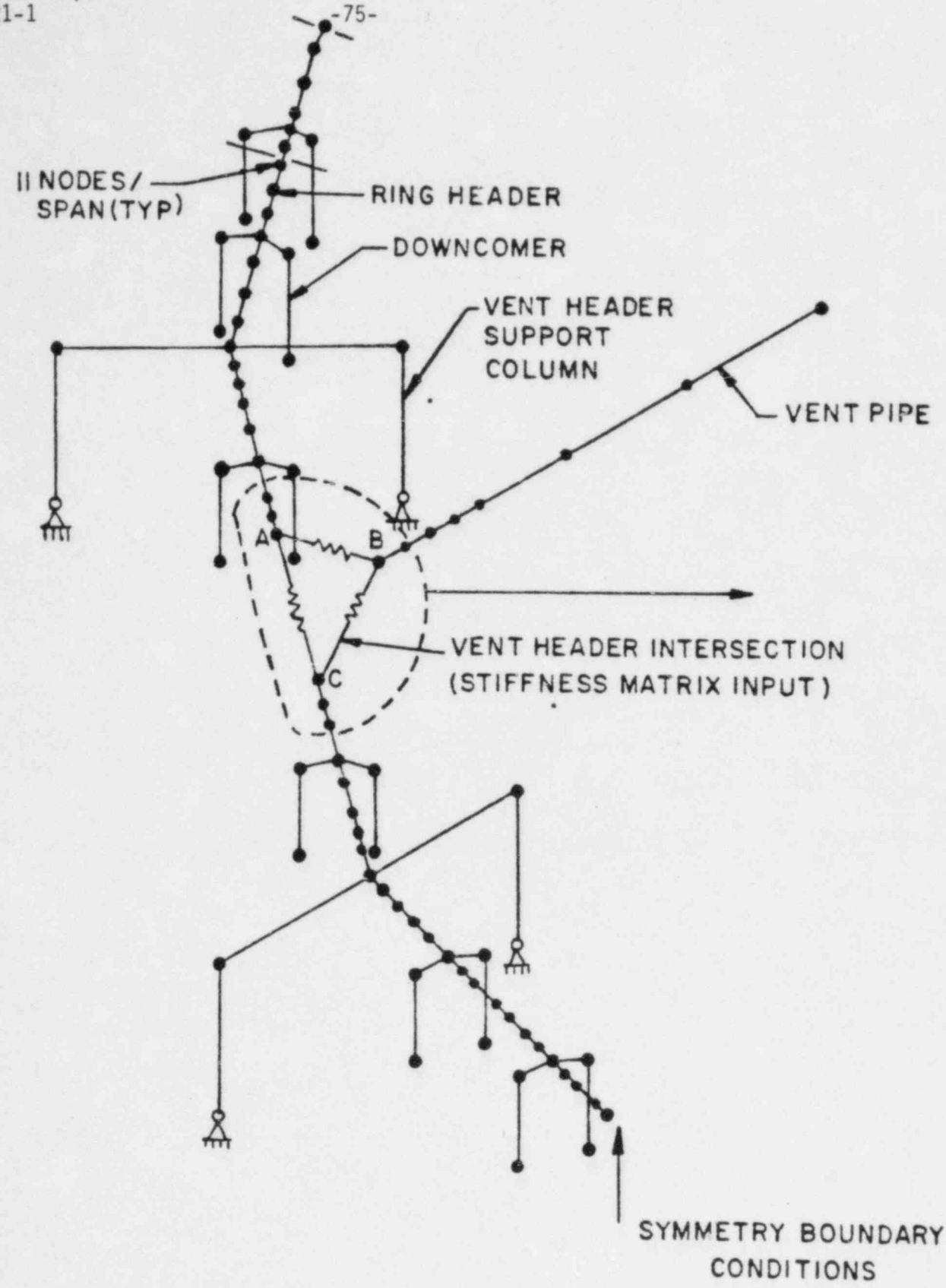

FIG. 4-4
VENT SYSTEM BEAM MODEL

STRUCTURAL FREQ. = 59.3 hz
LOAD FREQ. = 2 hz
DLF = 1.0

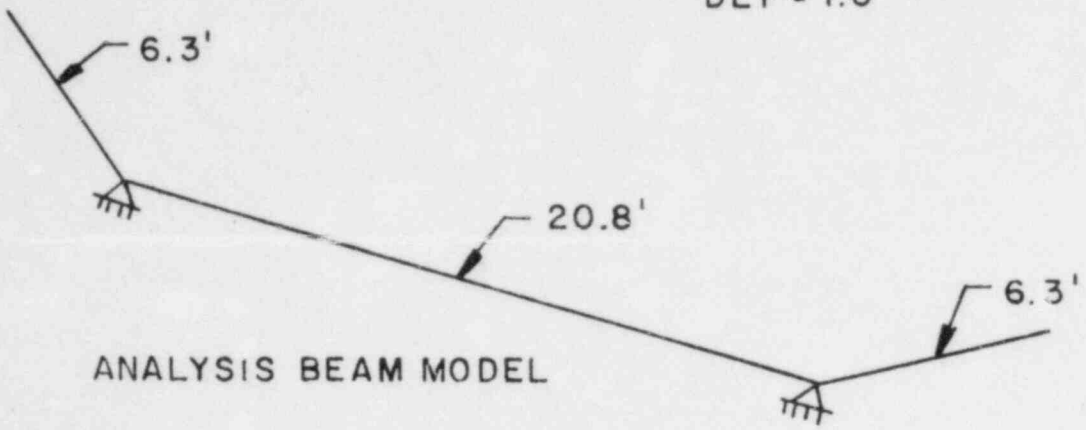

ANALYSIS BEAM MODEL

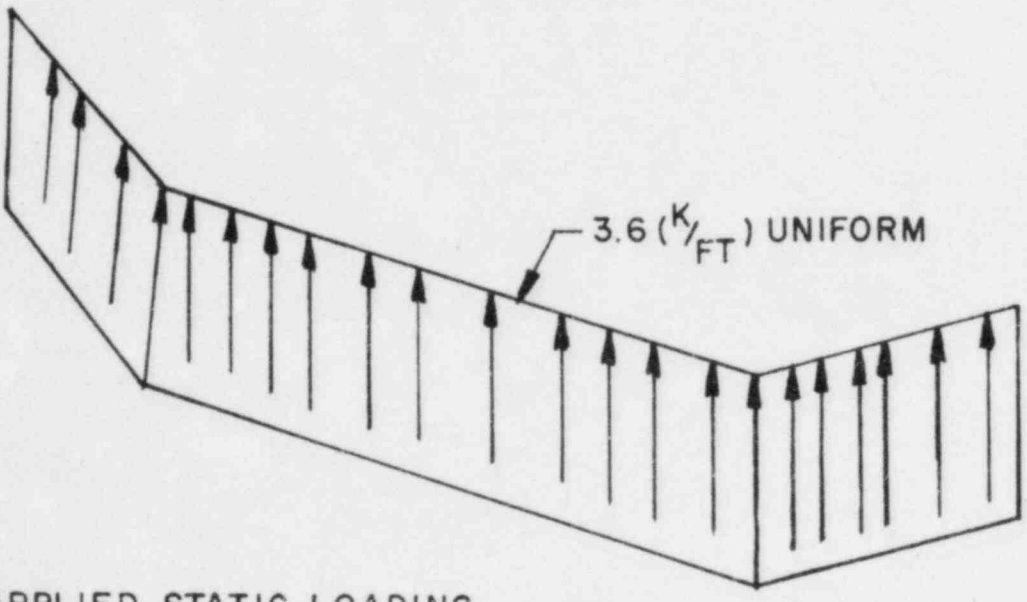

APPLIED STATIC LOADING

FIG. 4-5

VENT HEADER DEFLECTOR ANALYSIS - FITZPATRICK

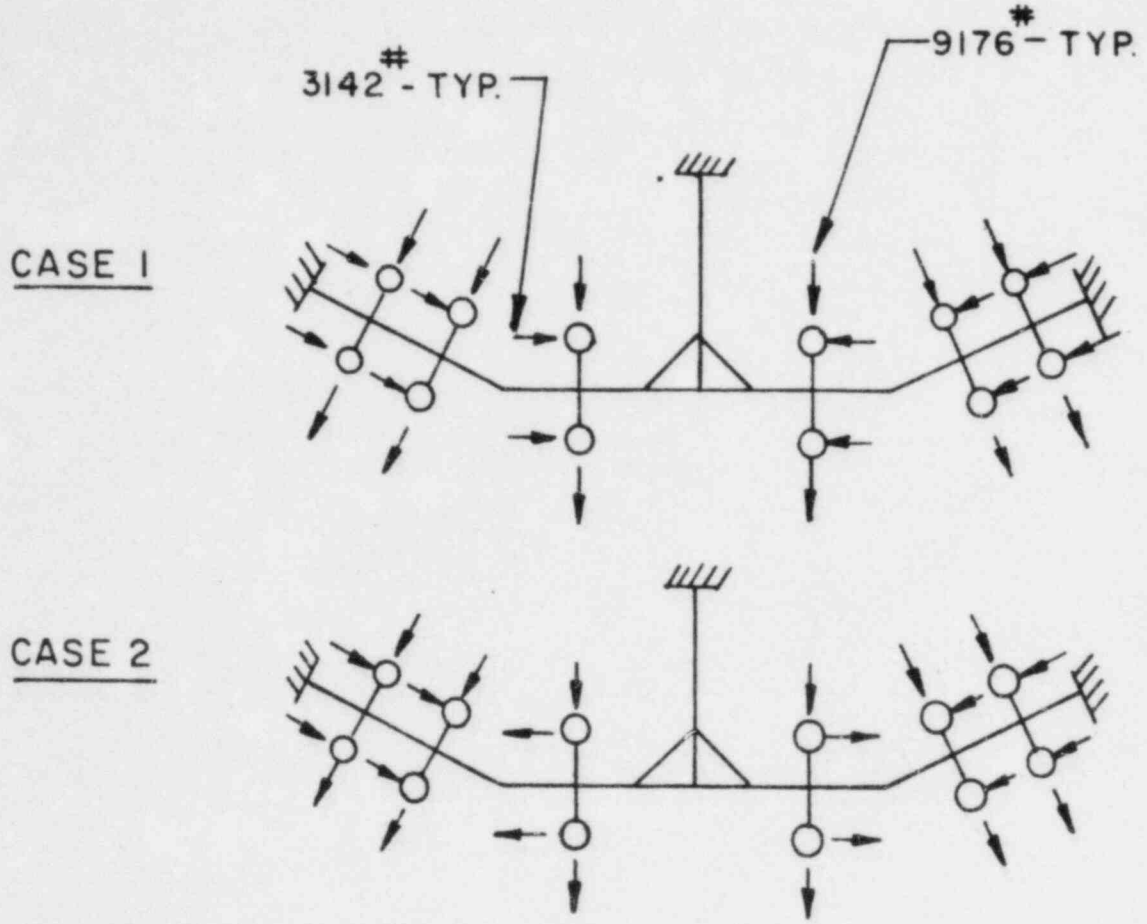

ANALYSIS CASES FOR SYNCHRONIZED LATERAL CHUGGING

FIG 4-6

5.0 RING GIRDER ANALYSIS

The ring girder for Fitzpatrick is shown in Figure 5-1. It is mounted in a vertical plane that passes through the support saddles and the support columns. Because all major internal structures are supported by the ring girders, the ring girders react to the largest number of individual loads.

5.1 Structural Elements Considered

Elements considered in this section are:

(a) The ring girder web and flange.
(b) The attachment weld to the shell.

Local stresses at attachments have also been considered and added; i.e., vent header support columns, catwalk, etc.

5.2 Computer Models

Two computer models were used as a part of the ring girder analyses; both are detailed models which also include the shell and external supports.

The first model is shown in Figure 5-2. This is a detailed model, which represents one-sixteenth of the torus structure; one half bay on each side of the mitre joint. It accurately simulates the ring girder offset (four-inches from the mitre joint), as well as structural differences between the vent and non-vent bays. Because the ring girder is not at the boundary of this model, out-of-plane motion of the ring girder can be accurately determined. This model was used to evaluate all direct loads on the ring girder; these include loads from attached structures such as the tee-quencher supports and vent header system, as well as all drag loads.

The one-sixteenth model used for the Fitzpatrick ring girder analysis was one that had been constructed for one of the other Mark 1 plants analyzed by TES. The dimensions of this other plant are very similar to Fitpatrick; the diameter of the torus, shell thickness and distance between the ring girder and mitre joint are all similar. The ring girder flange in this model is slightly smaller than Fitzpatrick and, therefore, produces conservative results since lateral loads control ring girder stresses. The comparison is:

Ring Girder Flange Dimensions (inches)

Fitzpatrick: 1.5 x 8
Model Used: 1.5 x 6

The second model used to determine ring girder loads is the Fitzpatrick 1/32 finite element model shown in Figure 3-1. This model was used previously to evaluate shell stresses of all symmetric loads that act on the shell. These same computer analyses produce information on ring girder stress for symmetric loads. Loads evaluated with this model include weight, internal pressure and all shell dynamic loads. The boundary conditions on this model restrict the ring girder to in-plane motion.

5.3 Loads Analysis

5.3.1 Loads Applied to Shell

As stated, the ring girder stresses for all symmetric loads applied to the shell were taken from the appropriate analyses described in Section 3.0; these include:

(a) Pool Swell Shell Load (Paragraph 3.2.1)
(b) Condensation Oscillation (3.2.2)
(c) Chugging (3.2.3)

(d) SRV Discharge*

(e) Seismic

(f) Deadweight, Thermal and Pressure

*SRV discharge is conservatively assumed to be a symmetrically applied load for shell analysis.

5.3.2 Drag Loads

The ring girder is subject to drag loads from each of the dynamic shell loads as well as Fluid Structure Interaction (FSI) effects from CO and CH. All these loads were evaluated by using the 1/16 model and applying static loads out-of-plane on the wetted nodes of the ring girder. The use of static analysis was based on the assumption that the stiffening effect of the saddle, columns, and column gussets make the ring girder very stiff and would prevent frequency interaction with the dynamic loads. Because of this, no dynamic load factors were applied to the static analysis results (DLF = 1.0). Drag loads considered were:

(a) Pool Swell Bubble

(b) Pool Swell Jet (bounded by a)

(c) SRV Jet

(d) SRV Bubble

(e) CO including FSI (bounded by g)

(f) Pre-chug including FSI (bounded by g)

(g) Post Chug including FSI

The effects of SRV jet (c) and SRV drag (d) were evaluated based on data collected from in-plant tests. A discussion of the in-plant tests and the use of drag data from these tests is given in Appendix 1.

Calculation of ring girder drag loads due to condensation oscillation and post chug FSI was not in accordance with NUREG 0661 (Reference 2). An alternate method of calculating drag volume was used in this load

calculation. It produced drag volumes for the ring girder of about half of those that the NUREG 0661 procedure would have produced. A discussion of this is included in Appendix 3. The FSI drag calculation was based on local pool accelerations at the ring girder resulting from the response of the entire shell. The post chug and FSI analysis considered frequencies to 31 Hz, which were combined by adding the values of the five maximum components to the SRSS sum of the others.

5.3.3 Loads Due to Attached Structure

Loads applied to the ring girder by structures attached to it were evaluated by equivalent static analysis, using the 1/16 model (Figure 5-2). The important loads are applied in the area of the support saddle and columns which make the ring girder very stiff and minimizes dynamic interaction. Because of this, dynamic amplification of the static ring girder stresses was not done (DLF = 1.0). The load input to the ring girder was a result of a dynamic analysis of the attached system (or had an appropriate DLF applied) and, therefore, included the effects of dynamic amplification on load.

The following loads are applied to the ring girder and were considered:

- Tee-quencher support beam thrust due to SRV discharge.
- Tee-quencher and support drag loads.
- Vent header support column reaction loads during pool swell.
- Vent header support column drag loads.

As stated in Section 5.1, stresses resulting from attached structure have been included in the following results.

5.4 Results and Evaluations

5.4.1 Ring Girder Web and Flange

The controlling load combination for the ring girder web and flange is load case 16 of Table 1; this includes:

Pool Swell (zero$\triangle$P) + Weight

The controlling stresses are:

STRESS LOCATION	STRESS TYPE	ACTUAL STRESS	ALLOWABLE STRESS
Web	Membrane	14.9 ksi	19.3 ksi
Flange	Membrane	16.9 ksi	19.3 ksi

5.4.2 Weld to Torus Shell

The controlling load combination for the shell weld is load case 21 of Table 1. The controlling stresses are:

DBA.CO + Seismic (SSE) + Weight

STRESS LOCATION	STRESS TYPE	ACTUAL STRESS	ALLOWABLE STRESS
Column Region Inside	Shear	7.64 K/in	8.53 K/in
Column Region Outside	Shear	8.27 K/in	8.53 K/in
Saddle Region	Shear	7.29 K/in	8.53 K/in

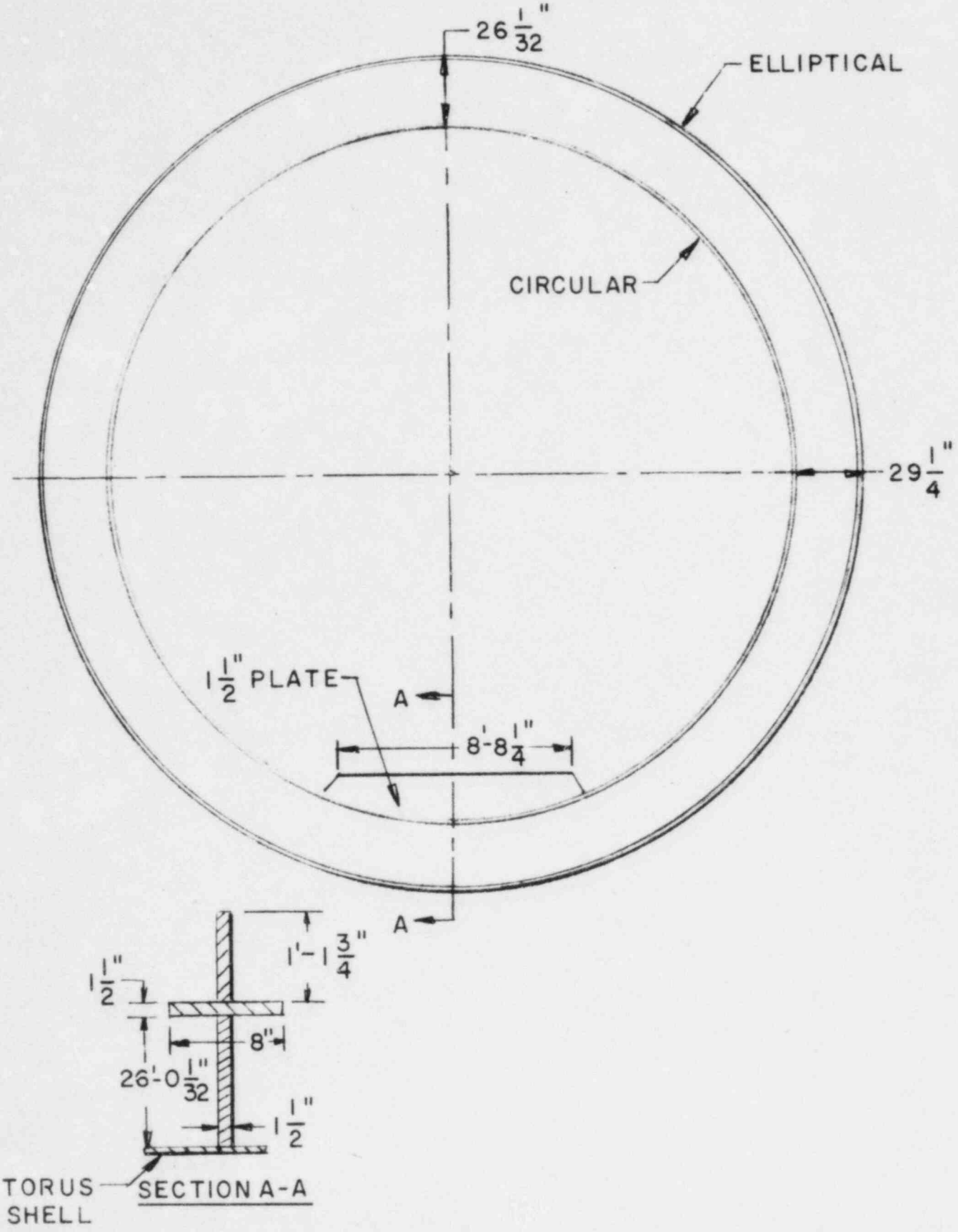

FIG. 5-1
RING GIRDER - FITZPATRICK

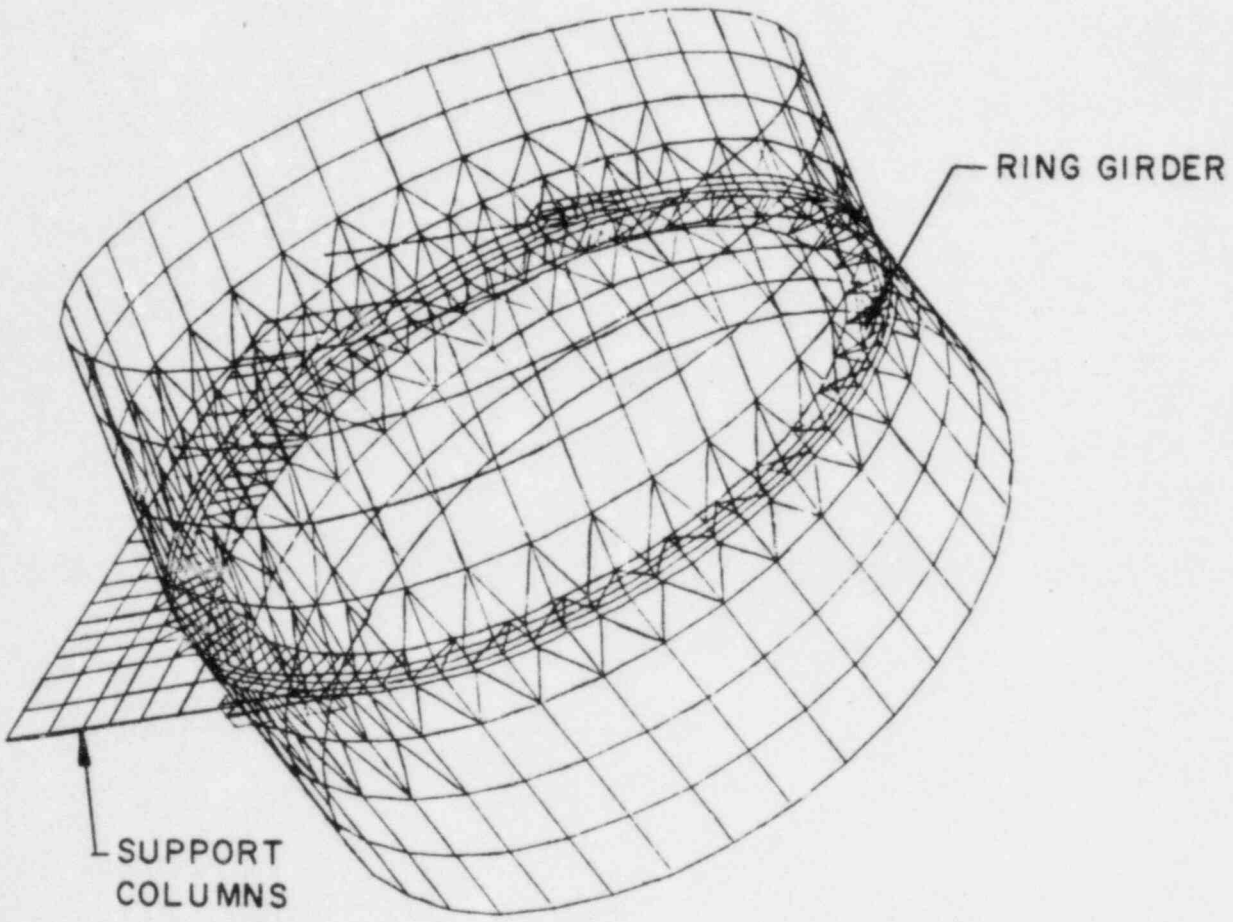

FIG. 5-2

DETAILED RING GIRDER - SHELL MODEL

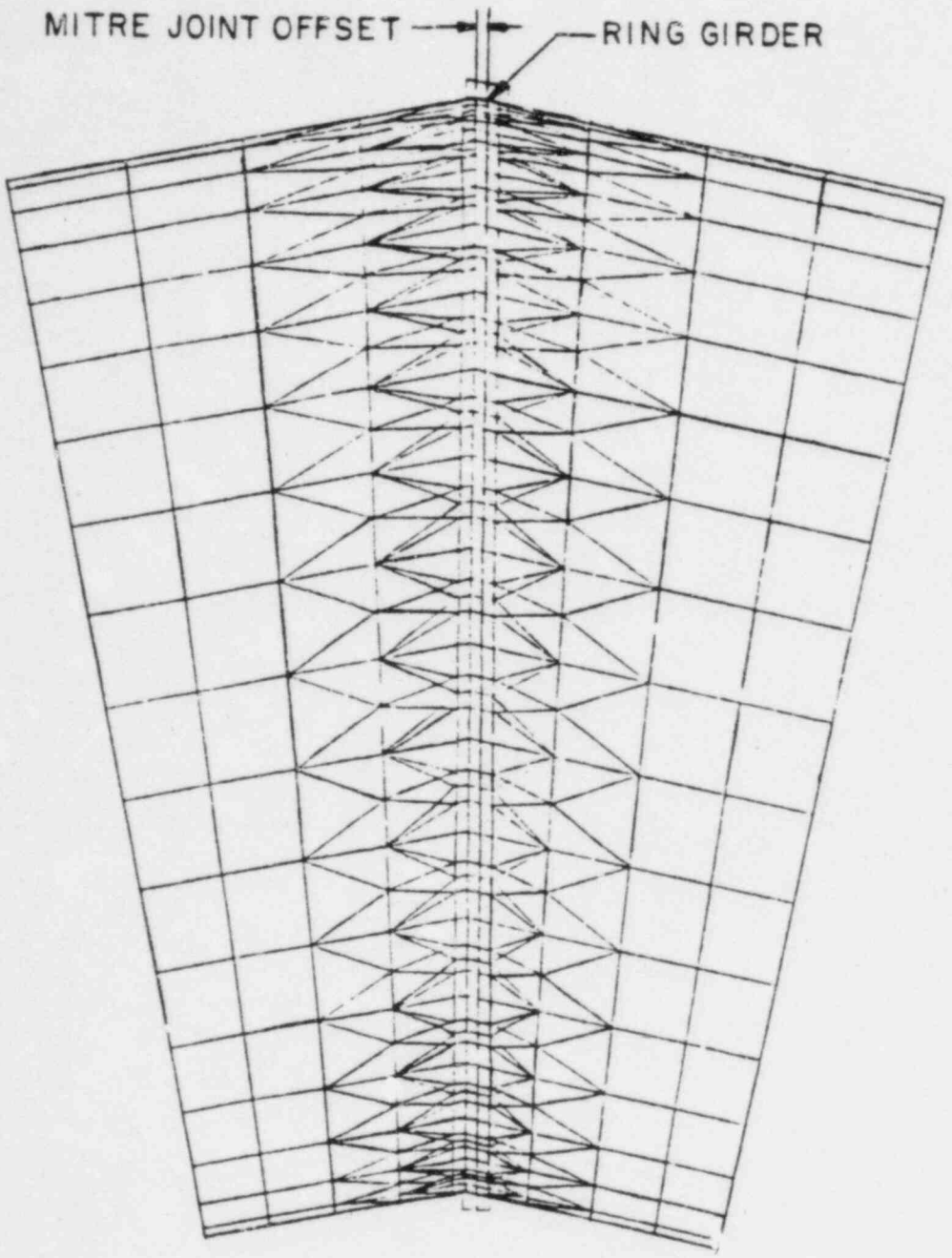

FIG. 5-3

DETAILED RING GIRDER - SHELL MODEL

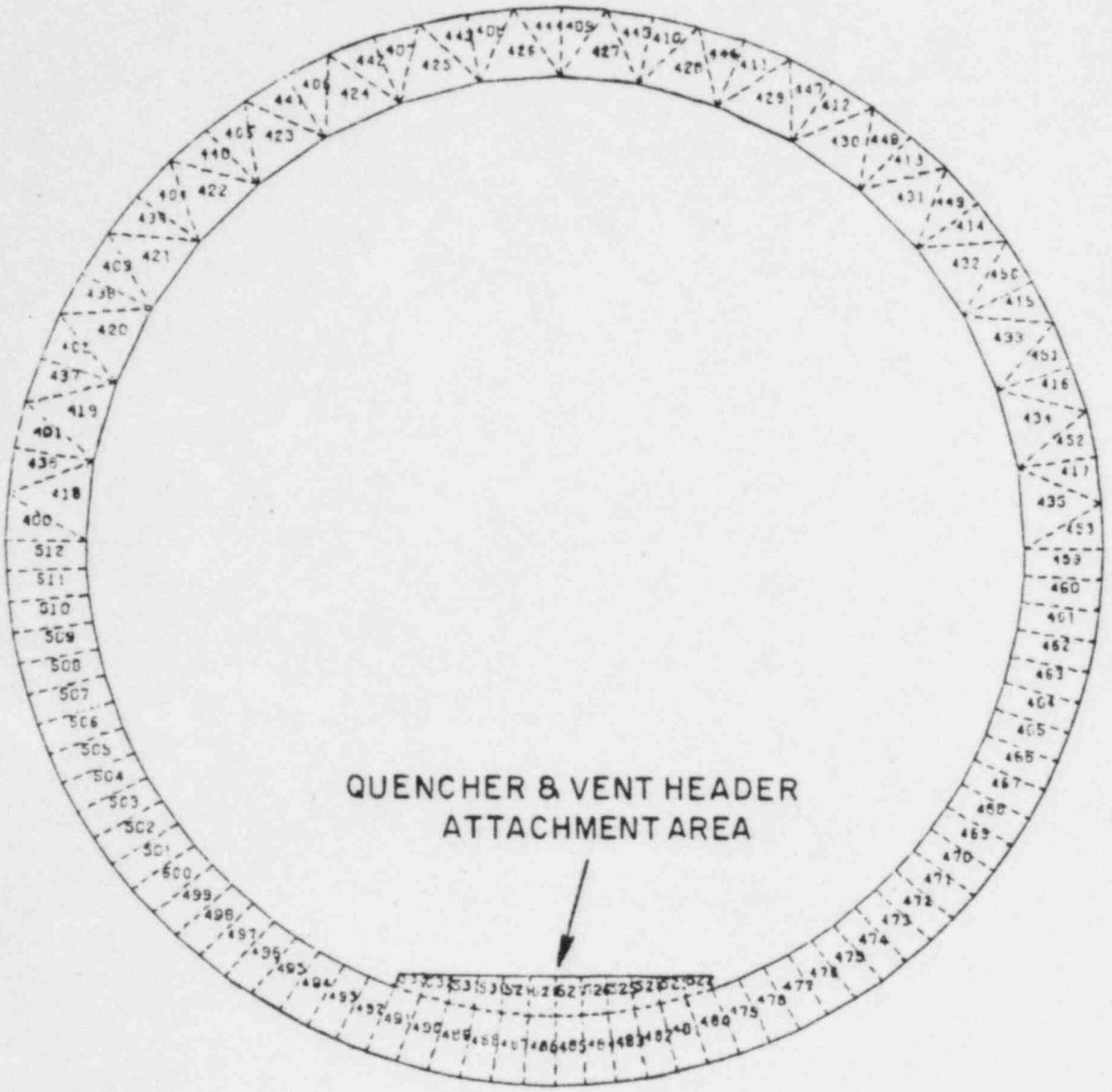

The model has additional elements, (not shown), which are for more detail in the lower ring girder section, the torus-to-column weld joint and the saddle.

FIG. 5-4

DETAILED RING GIRDER - SHELL MODEL

RING GIRDER ELEMENTS

6.0 TEE-QUENCHER AND SUPPORT

The following results for the tee-quencher and supports are conservative due to the combined effect of several factors, three of which are:

- The calculational methods to determine applied loads improved after this analysis was complete, and would provide reduced stresses.
- Some loads were intentionally bounded by conservative values from other plants so a single calculation could be used for more than one plant.
- For submerged drag loads, individual frequency components were added to produce maximum stress without regard to load direction.

The effect of these conservatisms vary among stresses, but can be significant in some cases.

6.1 Structural Elements Considered

The configuration of the quencher and support is shown in Figure 2-8. Fitzpatrick has eleven discharge lines, each enters the pool vertically.

The structural elements considered in this section include:

- The quencher.
- The submerged portion of the SRV line.
- The quencher support beam and attachments.

6.2 Computer Models

The computer model used in this analysis is shown in Figure 6-1.

This is a STARDYNE beam model which represents all piping and structure between the drywell jet deflector and the ring girder. For these analyses, the ring girder was assumed rigid and the vent pipe penetration was represented by a stiffness matrix which was developed from a finite element model of the penetration. Releases were modeled between the quencher and support plates to allow for free rotation of the quencher arms in the supports.

This model was used for both static and dynamic analysis.

6.3 Loads Analysis

6.3.1 SRV - Load

The calculation of stress due to SRV blowdown was done by applying the dynamic loads to the computer model and calculating the time-history response of the system. The applied loads included both the blowdown forces on the piping and the water clearing forces at the quencher. The controlling condition was for a second, multiple valve actuation after an SBA/IBA break (SRV case C3.3). This case produces a high reflood level at the time of the second actuation and produces maximum load on the support system. Loads for this analysis were developed using G.E. computer program RVFOR-04 and RVRIZ. The second actuation was assumed to occur at the point of maximum line reflood.

6.3.2 Pool Swell Loads

The effects of pool swell jet and bubble loads on the quencher and support system were conservatively estimated by static analysis and a dynamic load factor of 2. It was clear from this analysis that combined pool swell events would not control stresses - no further analysis was done.

6.3.3 Chugging Loads

Dynamic analysis of the quencher and support system was done for drag loads due to pre-chug, post chug and chugging FSI. All these analyses were based on a set of harmonic analysis which provided results for all steady-state frequency excitations from 1-31 Hz. Results for individual load conditions were determined by scaling individual frequency results of the computer analysis by the appropriate pressure amplitude.

The mass of the structure used in the computer analysis was adjusted to account for the "added mass" effect of the surrounding water. For FSI and post chugging analyses, individual frequency components were combined by adding the five maximum frequency contributors to the SRSS sum of the others (see Reference 12 for discussion). The maximum value of each frequency component was used in the combination, regardless of vector direction or time of instantaneous response. FSI loads were calculated by considering the calculated local accelerations in the pool due to response of the entire shell.

6.3.4 Condensation Oscillation Loads

The quencher and support system are subjected to condensation oscillation drag and CO-FSI drag. Analysis for these loads was based on the same harmonic analysis discussed in paragraph 6.3.3, scaled to the CO amplitudes. Each of the three CO spectra shown in Figure 4.4.1-1 of Reference 1 were considered.

All other discussion from paragraph 6.3.3 for chugging applies to the condensation oscillation analysis, except that the final load was determined by adding the four maximum frequency contributors to the SRSS sum of the others.

6.3.5 Other Loads

Calculations of stress due to weight, thermal and seismic loads was done by using the computer model in Figure 6-1 and static analysis. Pressure stresses for the piping and quencher were calculated by hand.

6.4 Results and Evaluation

The results reported in this section are conservative depending on the effect of factors discussed in Sections 1.0 and 6.0 of this report.

6.4.1 Tee-Quencher

The controlling stress in the tee-quencher, itself, occurs in the ramshead between the quencher arms. It is the result of load case 25 of Table 1. It includes:

Design Basis Accident + Seismic + SRV

The controlling stress is:

STRESS LOCATION	STRESS TYPE	ACTUAL STRESS	ALLOWABLE STRESS
Bifurcated Elbow	Bending	26,292 psi	37,440 psi

6.4.2 Submerged SRV Line

The controlling stress for the submerged portion of the SRV line occurs in the inclined lines and is a result of load case 25 in Table 1. This case includes:

Design Basis Accident + Seismic + SRV

STRESS LOCATION	STRESS TYPE	ACTUAL STRESS	ALLOWABLE STRESS
Vertical Section Above Reducer	Bending	25,085 psi	36,000 psi

6.4.3 Tee-Quencher Support

The controlling stress that was calculated for the tee-quencher support is the result of load case 25 of Table 1. This case includes:

Design Basis Accident + Seismic + SRV

The controlling stress for the beam is:

STRESS LOCATION	STRESS TYPE	ACTUAL STRESS	ALLOWABLE STRESS
At the Brace Connection	Bending	10,729 psi	36,000 psi

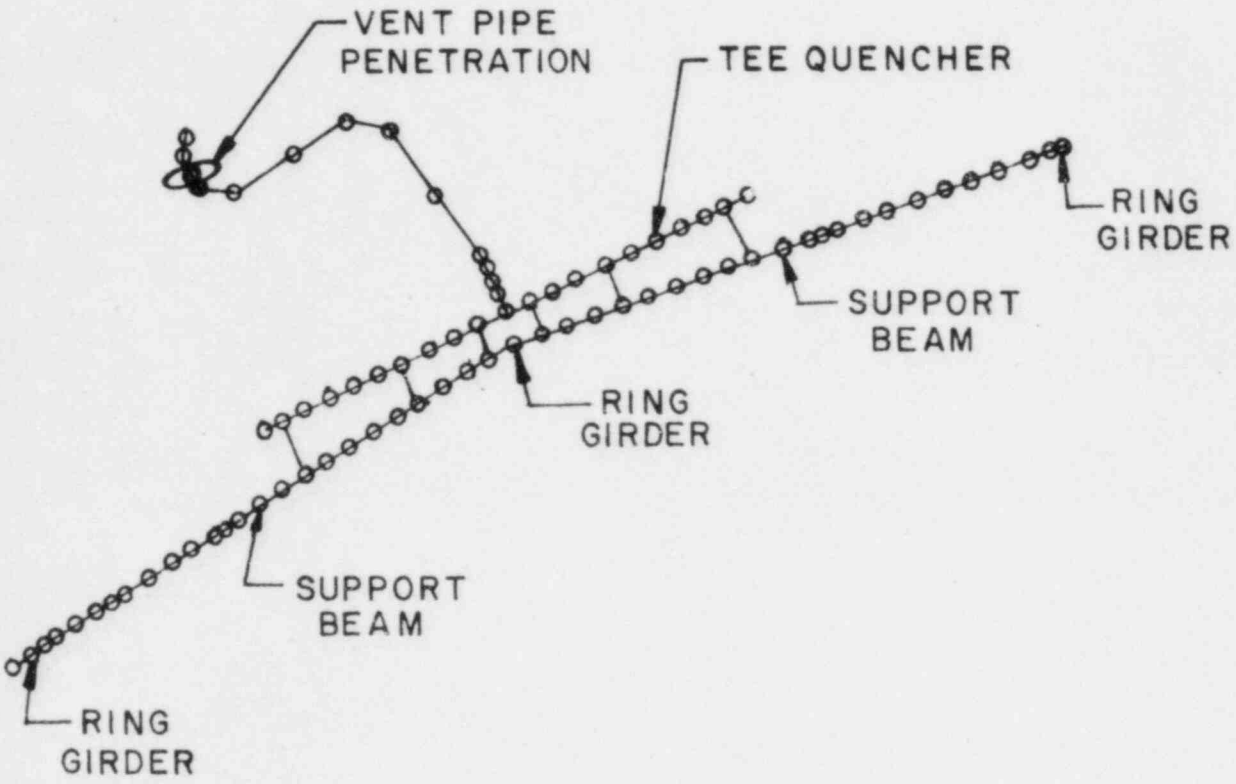

FIG. 6-1

FITZPATRICK ANALYTIC MODEL

7.0 OTHER STRUCTURES

7.1 Catwalk

Analysis of the catwalk structure at Fitzpatrick showed that major modifications would be necessary to meet allowable stresses. The necessary modifications were judged to be prohibitive and the entire catwalk was removed except for three bays. This partial catwalk was analyzed and that analysis is reported here.

Like the original catwalk, the partial catwalk consists of a horizontal frame structure which supports sections of open grating. The partial catwalk is supported from the ring girders and is fitted with handrails as shown in Figure 2-16. The handrails are ½-inch cable to reduce froth drag loads.

7.1.1 Computer Model

The computer models of the catwalk are shown in Figures 7-1 and 7-2 for the original and modified catwalks. They represent the structure for one full bay, beginning at mid-bay. They include all of the load carrying structural members, but do not include the grating or handrails. Loads from these elements are calculated and applied to the frame as forces at the points of attachment.

All catwalk analysis was performed on these linear models. All analysis used static application of loads, increased to account for dynamic amplification, where appropriate.

7.1.2 Loads Analysis

Loads analysis for the catwalk was performed for the direct effects of the following loads. Indirect effects due to motion of the ring girder at the attachments points were considered, but judged to be negligible.

7.1.2.1 Pool Swell Drag (4.3.4)

Pool swell drag loads are produced as the rising pool envelops the main frame, grating and handrails. Loads on the frame were calculated based on velocities taken from plant unique QSTF movies and the methods in Reference 1. These were multiplied by two to account for the dynamic effect. Loads on the grating were taken from Section 4.3.4 of Reference 1; these loads already include a dynamic factor, since they are based on test data.

7.1.2.2 Pool Swell Fallback (4.3.6)

Pool fallback loads were calculated and applied in accordance with Reference 1, except in unusual cases where fallback loads exceeded upward loads. In these cases, the maximum values of upward load were used for fallback also. Fallback affects the main frame and grating as well as the handrails.

7.1.2.3 Froth Load (4.3.5)

Froth loads have their major effect on the catwalk handrails; and, when applied horizontally, can produce high bending stresses in the vertical handrail members. Froth loads were calculated in accordance with Reference 1, except that the froth 1 influence region was redefined using plant-unique QSTF movies. These movies show clearly that froth 1 loads do not reach the catwalk railing; the analysis was therefore performed with froth 2 loads only.

Except for the handrails, the entire catwalk is submerged before froth loads reach this part of the torus; because of this, froth was only considered on the handrails.

7.1.2.4 Drag Loads (Support Columns)

The submerged portion of the catwalk support columns are subject to loading from drag forces from the following sources:

(a) Pool Swell
(b) SRV Discharge
(c) Condensation Oscillation
(d) Chugging

Loads from these sources were calculated and applied to the support columns as static loads. The natural frequency of the support was calculated using hand calculations and compared to the frequency(s) of each source. The statically determined stress was then multiplied by a dynamic amplification factor, developed by considering the worst case frequency ratio and the fact that this is a harmonic loading.

7.1.2.5 Weight and Seismic Loads

Stress due to weight loads were analyzed using static analysis and the one-sixteenth computer model shown in Figure 7-2. Seismic loads are small and were considered using hand analysis and scaling static stresses.

7.1.3 Results and Evaluation

Table 1 allows stresses in the catwalk structure (excluding attachments) to exceed yield and, in certain cases, to exceed ultimate. Our analysis was based on a linear model and all stresses were maintained below the stress at which a plastic hinge would form. Controlling stress and load combination for various catwalk elements are listed here.

7.1.3.1 Main Frame

The controlling stress in the catwalk frame occurs in the inboard supporting channel, Point A in Figure 7-2. It is a result of the combined condition that includes:

Pool Swell + SRV + Seismic + Weight (case 25, Table 1)

The maximum stress value is:

TYPE OF STRESS	ACTUAL STRESS	ALLOWABLE STRESS
Bending + Axial	31,500 psi	56,700 psi

7.1.3.2 Support Columns and End Joints

The controlling load case for the support column and end joints includes:

Pool Swell + SRV + Seismic + Weight (case 25)

Resulting stresses are:

TYPE OF STRESS	STRESS LOCATION	ACTUAL STRESS	ALLOWABLE STRESS
Bending	Column Under Extension	56,600 psi	56,700 psi

7.1.3.3 Welds to Ring Girder

The controlling load combination for this stress is also case 25:

Pool Swell + SRV + Seismic + Weight

For this condition, stresses are:

TYPE OF STRESS	ACTUAL STRESS	ALLOWABLE STRESS
Shear	27,903 psi	42,000 psi

7.2 Internal Spray Header

The internal spray header is attached to the ring girders and to a penetration on the shell. It is located at the top of the torus, above the vent header (Figure 2-3).

7.2.1 Computer Model

The computer model used to analyze the spray header is shown in Figure 7-3. It was constructed to allow determination of stresses in a typical multi-span area as well as at branch connections. This is a part of a piping system and piping elements were used in the model. All results were obtained through the use of static analysis, with factors applied to account for dynamic response.

7.2.2 Loads Analysis

The spray header is high enough in the torus so it does not experience direct water impact; froth is the only pool swell related load that is applied.

The motion of the ring girder that results from pool swell loads on the shell was considered but judged to be a negligible input to the spray header. Shell displacement at the nozzle connections was input to the computer analysis.

7.2.2.1 Froth Load (4.3.5)

Froth loads on the spray header were calculated as outlined in Reference 1. The worst stress condition existed for a vertically applied load. The loads were applied statically to the system.

7.2.2.2 Weight, Seismic & Ring Girder Displacement

The effects of weight, seismic, and shell displacement were all considered by using the model shown in Figure 7-3 and applying loads and displacments statically.

7.2.3 Results and Evaluation

The controlling stress for the spray header piping is a result of load case 19 in Table 1.

This case includes:

Froth (DBA), Weight, Seismic & Shell Motion

The controlling stress is:

SPRAY HEADER PIPING

STRESS LOCATION	STRESS TYPE	ACTUAL STRESS	ALLOWABLE STRESS
Tee at Branch Line	Bending	2,420 psi	24,660 psi

ATTACHMENTS TO RING GIRDER

STRESS LOCATION	STRESS TYPE	ACTUAL STRESS	ALLOWABLE STRESS
Support Hold-down Plate	Shear + Bending	14,427 psi	18,000 psi

WELDS TO RING GIRDER

STRESS LOCATION	STRESS TYPE	ACTUAL STRESS	ALLOWABLE STRESS
At Ring Girder	Shear + Bending	1,160 psi	18,000 psi

7.3 Vent Pipe Bellows

The vent pipe bellows forms the pressure seal between the vent pipe and torus; and allows for relative motion between these parts. It is illustrated in Figure 7-4.

7.3.1 Analysis Method

Analysis of the bellows at Fitzpatrick considered the capability of the bellows to respond to the dynamic motion applied to it; and also the possibility of direct water impact during pool swell (the bellows is inside the torus).

The effect of dynamic motion on the bellows was evaluated by considering the manufacturer's rating for differential motion both axially and radially. These ratings are intended to define static differences which occur over a long enough time so that dynamic response of the bellows itself can be ignored.

In the present analysis, both ends of the bellows are experiencing dynamic motion; one end is controlled by the vent pipe - the other by the torus shell. We expect that the dynamic characteristics of the convoluted bellows should increase stresses over their static equivalents. We also expect that the convolutions will produce complex modes and stress patterns that will not couple efficiently with specific input frequencies, i.e., high dynamic response is not expected. Further, the "pogo" and "rolling" modes of the convolutions are non-linear, highly cross-coupled modes that would not be predicted by ordinary structural codes.

Our approach to the bellows evaluation for motion input is to compare the maximum calculated difference in dynamic response across the bellows to the manufacturers allowable. We accept the bellows as adequate for all cases where a large margin occurs between the predicted input motions and the static capacity, as stated by the manufacturer.

Our evaluation of bellows stress, due to direct impact after pool swell, began with calculations for pool impact velocity. This analysis showed that the rising pool would not reach the bellows for the full P case. There was slight impact for the 0 P case and the stress was insignificant.

7.3.2 Loads Analysis

Calculation of vent pipe motion and torus shell motion was done as a part of the analysis work discussed in Sections 3.0 and 4.0 of this report. The analysis of the torus shell in Section 3.0 was based on a computer model of the non-vent bay and, therefore, did not account for the presence of the vent pipe hole, or the heavy shell reinforcement in that area.

7.3.3 Results and Evaluation

The maximum differential motion across the bellows occurs as a result of case 25 in Table 1; this case includes:

Pool Swell Pressure on Shell + Water Impact on the Vent System + Vent System Thrust + Pressure + Weight + SRV + Seismic

For this case, the following deflections occurred:

	MAXIMUM DIFFERENTIAL MOTION	MANUFACTURERS' STATIC ALLOWABLE
Axial Compression (in.)	.036	.375
Axial Extension (in.)	.036	1.125
Lateral Motion (in.)	.123	.625

All calculated values are less than 20% of the manufacturer's allowables. We consider that this large difference demonstrates the acceptability of the bellows, especially if we consider that much of the load is either static or a single-pulse transient (maximum amplification of 2).

7.4 Monorail

The monorail is attached to the torus ring girders at about 45^{o} above the water level. It is a non-containment related structure and therefore in the same category as the catwalk. It is illustrated in Figures 2-18 and 7-5.

7.4.1 Computer Model

The computer model used to analyze the monorail is shown in Figure 7-5. It is a beam model that represents the monorail through 180^{o} of the torus structure. Two sections of the monorail, 180^{o} apart, were removed to relocate the RHR return lines for circulating the torus pool. The monorail beam model ends are represented by the three foot cantilevered section with tne ends unrestrained.

All loads were applied to the monorail statically and dynamically.

7.4.2 Loads Analysis

The monorail is high enough over the pool so that it does not experience direct water impact. The only pool swell related load is froth 1. As with the catwalk, ring girder motion was considered, but judged to be negligible.

7.4.2.1 Froth Loads

The monorail is located in the Froth 1 region of the torus and was analyzed for these loads, oriented to produce maximum stress. This orientation was 45^{o} to the horizontal. Froth loads were calculated in accordance with the methods of Reference 1, and applied statically to the computer model.

7.4.2.2 Weight & Seismic

Weight and seismic analysis was performed using the model shown in Figure 7-5 and static analysis.

7.4.3 Results and Evaluation

The combination of froth, weight and seismic SSE (load case 19, Table 1) produce the following controlling stresses:

MONORAIL BEAM

STRESS LOCATION	STRESS TYPE	ACTUAL STRESS	ALLOWABLE STRESS
At Support	Bending	37,310 psi	42,280 psi

MONORAIL BUILT-UP COLUMN

STRESS TYPE	ACTUAL STRESS	ALLOWABLE STRESS
Axial + Bending	54,160 psi	57,290 psi

WELD ON RING GIRDER

STRESS TYPE	ACTUAL STRESS	ALLOWABLE STRESS
Bending + Tension	53,067 psi	57,290 psi

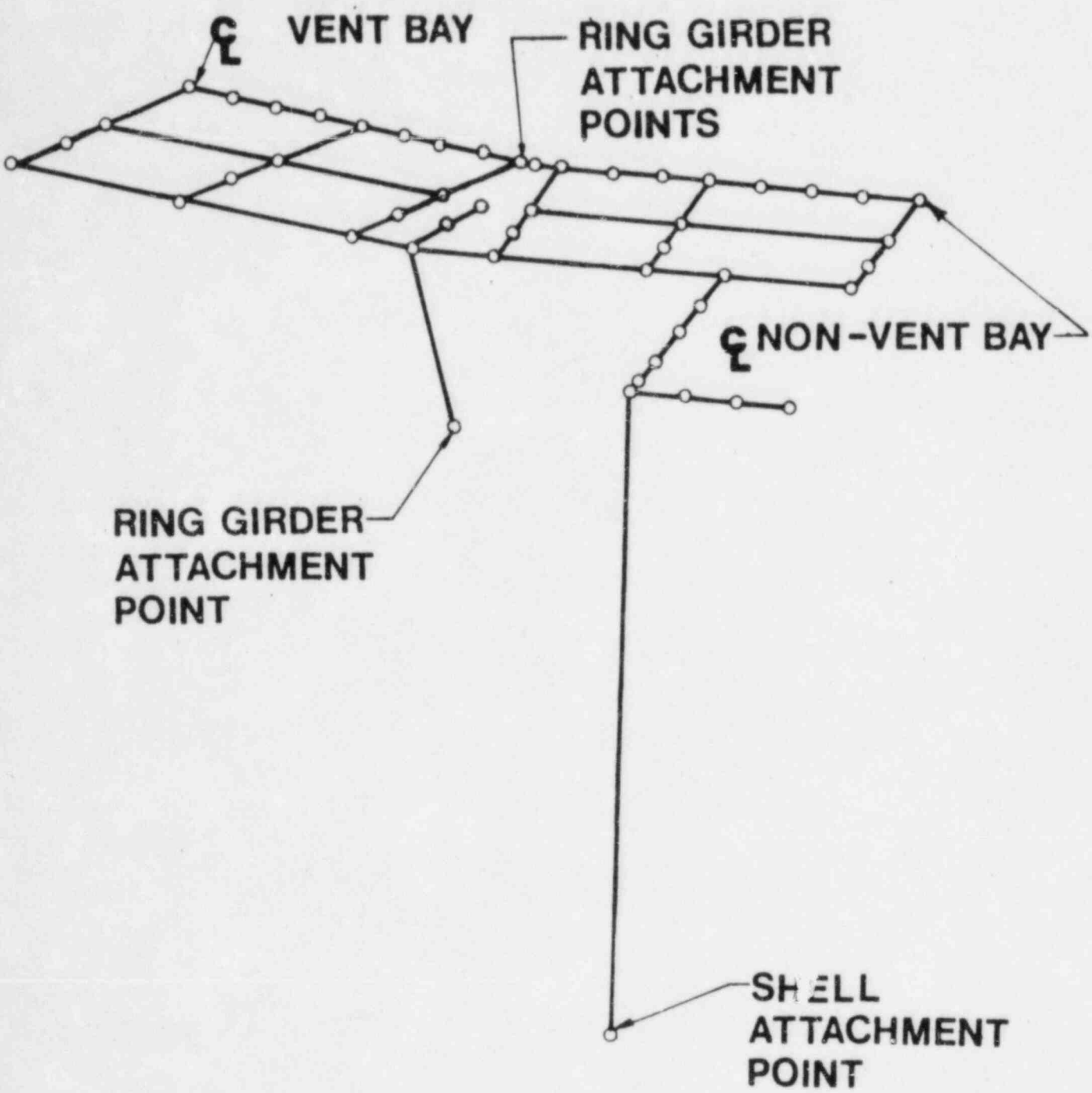

FIG. 7-1

UNMODIFIED CATWALK COMPUTER MODEL AT 315° AZ
FITZPATRICK

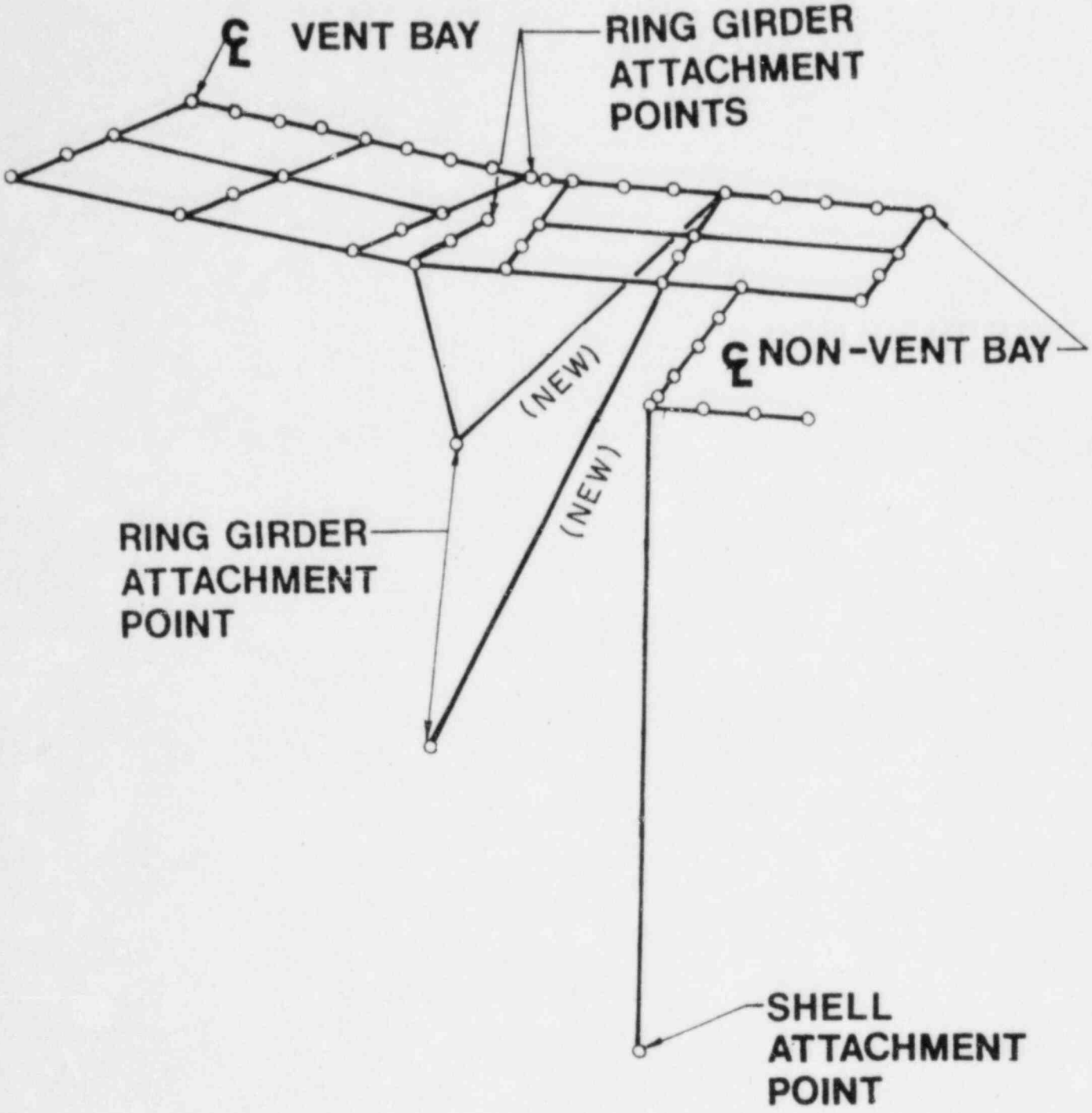

FIG. 7-2

MODIFIED CATWALK COMPUTER MODEL AT 315° AZ

FITZPATRICK

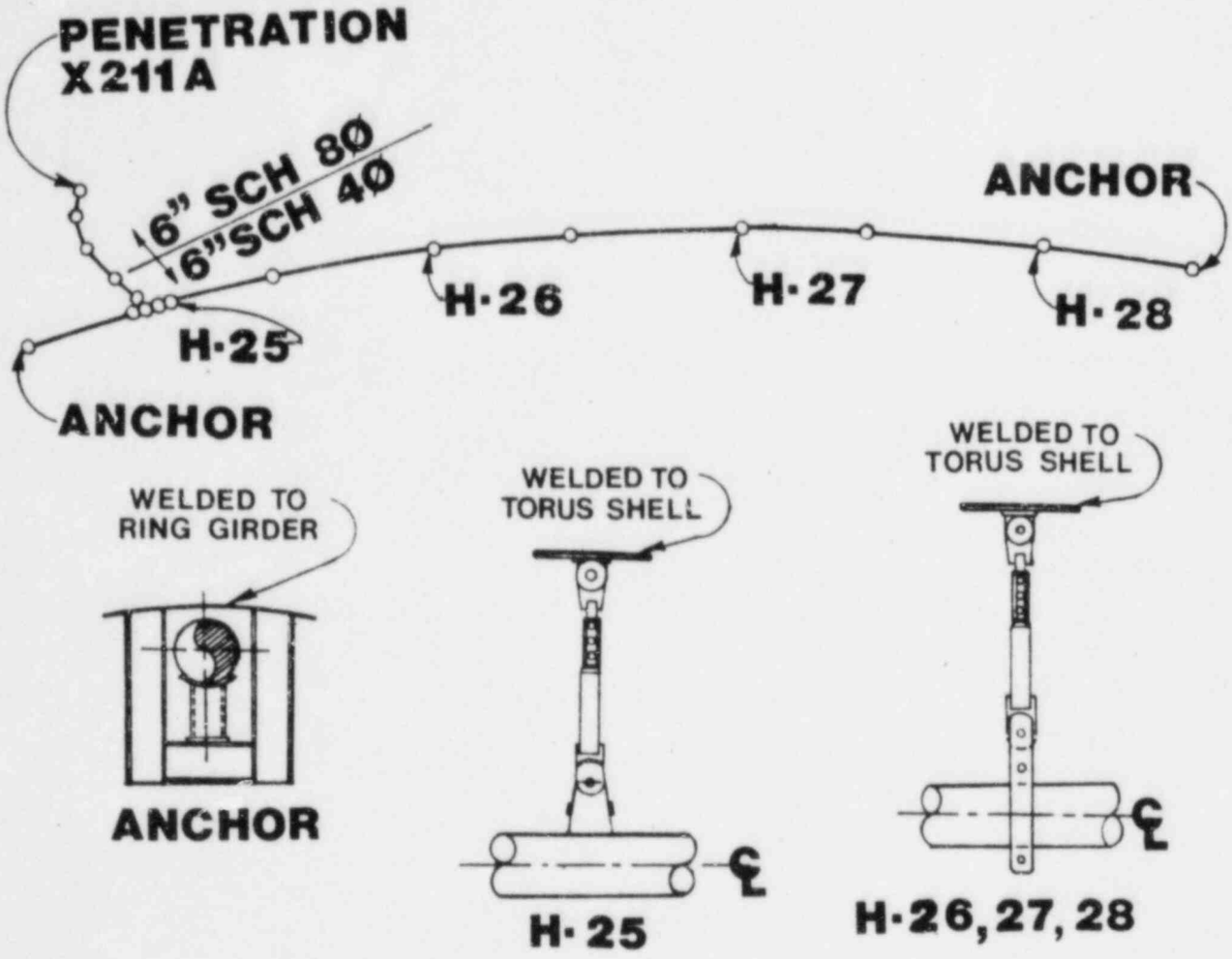

FIG. 7-3
INTERNAL SPRAY HEADER DOUBLE TORUS BAY
COMPUTER MODEL-FITZPATRICK

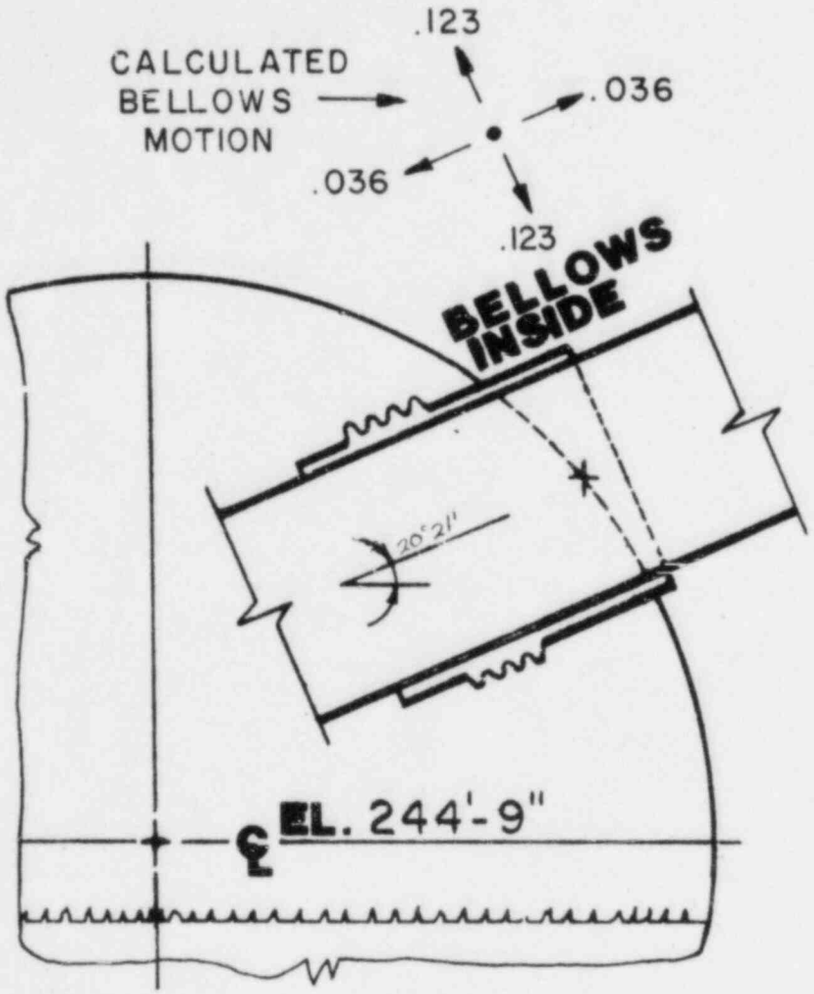

FIG. 7-4
MAXIMUM VENT PIPE - TORUS SHELL RELATIVE MOTION
ZERO - ΔP POOL SWELL - FITZPATRICK

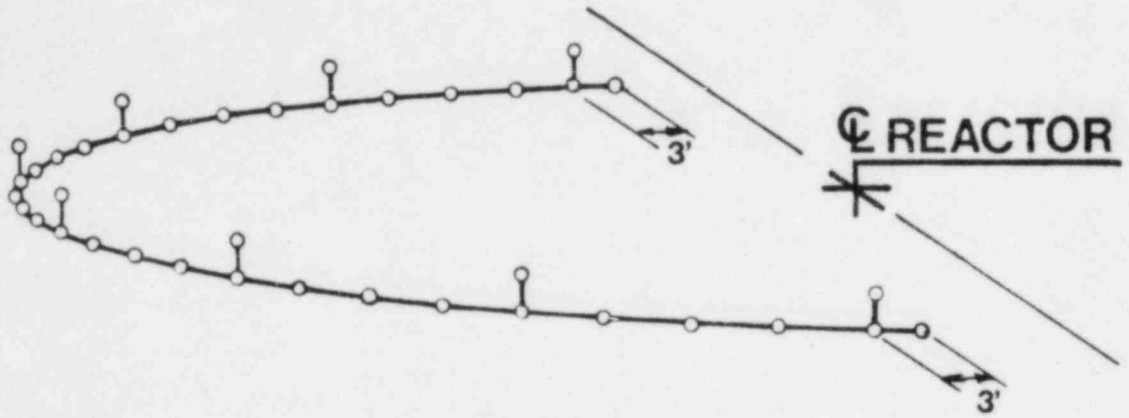

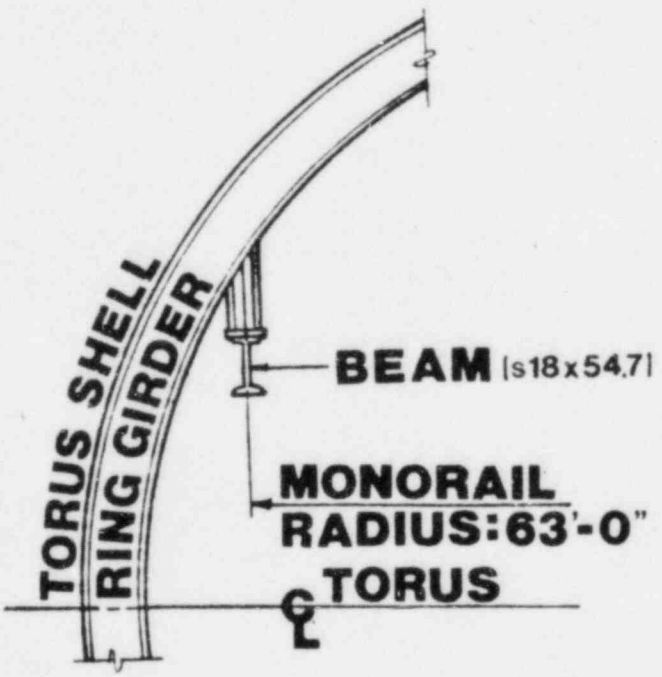

FIG. 7-5

TORUS MONORAIL 180° COMPUTER MODEL - FITZPATRICK

8.0 SUPPRESSION POOL TEMPERATURE EVALUATION

The Mark 1 modification which added tee-quenchers at the discharge end of the SRV lines required that we consider the high temperature performance characteristics of these devices. An important consideration in high temperature performance, is the mixing characteristics of the device and the attendent local-to-bulk temperature difference (Δt).

In response to these concerns and to assure reliable operation of these devices, the NRC has set limits on maximum pool temperatures for tee-quencher operation, as well as guidelines for a temperature monitoring system for the suppression pool. These requirements are stated in NUREG 0661 (Reference 2).

8.1 Maximum Suppression Pool Temperature

Reference 15 presents an evaluation showing the local temperature does not exceed the maximum pool temperature limits for tee-quencher operation at different flow rates, and for several different plant conditions. The evaluation of the Fitzpatrick Plant for these conditions was done by General Electric Company under contract to the Power Authority of the State of New York. The results of that work are reported here.

The local pool temperature limits for Fitzpatrick, and in accordance with NUREG-0661, is 200^{0}F. The General Electric evaluation of the Plant for the following seven conditions shows the limit is not exceeded:

1A Stuck-open SRV during power operation with one RHR loop available.

1B Stuck-open SRV during power operation assuming reactor isolation due to MSIV closure.

2A Isolation/scram and manual depressurization with one RHR loop available.

2B Isolation/scram and manual depressurization with the failure of an SRV to reclose (SORV).

2C Isolation/scram and manual depressurization with two RHR loops available. This case demonstrates the pool temperature responses when an isolation/scram event occurs under normal power operation, i.e., when all systems are operating in normal mode.

3A Small-break accident (SBA) with manual depressurization; accident mode with one RHR loop available.

3B Small-break accident (SBA) with manual depressurization and failure of the shutdown cooling system.

Table 8-1 summarizes the results of the evaluation of the conditions listed.

8.2 Pool Temperature Monitoring System

The NRC criteria also presents guidelines for a monitoring system to constantly monitor pool temperature. A monitoring system has been installed at Fitzpatrick which uses a network of 16 RTDs set in thermowells in the torus wall. The RTDs are hardwired to display consoles and an alarm in the control room. The system is described more fully in Section 2.2.1 of this report and is illustrated in Figures 2-9, 2-14 and 2-21.

Case No.	Event	Number of SRVs Manually Opened	Maximum Cooldown Rate (°F/hr)	Maximum Bulk Pool Temperature (°F)	Maximum Local Pool Temperature (°F)
1A	SORV at Power, 1 RHR Loop	2	1160	157	193
1B	SORV at Power, Spurious Isolation, 2 RHR Loops	1	570	172	198
2A	Rapid Depressurization at Isolated Hot Shutdown, 1 RHR Loop	5	1500	166	203 w/o end cap holes 195 w/end cap holes
2B	SORV at Isolated Hot Shutdown, 2 RHR Loops	1	570	174	194
2C	Normal Depressurization at Isolated Hot Shutdown, 2 RHR Loops	5	100	179	193
3A	SBA-Accident Mode, 1 RHR Loop	6 (ADS)	5000	163	196
3B	SBA-Failure of Shutdown Cooling Mode, 2 RHR Loops	5	100	178	188

*When the main condenser becomes available.

TABLE 8-1

SUMMARY OF RESULTS

FITZPATRICK POOL TEMPERATURE RESPONSE

REFERENCES

1. G.E. Report NEDO-21888, Rev. 2, "Mark 1 Containment Program Load Definition Report", dated November 1981.

2. NRC "Safety Evaluation Report, Mark 1 Containment Long-Term Program", NUREG 0661, dated July 1980.

3. G.E. Report NEDO-24583-1 "Mark 1 Containment Program Structural Acceptance Criteria Plant Unique Analysis Application Guide" dated October 1979.

4. G.E Report NEDO-21944 "...¼ Scale 2-D Plant Unique Pool Swell Test Report" dated August 1979.

5. G.E. Report NEDO-24615 "....¼ Scale Suppression Pool Swell Test Program: Supplemental Plant Unique Test", dated June 1980.

6. G.E. Report NEDE-24840 "Mark 1 Containment Program - Evaluation of Harmonic Phasing for Mark 1 Torus Shell Condensation Oscillation Loads" October 1980.

7. G.E. Report NEDE-24519-P "Mark 1 Torus Program Seismic Slosh Evaluation" dated March 1978.

8. G.E. Report NEDE-21968 "Analysis of Vent Pipe - Ring Header Intersection" dated April 1979.

9. Deleted.

10. G.E. Report NEDO-24578, Rev. 1, "Mark 1 Containment Program - Plant Unique Load Definition - James A. Fitzpatrick Nuclear Power Plant, dated April, 1981.

REFERENCES (CONTINUED)

11. ASME B&PV Code, Section III, Division 1, through Summer 1977.

12. Structural Mechanics Report SMA-12101.05-R001, "Design Approach for FSTF Data for Combining Harmonic Amplitudes for Mark 1 Post Chug Response Calculations", dated May, 1982.

13. Mark 1 Containment Program Report WE8109.31 "Buckling Evaluation of a Mark 1 Torus", dated January, 1982.

14. Structural Mechanics Assoc. Report SMA-12101.04-R003D, "Response Factors Appropriate for Use with CO Harmonic Response Combination Design Rules", dated March, 1982, pg. 3.

15. G.E. Report NEDC-24351-P "James A. Fitzpatrick Nuclear Power Plant Suppression Pool Temperature Response", dated August 1981.

16. Welding Research Council Bulletin No. 107, "Local Stresses in Spherical & Cylindrical Shells due to External Loadings", dated August 1965.

17. Welding Research Supplement, "Local Stresses in Spherical Shells from Radial and Moment Loadings", P.P. Bijlaard, dated May 1957.

18. "On the Effects of Tangential Loads on Cylindrical & Spherical Shells", P.P. Bijlaard, Unpublished, Available from PVRC, Welding Research Council.

19. James A. Fitzpatrick, Final Safety Analysis Report Update, 1978, Page 16.7-7.

CLASS MC COMPONENTS AND INTERNAL STRUCTURES

TABLE I

EVENT COMBINATIONS		SRV	SRV + EQ		SBA IBA		SBA + EQ IBA + EQ				SBA + SRV IBA + SRV		SBA + SRV + EQ IBA + SRV + EQ				DBA		DBA + EQ				DBA + SRV		DBA + EQ + SRV			
						CO, CH			CO, CH			CO, CH			CO, CH		PS (1)	CO, CH	PS		CO, CH		PS	CO, CH	PS		CO, CH	
TYPE OF EARTHQUAKE			O	S			O	S	O	S			O	S	O	S			O	S	O	S			O	S	O	S
COMBINATION NUMBER		1	2	3	4	5	6	7	8	9	10	11	12	13	14	15	16	17	18	19	20	21	22	23	24	25	26	27
LOADS																												
Normal (2)	N	X	X	X	X	X	X	X	X	X	X	X	X	X	X	X	X	X	X	X	X	X	X	X	X	X	X	X
Earthquake	EQ		X	X			X	X	X	X			X	X	X	X			X	X	X	X			X	X	X	X
SRV Discharge	SRV	X	X	X							X	X	X	X	X	X							X	X	X	X	X	X
LOCA Thermal	T_A				X	X	X	X	X	X	X	X	X	X	X	X	X	X	X	X	X	X	X	X	X	X	X	X
LOCA Reactions	R_A				X	X	X	X	X	X	X	X	X	X	X	X	X	X	X	X	X	X	X	X	X	X	X	X
LOCA Quasi-Static Pressure	P_2				X	X	X	X	X	X	X	X	X	X	X	X	X	X	X	X	X	X	X	X	X	X	X	X
LOCA Pool Swell	P_{FS}																X		X	X			X		X	X		
LOCA Condensation Oscillation	P_{CO}					X			X	X		X			X	X		X			X	X		X			X	X
LOCA Chugging	P_{CH}					X			X	X		X			X	X		X			X	X		X			X	X
STRUCTURAL ELEMENT	ROW																											
External Class MC																												
Torus, External Vent Pipe, Bellows, Drywell (at Vent), Attachment Welds, Torus Supports, Seismic Restraints	1	A	B	C	A	A	B	C	B	C	A	A	B	C	B	C	A (3, 6)	A	B (3, 6)	C	B	C	C	C	C	C	C	C
Internal Vent Pipe																												
General and Attachment Welds	2	A	B	C	A	A	B	C	B	C	A	A	B	C	B	C	A (3, 5)	A	B (3, 5)	C	B	C	C	C	C	C	C	C
At Penetrations (e.g., Header)	3	A	B	C	A	A	B	C	B	C	A	A	B	C	B	C	A (3)	A	B (3)	C	B	C	C	C	C	C	C	C
Vent Header																												
General and Attachment Welds	4	A	B	C	A	A	B	C	B	C	A	A	B	C	B	C	A (3, 5)	A	B (3, 5)	C	B	C	C	C	C	C	C	C
At Penetrations (e.g., Downcomers)	5	A	B	C	A	A (4)	B	C	B (4)	C	A	A (4)	B	C	B (4)	C	A (3, 4, 5)	A (4)	B (3, 4, 5)	C	B (4)	C	C	C	C	C	C	C
Downcomers																												
General and Attachment Welds	6	A	B	C	A	A	B	C	B	C	A	A	B	C	B	C	A (3, 5)	A	B (3, 5)	C	B	C	C	C	C	C	C	C
Internal Supports	7	A	B	C	A	A	B	C	B	C	A	A	B	C	B	C	A	A	B	C	B	C	C	C	C	C	C	C
Internal Structures																												
General	8	A	B	C	A	A	C	D	C	D	C	C	D	E	D	E	E	E	E	E	E	E	E	E	E	E	E	E
Vent Deflector	9	A	B	C	A	A	C	D	C	D	C	C	D	D	D	D	D	D	D	D	D	D	D	D	D	D	D	D

TABLE 2

PLANT PHYSICAL DIMENSIONS

FITZPATRICK

TORUS

Inner Diameter	29'6"
Number of Sections	16
Shell Plate Thickness	
Vent Pipe Penetration	1.125"
Top Half	.568"
Bottom Half	.632"

SUPPORT COLUMNS

	Quantity	Size
Outer	16	12WF161 structural shape with fabricated
Inner	16	I section near top
Base Assembly	Sliding, not anchored	

RING GIRDER

Quantity	16
Size	T-Beam (8" x 1.5" Flange, 1.5" x 27.5" (Average) Web)

EARTHQUAKE RESTRAINT SYSTEM

Quantity	4
Type	Shell Mounted - Pinned to Floor

DRYWELL VENT SYSTEM

	Quantity	Size
Vent Pipe	8	6'9" I.D.
Vacuum Breakers	5	30" I.D.
Vent Header Support Columns	16 pairs	6" Sch. 80
Downcomers	96	24" O.D.
Minimum Submergence	4.29'	

TABLE 3

PLANT ANALYSIS INFORMATION

FITZPATRICK

Seismic Acceleration Values (G's)

	OBE	SSE
Vertical	.06	.10
Horizontal	.08	.15

Effective Water Mass for Horizontal Seismic Load (Reference 7)

22.1%

Effective Water Mass during Pool Swell Uplift (Reference 4)

Full ΔP - 71%

Zero ΔP - 63%

Plant Unique C.O. Multiplier (Reference 1)

.892

TABLE 4

SRV LOAD CASE/INITIAL CONDITIONS

	Design Initial Condition	Any One Valve	ADS* Valves	Multiple Valves
		1	2	3
A	1 NOC*., First Act.	A1.1		A3.1
	2 SBA/IBA,* First Act.	A1.2	A2.2	A3.2
	3 DBA,* First Act.[1]	A1.3		
C	1 NOC, Subsequent Act.			C3.1
	2 SBA/IBA, Sub. Act. Air in SRV/DL			C3.2
	3 SBA/IBA, Sub. Act. Steam in SRV/DL			C3.3

(1) This actuation is assumed to occur coincidently with the pool swell event. Although SRV actuations can occur later in the DBA accident, the resulting air loading on the torus shell is negligible since the air and water initially in the line will be cleared as the drywell to wetwell ΔP increases during the DBA transient.

* ADS = Automatic Depressurization System

NOC = Normal Operating Condition

SBA = Small Break Accident

IBA = Intermediate Break Accident

DBA = Design Basis Accident

APPENDIX 1

Use of SRV In-Plant Test Data for Analysis

Test Data

The in-plant SRV tests used to support structural analysis were run at Fitzpatrick in April, 1982. The data was collected in a series of four tests, each consisting of one actuation with a cold line and a second about one minute later (hot line). Each of the four test pairs was run at approximately one week intervals.

The torus shell was instrumented with a combination of strain and pressure transducers as shown in Figure A1-1. Strain gages were mounted in pairs on both sides of the shell to allow separation of bending and membrane stresses. Additional gages were located on the tee-quencher and support (Figure A1-2), vent header support column (Figure A1-3), and downcomers (Figure A1-4). Pressure transducers were mounted on the shell and ring girder as illustrated in Figure A1-1.

Two independent data collection systems were used to provide a check on system accuracy. The major system was a multiplexed FM tape system on which all data was collected. The second system was a hard wired oscillograph to produce direct, quick-look readout on several channels.

In all, 100 transducers were used during the testing; as follows:

Strain Gages		
	Shell	42
	Internal Structures	28
Pressure Transducers		
	Shell	19
	Ring Girder	8

DCDT's

Shell	1
Attached Piping	2

Use of Data - Applications

The SRV test data was used to calibrate computer analysis of the shell and support systems and also to establish actual numbers for SRV drag loads on submerged structures.

Use of Data - Shell & Support System Analysis

Evaluation of shell stress and support system loads due to SRV actuation was done with a large detailed computer model as discussed in para. 3.2.4 of the report. Data collected from the in-plant tests was used to define the actual shell pressures and decay time for a benchmark (test) condition and to develop correction factors between these measured results and values predicted by generic analytical methods. The steps involved are these:

1. Determine maximum average shell pressure, average frequency and waveform for the four cold tests.

2. Calculate these same quantities for the test conditions using the generic computer programs (QBUBS 02).

3. Calculate calibration factors relating predicted-to-actual pressure and predicted-to-actual frequency.

4. Calculate predicted pressures and frequencies using the generic computer program, for other SRV conditions.

5. Apply the calibration factors calculated in step (3) to all other predictions for pressure and frequency. The duration of the pres-

sure transient, as measured in the test, is affected proportionally by the frequency correction and used as the basis for all computer model loading.

Verification of Computer Model

The test data was also used to verify the accuracy of the computer model. This was done by the following method:

1. The computer model was loaded with the measured shell pressures.

2. The model was run and stresses at all strain gage locations were calculated.

3. Comparisons were made between computer predicted shell stress and measured shell stress at the same points.

Correlations for shell stress were excellent - generally within 5%. Correlations to column loads were not so good - generally off by about 50%. This difference in computer results for test conditions was handled by developing a second calibration factor for supports only, and combining it with the previous pressure calibration factor. The results were two different calibration factors to be applied to final analysis - one for the shell and one for the columns. The factors developed and used are:

Shell pressure = .34 x predicted

Support load = .4 x predicted

Multiple Valve Contributions

For cases where more than one valve actuates, the contributions from other valves were added directly (same signs). The maximum value used was 1.65 x the pressure from a single valve (Reference 2).

SRV Test Data for Drag Loads

The data collected during the Fitzpatrick in-plant test included strains and pressures measured on submerged structures. Strain gages, positioned to show bending stress due to drag loads, were installed on the downcomer and vent header support column. Figure A1-4 shows the locations of these gages, relative to the quencher. Pressure transducers were mounted on the ring girder. The test data showed these results:

1. Structural response occurred at the natural frequency of the structure only.

2. Responses were much less than would be predicted by Program analysis methods - as much as an order of magnitude lower.

The data collected from Fitzpatrick was evaluated along with the data collected by TES in three other in-plant tests. The matrix of data collected is as follows:

	Catwalk Supports	Vent Column	Downcomer	Ring Girder (Pressure)
Millstone	X	X	X	
Nine Mile Point		X	X	
Vermont Yankee	X	X		
Fitzpatrick		X	X	X

An important consideration in the application of this data was the possibility that resonant structural response might occur at some other SRV condition. This was considered and dismissed based on two separate arguments; they are:

1. If a major frequency component existed in the drag force, it would be detectable on each of the structural responses for a given test. This did not occur.

2. The response frequencies of the structures tested (structural natural frequencies) ranged from 8.1 to 38 Hz.* If any single strong frequency existed in the drag load, one of the structural responses should have demonstrated some degree of resonant response - none did.

We conclude from this that the structures involved are responding to a fairly uniform random field and that the test data represents usable data for all SRV conditions.

The next step in the process was to calculate an equivalent static load for each structure. This is the static load that produces the same bending stresses measured in the test, when applied uniformly to the submerged area. These static pressure values were plotted against distance from the quencher and Figure A1-5 was developed. This curve represents the equivalent static drag pressures, including quencher jet loads. It is scaled upward from test conditions to more severe SRV cases by the ratio of the calculated shell pressures for the two cases, for application to structures under different loading conditions.

*Actual values were 8.1, 8.2, 14.5, 15, 21, 23, 24, 25, 29, 30, 34 and 38 Hz.

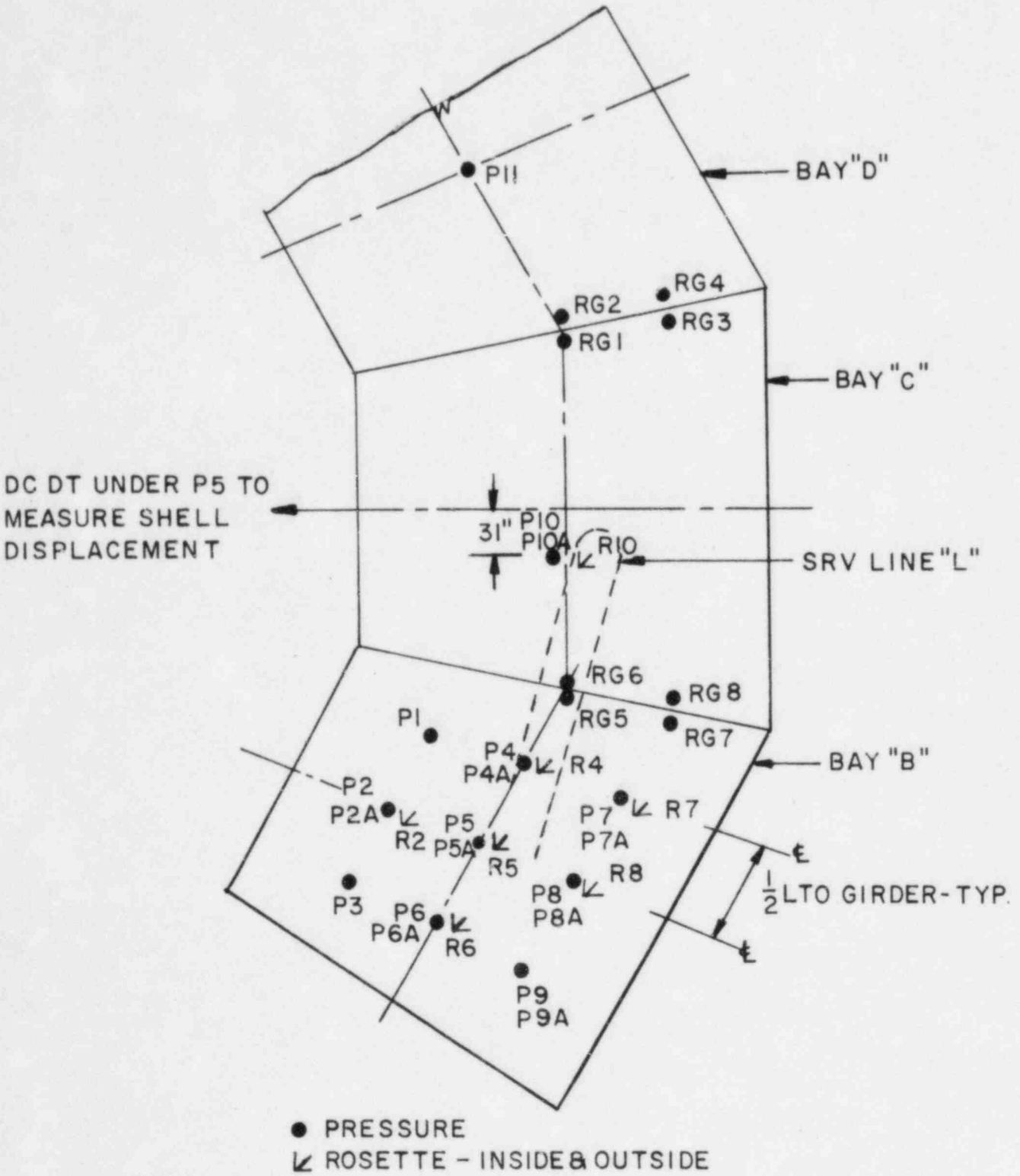

FIG. A1-1

PRESSURE & SHELL GAGE LOCATIONS - FITZPATRICK

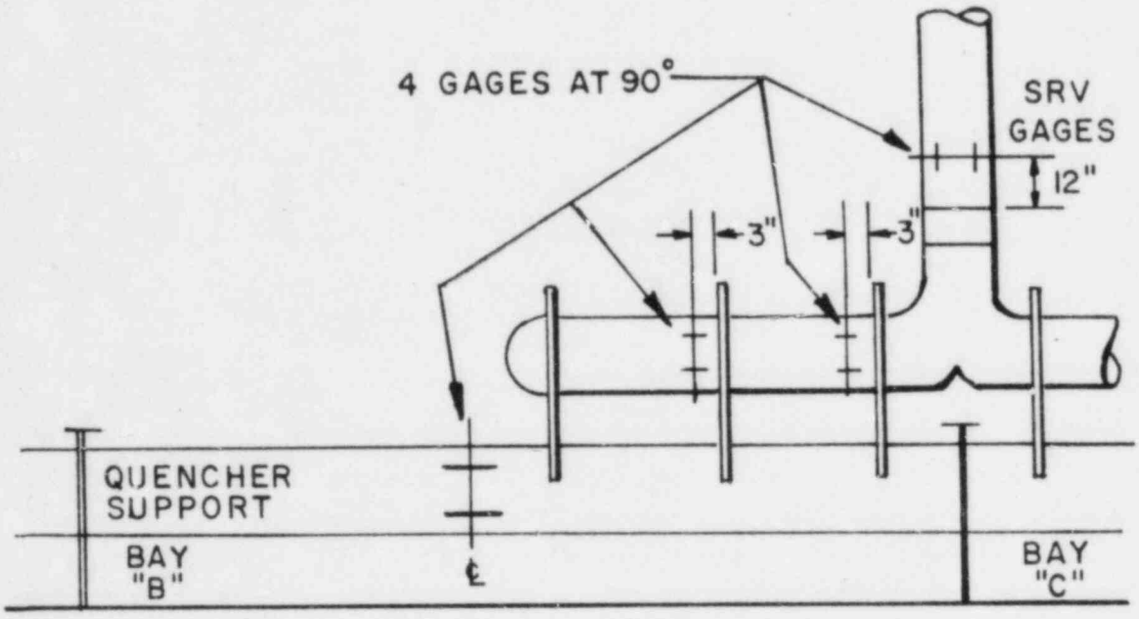

FIG. A1-2

SRV TEST - TEE QUENCHER & SUPPORT GAGES
FITZPATRICK

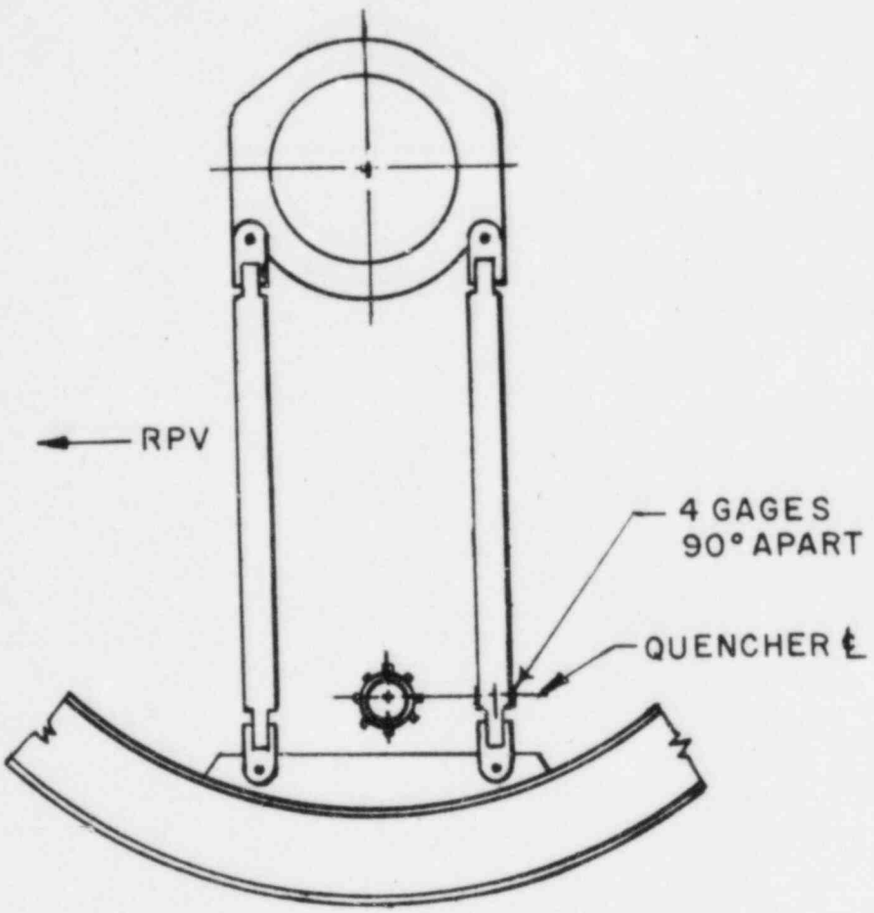

FIG. A1-3

SRV TEST-VENT HEADER SUPPORT GAGES

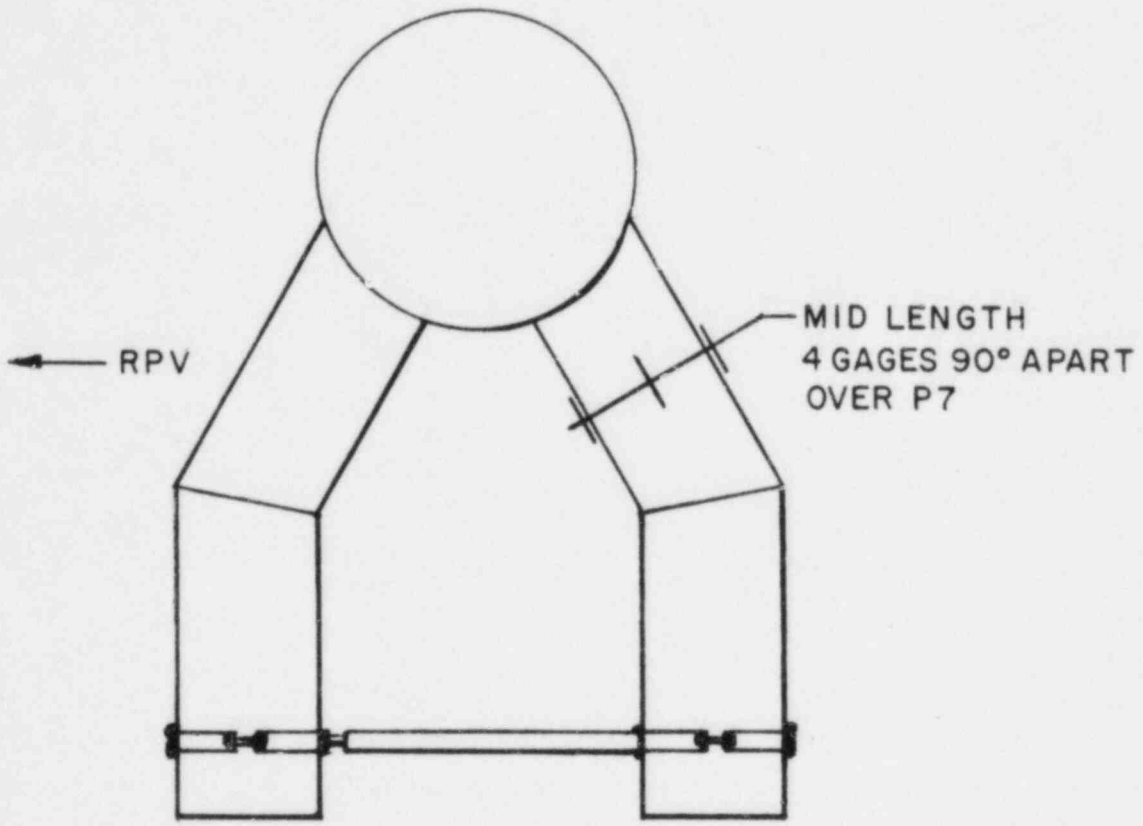

FIG. A1-4

DOWNCOMER GAGES

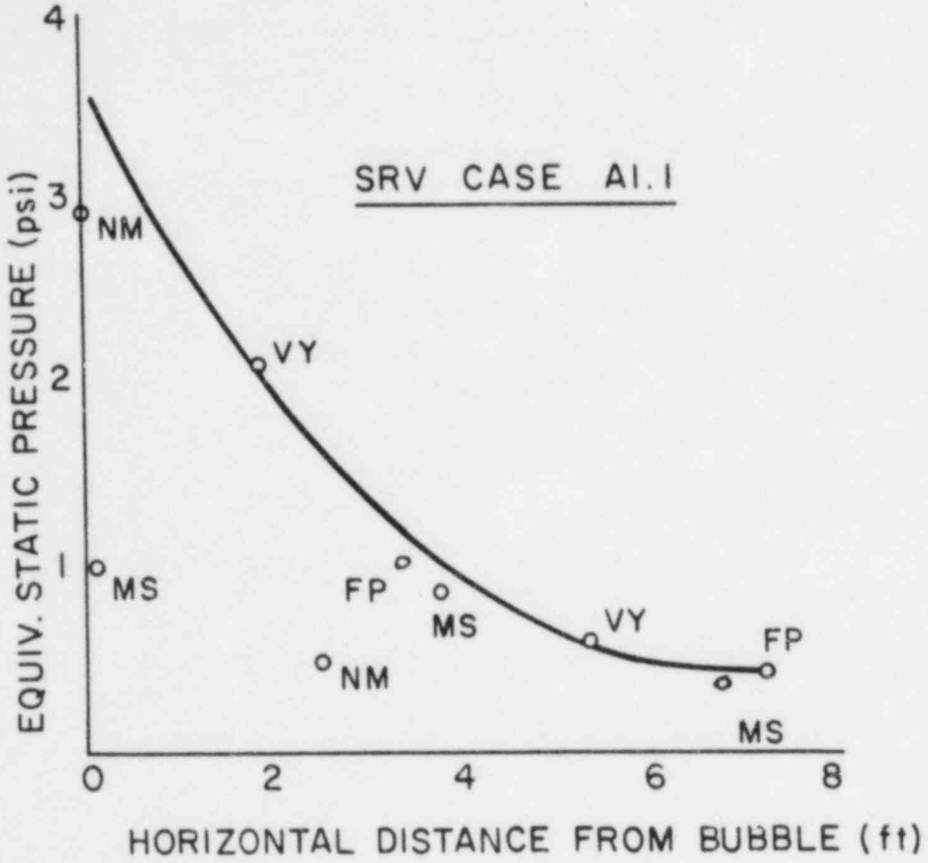

EQUIVALENT SRV DRAG FROM IN PLANT TESTING

FIG A1-5

APPENDIX 2

Discussion of 32 Hz Frequency Cut-off for Condensation Oscillation and Post Chug Analysis

TES made the decision to limit CO and Post Chug response analysis to frequencies below 32 Hz early in the program. The decision was the result of several considerations that led to the conclusion that the 32 Hz cut-off would produce realistic results.

The basis for use of a 32 Hz cut-off involved strong fundamental arguments, both in the loads used for the analysis, and in the stress analysis itself. The primary arguments are different for CO, and for Post Chug, and are given here:

For condensation oscillation analysis.

1. Load Definition - A PSD study of the CO pressure data showed that frequencies above 25 Hz accounted for only 10% of total power (Reference 1, page 4.4.1-10). This means that a system with flat frequency response to 50 Hz would suffer a 10% unconservative stress error if a 25 Hz cut-off was used. Since we are using a 32 Hz cut-off and our system is highly responsive at low frequencies (not flat), we should expect a much smaller error.

2. Structural Response Analysis - The relative importance of loads below and above 32 Hz can be judged based on examination of the modal frequencies and generalized coordinates of the structure in both frequency ranges. If we consider the characteristics of a typical torus model in these ranges, we find:

	Number of Frequencies	Number of* $GX\emptyset^2$ > 1000	Number of $GX\emptyset^2$ > 2000	Max. Value $GX\emptyset^2$
Below 32 Hz	44	25	14	167,858
32-50 Hz	34	5	1	4,594

*Product of generalized weight and the square of the participation factor - used as an indicator of modal response strength.

These figures show that for condensation oscillation, frequencies below 32 Hz clearly dominate the response and frequencies above 32 Hz are relatively insignificant. They provide a strong indication that the 10% worst-case unconservatism discussed above will be greatly reduced by the selective nature of the structural response. We should logically expect the structural response characteristics, and the fact that we are using a 32 Hz cut-off, instead of 25, to reduce the 10% maximum error to less than 5%. An error of this magnitude is consistent with other assumptions which must be made in the analysis and is considered acceptable.

A further statement regarding the validity of this approach may be found in References 11 and 14.

For the Post Chug load, the second consideration of structural response is also valid, but the load definition is not as heavily skewed toward the low frequency end as is C.O. The decision for handling post chug was heavily influenced by the fact that it produced very low stress. This is discussed further in Section 3.2.3.2 of this report.

APPENDIX 3

CO/CH Drag Loads for Ring Girder Analysis

TES did not follow the calculational methods of NUREG 0661 (Reference 2) for calculation of CO/CH drag loads on the ring girder. This appendix describes the method that was used, the differences from the NUREG method and the basis for the change.

The NUREG analysis method specifies that acceleration drag forces (and effective hydrodynamic mass) for flat plates be based on an equivalent cylinder with radius equal to 2 times the radius of the circumscribed circle. It also specifies that the drag forces be increased by an additional factor of 2 for structures attached to the torus shell, to account for wall interference.

Application of the NUREG criteria produces a factor of 4 multiplier for drag force for flat plate structures in the fluid; and a factor of 8 multiplier for flat plate structures in the fluid and attached to the shell. These values are referenced to a drag force equal to 1.0 for flat plate calculations based on potential flow theory and neglecting interference effects.

These increases in loads are supported by data available in Reference A3-1 and A3-2. Keulegan and Carpenter show in Reference A3-1 that the drag forces on a plate in an oscillating flow may be as much as a factor of 4 higher than the theoretical force based on potential flow. Sarpkaya shows in Reference A3-2 that forces on a cylinder near a boundary, may be twice as high as forces away from the boundary.

Both References A3-1 and A3-2 present results as a function of the VT/D ratio where:

V = maximum velocity

T = period of flow oscillation

D = diameter

Keulegan and Carpenter (Reference A3-1) show the effective hydrodynamic mass coefficient for a plate varies from a maximum of 4 at $\frac{VT}{D}$ = 125 to 1 at VT/D = 0. (pure potential flow). Sarpkaya (Reference A3-2) shows an increase in the hydrodynamic mass coefficient for a cylinder near a boundary that varies from a maximum factor of 2 at $\frac{VT}{D}$ = 15 to a minimum of 1.65 at VT/D = 0.

NUREG 0661 appears to use the bounding values from both of these references to formulate its' analysis method. It implies by this that large values of $\frac{VT}{D}$ will exist in the torus. In fact, this is not true for CO and CH drag loads on the ring girder. For this structure, under this load, $\frac{VT}{D}$ ratios are near zero and the use of maximum multipliers should not be necessary. It is on this basis that we have used an alternate method to calculate CO and CH drag loads on the ring girder.

The TES method to calculate these drag loads on the ring girder used the same references as above (A3-1 and A3-2), but accounted for calculated values of $\frac{VT}{D}$, rather than the values corresponding to the maximum increases. Consid-sideration of the actual $\frac{VT}{D}$ ratio for wall interference led to an interference factor of 1.65 (instead of 2).

Low values of $\frac{VT}{D}$ suggest that the theoretical hydrodynamic mass coefficient for the ring girder is appropriate. The theoretical coefficient for this structure is estimated by an equivalent cylinder with a radius equal to the circumscribing radius. Use of this cylinder results in a hydrodynamic mass coefficient equal to two. The total factor used was related to the NUREG multiplier by:

$$\frac{2.0}{4.0} \times \frac{1.65}{2.0} = .41$$

The factor used by TES was .41 x the NUREG 0661 factor.

REFERENCES

A3-1 Keulegan and Carpenter, "Forces on Cylinders and Plates in a Oscillating Fluid," National Bureau of Standards, Vol. 60, No. 5, May 1959.

A3-2 Sarpkaya, "Forces on Cylinders near a Plane Boundary in a Sinusoidally Oscillating Fluid", Journal of Fluids Engineering, September 1976.